KOÇ ÜNİVERSİTESİ
GRADUATE SCHOOL OF HEALTH SCIENCES

KOÇ UNIVERSITY

GRADUATE SCHOOL OF HEALTH SCIENCES

THE ROLE OF PERICYTES IN THE PATHOPHYSIOLOGY OF MULTIPLE SCLEROSIS

EMINE SEKERDAG

NEUROSCIENCE

PHD THESIS

ISTANBUL 2019

KOÇ ÜNİVERSİTESİ
GRADUATE SCHOOL OF HEALTH SCIENCES

KOÇ UNIVERSITY

GRADUATE SCHOOL OF HEALTH SCIENCES

THE ROLE OF PERICYTES IN THE PATHOPHYSIOLOGY OF MULTIPLE SCLEROSIS

NEUROSCIENCE

PHD THESIS

EMINE SEKERDAG

Advisor: Prof. Dr. Yasemin Gürsoy-Özdemir

Thesis Approval

Koç University Graduate School of Health Sciences, Neuroscience Department, PhD student **EMINE SEKERDAG**, has successfully completed her PhD thesis titled '**THE ROLE OF PERICYTES IN THE PATHOPHYSIOLOGY OF MULTIPLE SCLEROSIS**' on ……

Jury Members:

Prof. Dr Yasemin Gürsoy-Özdemir Signature:

Prof. Dr. Turgay Dalkara Signature:

Prof. Dr. Erdem Tüzün Signature:

Assoc. Prof. Dr. Müjdat Zeybel Signature:

Dr. Atay Vural Signature:

Statement

Hereby I declare that this thesis study is my own work, and that from the planning of the thesis to the writing of all phases there were no ethical issues. I declare, that I have obtained all the information in this thesis within academic and ethical rules, and all literature information and interpretations used in this thesis have been referred to their sources. I also, declare that there is no violation of patent and copyright rights during the study and writing of this thesis.

Emine Sekerdag

Acknowledgements

Undertaking this PhD has been an exciting challenge for me and it would not have been possible without the support and guidance of many people around me.

First of all, I would like to express my deepest gratitude to my supervisor Prof. Dr. Yasemin Gürsoy-Özdemir for her support and motivation as well as her excellent mentoring at all times during these 4 years of my PhD study. I am very happy that I met her here in Turkey, and that I continued a PhD in her research group. She has been and still is one of my role models.

I further would like to thank Assoc. Prof. Dr. Müjdat Zeybel, Prof. Dr. Erdem Tüzün, Assoc. Prof. Dr. Cem İsmail Küçükali, Dr. Özgür Öztop Çakmak, Dr. Atay Vural, Prof. Dr. Meryem Aslı Tuncer for their excellent support and professional advices as well as motivation concerning this project and my overall PhD progression. I also thank my colleagues Dila Atak, Canan Ulusoy, Aysu Bilge Yılmaz, and Esra Özkan for their excellent assistance and contribution to the enormous amount of *in vivo* and *in vitro* experiments throughout the progression of this thesis project. Many thanks also go to my lovely internship students Seddiq Seyaj and Gülsüm Deniz for their help with cryosections and immunofluorescence studies.

I also acknowledge the funding received from TUBITAK, without it, it would not have been possible to conduct the research in this thesis.

I am also very grateful to all of those at KUTTAM for sharing their scientific knowledge with me, and many thanks go to Şimal Laçin and Tayfun Barlas for their technical assistance in the lab, as well as for providing practical solutions during hard times.

Finally, my deepest appreciation goes out to my family and dear ones for always believing in me and encouraging me to follow my dreams.

Content List

Figures & Tables List

Abbreviations

ADAMTS1 = ADAM Metallopeptidase with Thrombospondin Type 1 Motif 1

αSMA = Alpha Smooth Muscle Actin

BBB = Blood-brain Barrier

CC3 = Cleaved Caspase 3

CD13 = Amino-peptidase-N

CFA = Complete Freund's Adjuvant

CNS = Central Nervous system

CNTF = Ciliary Neurotrophic Factor

CY3 =Cyanine

DAPI = 4',6-diamidino-2-phenylindole

DMEM = Dulbecco's Modified Eagle Medium

DPBS = Dulbecco's Phosphate Buffered Saline

EAE = Experimental Autoimmune Encephalomyelitis

ECM = Extracellular Matrix

FBS = Fetal Bovine Serum

FITC = Fluorescein Isothiocyanate

H&E = Hematoxylin and Eosin

HBVP = Human Brain Vascular Pericytes

i.p = Intraperitoneal

IB4 = Isolectin

IL-10 = Interleukin 10

IP-10 = Interferon Gamma-Induced Protein 10

LFB = Luxol Fast Blue

LOX = Lysyl Oxidase

MAG = Myelin Associated Glycoprotein

MAP2 = Microtubule-associated Protein 2

MBP = Myelin Basic Protein

MCP-1 = Monocyte Chemoattractant Protein-1

MMP = Matrix Metallopeptidases

MOG = Myelin Oligodendrocyte Glycoprotein

MS = Multiple Sclerosis

NfKB = Nuclear Factor Kappa B

NG2 = Neural/glial antigen 2

NO = Nitric Oxide

NVU = Neurovascular Unit

OCT = Optimal Cutting Temperature compound

PBS = Phosphate Buffered Saline

PDGF-BB = Platelet-derived Growth Factor BB

PDGFRβ = Platelet Derived Growth Factor Receptor Beta

PFA = Paraformaldehyde

PI = Post Immunization

PLL = Poly-L-Lysine

PLP = Proteolipid Protein

PPMS = Primary Progressive MS

P/S = Penicillin/Streptomycin

PTX = Pertussis Toxin

RGS-5 = Regulator of G-protein Signaling 5

RRMS = Relapsing Remitting MS

s.c. = Subcutaneous

SJL = Swiss James Lambert

TGFβ = Transforming Growth Factor beta

TIMP3 = TIMP Metallopeptidase Inhibitor 3

TNFα = Tumor Necrosis Factor alpha

VEGF = Vascular Endothelial Growth Factor

ZO-1 = Zonula occludens-1

Abstract

Aim. Pericytes are multifunctional cells located at the blood-brain barrier (BBB). They maintain BBB integrity, regulate cerebral blood flow and possess immunological roles which indicate that pericytes could be the main players in the pathophysiology of Multiple sclerosis (MS), a chronic inflammatory demyelinating disease of the central nervous system (CNS). This study investigated the role of pericytes in the pathophysiology of MS with a special focus on vascular pathology. **Methods.** Experimental Autoimmune Encephalomyelitis (EAE) models were induced with myelin oligodendrocyte glycoprotein (MOG) or proteolipid protein (PLP). Two time-point models were developed, 15 days (early EAE) and 40 days (late EAE) to investigate the progression of both models. Cryosections of spinal cord and brain were assessed for BBB leakage, demyelination, inflammation, axonal loss and gliosis, vascular pathology, pericytes and fibrosis. Furthermore, to relate the obtained *in vivo* outcomes to pericyte function, cell culture of human brain vascular pericytes (HBVP) were exposed to MS serum and compared to *in vivo* data. **Results and Discussion.** In both MOG and PLP induced EAE models, pericytes were increased at lesion sites. In MOG EAE model pericyte coverage was decreased on the endothelial walls but increased and scattered throughout the lesions. In MOG EAE, detached PDGFRβ+ and αSMA+ pericytes were present according to co-localization studies with endothelium. On the other hand, PLP EAE model showed increased PDGFRβ+ pericytes accumulated at the vasculature throughout the EAE tissue. Additionally, these pericyte accumulations were enhanced at lesion sites in the white matter. Upon exposure of HBVP to MS patient serum, it was found that pericytes proliferate upon contact with MS serum and produce Collagen I & Collagen IV and Fibronectin which was in line with our *in vivo* findings. **Conclusion:** Abovementioned data implicates that pericytes are possibly involved in both progression and suppression of EAE by mediating fibrosis.

Keywords: Multiple Sclerosis, EAE, Pericytes, Fibrosis, Collagen I, Collagen IV

1 Introduction

Multiple sclerosis (MS) is a chronic, inflammatory, demyelinating and neurodegenerative disease of the central nervous system (CNS). The incidence of this disease varies depending on the geographical and ethnic (racial) characteristics with a prevalence of 2-200/100000. Despite the rapid accumulation of information in recent years, MS is still a complex disease with unknown pathophysiology. It is believed that both autoimmune and infectious mechanisms may play a role in MS (1). Genetic and environmental factors have also been emerged as a potential factor for the onset of the disease (2-4). Although the specific factors that trigger MS are not known, autoreactive T cells and antibodies against CNS structures are believed to play a major pathogenic role in the development of inflammation and tissue damage. The same mechanism is also responsible for the progression of neurological disability and function loss (5).

Immune histopathology of MS lesions indicate T and B lymphocytes infiltration in the white matter of the brain and spinal cord (6-8). However, it is unknown what the underlying antigenic structure is. It is understood that T lymphocytes in MS react to myelin and activate macrophages with microglia and disrupt the nerve axons by damaging their myelin sheath (9, 10). However, it is unknown whether this is a primary reaction or an epiphenomenon that occurs during the course of the disease. Although it is likely that autoreactive T cells mediate MS pathogenesis, it is unclear which factor(s) trigger their migration to and subsequent activation in the CNS (11). One important aspect in this regard is the blood-brain barrier (BBB). The BBB hinders reachability of the CNS by immune cells, however also secretes and/or mediates the release of chemoattractant molecules as an interface between CNS cells and the immune system and is therefore also responsible for mediating cell entry into the CNS. The determining factors that play a role in cell migration into the CNS are currently being investigated and subsequent novel treatment strategies are being considered.

Next, there is evidence of an immunological function of astrocytes and microglia in CNS inflammation, however their specific roles in MS lesion pathology are still controversial (12-15). In MS, both microglia and astrocytes are activated and express a high level of major histocompatibility complex (MHC) class II molecules (16) but on the other hand can also secrete anti-inflammatory cytokines such as transforming growth factor beta (TGFβ) and Interleukin 10 (IL-10) to suppress T helper cell responses. It has also been shown that microglia and/or macrophages play important roles as antigen presenting cells (17). Although the role of T cells is known to be prominent in the pathogenesis of MS and Experimental Autoimmune Encephalomyelitis (EAE), the importance of humoral immune response in MS patients has gained great interest as well. Recently reported MS pathology studies draw attention to the important contribution of B cells in MS pathogenesis (18, 19).

MS is a heterogeneous disease when evaluated in terms of clinical, radiological and treatment responses. In MS lesions, demyelination mechanisms are divided into four separate patterns (20, 21):

Pattern 1: Macrophage related demyelination which is similar to EAE model in which myelin is destroyed by the action of toxic products (tumor necrosis factor α; TNFα, and nitric oxide; NO) released from activated macrophages (22, 23).

Pattern 2: Lesions in this pattern are resembling the EAE model formed by sensitizing against myelin oligodendrocyte glycoprotein (MOG), where areas with destructed myelin are associated with the accumulation of immunoglobulin and activated complement (24).

Pattern 3: Lesions contain an infiltrated bulk of inflammatory cells consisting of macrophages, activated microglia and T cells, and there is a significant loss of myelin associated glycoprotein (MAG). This pattern is accompanied by a loss of oligodendrocytes and the presence of minimal remyelination. It is believed that the loss of MAG leads to the development of

oligodendrogliopathy from distal to proximal area where necessary metabolic needs of the axon cannot be met (25).

Pattern 4: In this pattern, rarely found in patients presenting a primary progressive MS (PPMS), lesions are infiltrated by a bulk of inflammatory cells including macrophages, activated microglia and T cells. However, there is no loss of MAG and no presence of immunoglobulin or complement accumulation. Interestingly, non-apoptotic oligodendrocyte death is observed in the white matter area adjacent to the lesion. The latter suggest that a metabolic disorder in oligodendrocytes can sensitize these cells especially against toxic damage by inflammation (25).

Researchers have suggested that MS patients have intra-individual and inter-individual heterogeneous lesions. In these studies, the researchers interpret their findings as the evolution/development of a single pathophysiological mechanism rather than the etiology of a heterogeneous disease (26).

Due to complexity and difficulty of taking samples from the CNS, different animal models are used to simulate the disease in order to examine MS and the BBB. It is possible to sort these models briefly as: 1. Autoimmune models; 2.Mutant models, 3.Viral models and 4. Chemical based models.

Autoimmune models are mainly referred to as EAE, most common model used for MS research. Although not exactly presenting MS, EAE simulates many steps of MS. In the EAE model, various myelin forming proteins such as Myelin Basic Protein (MBP), Proteolipid Protein (PLP) or MOG, are mixed with complete Freund's adjuvant (CFA) and pertussis toxin (PTX) as whole or partial (antigen) and injected into the subject animal. As a result, the BBB loses its integrity, inflammatory cells infiltrate into the CNS and react against the myelin tissue (27). EAE is a disease that is progressively worsening with the presence of inflammation and demyelination. The clinical manifestation of the EAE model varies depending on the species of the subject animal, the strain, and the type of antigen used to generate autoimmunity. For example, MOG protein injection

in C57BL/6J mouse line results in a progressive paralyzed model. On the other hand, PLP injection in Swiss James Lambert (SJL) mice results in a relapsing remitting EAE model with attacks (28). As mutant models, mutant mice containing mutant versions of proteins in their myelin structure have been developed, these include the Shiverer mutant (MBP mutant) and Rumpshaker Jimpy (PLP mutant). Besides, also MAG knockout mice have been developed (28).

According to literature, many studies have investigated the relationship between MS and the BBB with a main focus on the causes of deterioration of BBB integrity and the inflammatory mechanisms that play a role in the process. However, there are very few studies focusing on pericytes, which are a prominent component of the BBB. Pericytes are part of the neurovascular unit (NVU) located around and/or wrapping the endothelial wall and are responsible for a variety of mechanisms in both healthy and disease conditions. Together with microvascular smooth muscle cells, pericytes form microvascular mural cells. Pericyte distribution is continuum along the walls of arterioles, venules and capillaries (29). Their coverage and number is associated with the permeability of the biological-barriers, a lower coverage correlates with a higher permeability (30). Moreover, pericytes are able to regulate the capillary structure and diameter (31-33) and even guide vessel sprouting (34, 35).

Pericytes are initially classified according to their location in the microvascular system. However due to novel findings in several disease conditions where pericytes are leaving the microvascular bed (36) and migrate or even proliferate into different phenotypes in the perivascular area (37-39), this classification is difficult to assess. To some degree it may be possible to track down if the cell is a pericyte or smooth muscle cell based on its location, but pericytes have been more prominently classified according to a number of co-localizations of intrinsic and surface markers. Although the latter seems 'problem solved', it has actually made it even more difficult. Different combinations of marker co-localizations are present in pericytes, concluding that pericytes are multipotent cells which may

differentiate into other phenotypes depending on the need, the activation and/or response. On top of this, pericytes function in a tissue-context-dependent manner (40). Therefore, their organ-specific functional roles and phenotypic heterogeneity as well as their origin remain poorly defined (40).

Even more, the phenotype of pericytes not only varies based on the organ tissue and vessel size, but also on whether they are active or quiescent. It is found that active pericytes tend to shorten their processes and increase their somatic volume (41). Activated pericytes can regulate migration associated genes by upregulating ADAM Metallopeptidase with Thrombospondin Type 1 Motif 1 (ADAMTS1) peptidase and downregulating TIMP Metallopeptidase Inhibitor 3 (TIMP3) (42). Other factors related to migration and motility of pericytes are Vascular Endothelial Growth Factor (VEGF), Platelet-derived Growth Factor BB (PDGF-BB) and Ciliary Neurotrophic Factor (CNTF) (39, 43). Pericytes can also migrate upon upregulated cell surface proteases and angiogenesis. In recent studies, it is demonstrated that pericytes control the migration of leukocytes in response to inflammatory mediators by up-regulating the expression of adhesion molecules and releasing chemo-attractants (44); however, under physiological conditions they appear to be immune-suppressors. Activated pericytes further guide angiogenesis upon injury. When activated, pericytes become highly proliferative and migrate through the basal lamina. This migrating behavior of pericytes is needed in order to activate its stem cell capacity (36). It is believed that pericyte-originated cells migrate towards the newly formed vessels and regulate its stability (45).

Pericytes regulate capillary permeability and contraction (31-33) and can secrete cytokines, chemokines, NO and matrix metalloproteinases (MMPs). They further express, gap junctions, tight junctions and focal adhesions with endothelial cells (46) and promote reduction in vesicular transport (33) and endothelial tight junction protein expressions (zona occludens, ZO-1, claudin-5, occludin) (31, 33, 47). Generally accepted pericyte markers include Alpha Smooth Muscle Actin (αSMA), Desmin, Regulator of G-protein Signaling 5 (RGS-5), Neuron-Glial

Antigen 2 (NG2), Platelet-derived Growth Factor Receptor Beta (PDGFRβ) and Amino-peptidase-N (CD13) (48, 49). Pericytes wrapping around capillaries are expressing $NG2^{+}/\alpha SMA^{-}$, wrapping around venules are expressing $NG2^{-}/\alpha SMA^{+}$ and wrapping around arterioles are expressing $NG2^{+}/\alpha SMA^{+}$. Pericyte markers CD146 and PDGFRβ are expressed throughout the vascular bed (50).

Upon exposure to neurotransmitters, neuro-hormones and inflammatory mediators, pericytes may change their phenotype into fibroblasts, smooth muscle cells, macrophages, myofibroblasts, microglia and stromal cells (51, 52). Furthermore, upon stimulation pericytes can secrete interleukin-1β, Interleukin-6, TNFα, reactive oxygen species, NO, MMP2 and MMP9, Prostaglandin-E receptors, TGFβ (fibronectin increases), Monocyte Chemoattractant Protein-1 (MCP-1) and Interferon Gamma-Induced Protein 10 (IP-10) (53-57). Pericyte detachment from endothelial cells and differentiation correlates with increased vesicle numbers in endothelial cells, tight junction disruption, immune cell recruitment, pericyte derived fibrin and collagen (scar formation), antigen presentation on pericytes and Nuclear factor Kappa B (NfKB) translocation to the nucleus (53-57).

Myofibroblasts are activated fibroblast-like and αSMA expressing cells, and it is believed that pericytes are involved in fibrosis by differentiating into myofibroblasts and secreting extracellular matrix (ECM) components (38, 58, 59). In several models such as spinal cord injury, dermal scarring, liver, lung and kidney fibrosis, pericytes transdifferentiate into fibrogenic phenotypes and produce collagen at the injured sites (37, 60, 61).

In a spinal cord injury model, Goritz et al. found that scar formation and fibrosis are associated with the migration of pericytes. They primarily concluded that there are two types of pericytes: Type A pericytes were marked by $PDGFR\beta^{+}/CD13^{+}/Desmin^{-}$ and type B pericytes by $\alpha SMA^{+}/Desmin^{+}$. The study found out that type A pericytes ($PDGFR\beta^{+}/CD13^{+}/Desmin^{-}$) detached from the vascular bed and infiltrated the perivascular area where they contributed to scar formation in the spinal cord injury (37). After detaching, pericytes who lost their

contact with capillaries also lost CD13 and PDGFRα expression, but remained expressing PDGFRβ. Moreover, these cells also became expressing the fibroblast marker Fibronectin as well as temporarily expressed the myofibroblast marker αSMA (62).

Fibrosis is characterized by an excessive accumulation of ECM components at the site of injury. When fibrosis occurs, the tissue is no longer able to recover. Research has found that PDGFRB+ pericytes are playing a crucial role in scar formation in brain injury (63). It is further believed that PDGFRB+ pericytes may express fibroblast-associated markers Collagen IV, Fibronectin and fibroblast surface proteins.

Until now, MS has been associated with gliosis, astrocytes mediating the lesions in the brain and spinal cord, however there are no studies relating MS with fibrosis. Besides, the role of pericytes in fibrosis has been investigated in organs such as liver, kidney, lung, dermal scarring and spinal cord injury, but no study has yet revealed the role of in particular fibrotic pericytes in MS. This thesis is therefore the first study that thoroughly investigated the role of pericytes in the pathophysiology of MS indirectly in two EAE mice models. Within these two EAE models (MOG and PLP) both early stage (15 days) and late stage (40 days) EAE models were developed to investigate pericytes at both time points and correlate its function and/or role within the progression of the disease. Furthermore, the obtained fibrotic pericyte response *in vivo* and its proliferation ability was compared with *in vitro* studies where a pericyte cell line was exposed to MS and/or healthy human serum.

2 Materials and Methods

2.1 MOG EAE Model

To generate the EAE model that mimics the progressive MS disease subtype, C57BL/6 mice were immunized with MOG antigen and the first clinical findings started to manifest after the 10-15th day of immunization. Kılıç et al. observed a stable progression after 30 days in this EAE model (27). Based on the knowledge that the model becomes stable after the 30th day, experiments were ended at the end of the 40th day. In order to find an answer to the question of whether pericyte function is impaired in the early or late stage of the disease, we proposed to work with two different groups of mice to be sacrificed at the end of the 15th and 40th days after immunization. After three trials of optimization, MOG EAE model induction is described below. All materials used in this thesis project are listed with their corresponding manufacturer and catalog numbers in Appendix I.

C57BL/6 wild type mice (Ethical approval number 2016-02, see Appendix II) produced at Koç University Experimental Animal Production Center were used for MOG EAE immunization. 6 weeks old female mice were used for the EAE model as schematized in Figure 1. Both 40 days (SHAM n=11, MOG EAE n=13) and 15 days (SHAM n=4, MOG EAE n=11) experimental groups were immunized with the protocol described below. MOG35-55 (ANASPEC, AS-60130-10) was dissolved in phosphate buffered saline (PBS) with a stock concentration of 2 mg/mL. 300 µg of MOG35-55 peptide per mouse (64) and CFA (Difco laboratories, 263910) containing 800 µg of inactivated Mycobacterium tuberculosis (65) were prepared as 1:1 (v/v) ratio with a total volume of 300 µl. The SHAM group received PBS:CFA with a ratio of 1:1 (v/v). All immunizations were subcutaneously (s.c) injected (300 µl divided) at four areas under isoflurane anesthesia. Both SHAM and MOG EAE groups were followed by intraperitoneal (i.p.) 500 ng/mice PTX (Sigma, P7208-50UG) injections 1 hour and 48 hours after the immunization (27).

A second boost of immunization was injected 7 days after the first injection to both SHAM and MOG EAE groups (Figure 1 and Table 1) (64). 1 hour after the second boost, a 3rd PTX injection was administered i.p. to all groups.

Table 1: Overview of compounds used in the MOG EAE model.

Compound	Stock Concentration	Injected Dose	Total Volume	Ratio, Administration
MOG	2 mg/mL	300ug	150 µl	1:1, s.c.
CFA	5.33 mg/mL	800ug	150 µl	
PTX	5 µg/mL	500ng	100 µl	i.p.

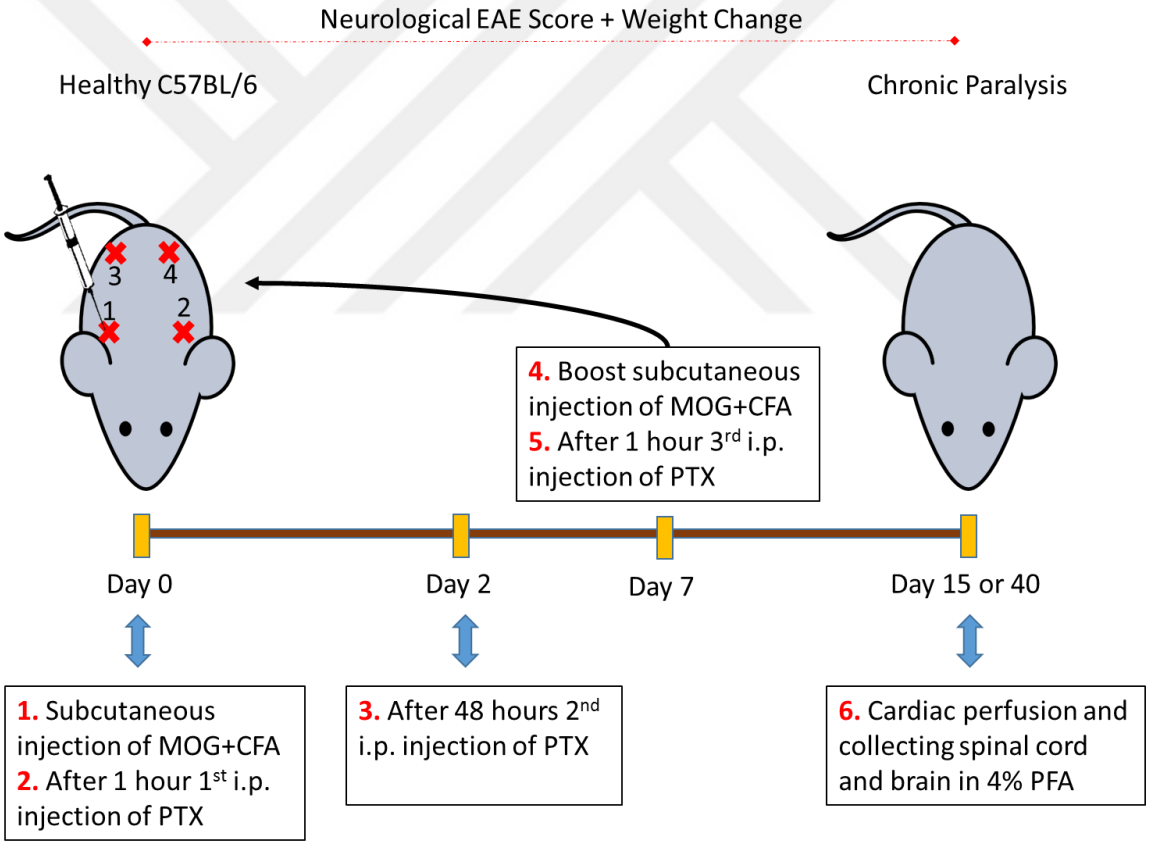

Figure 1: Scheme of MOG EAE model setup.

Weight change and EAE scores of experimental animals were recorded every two days. For clinical onset, score 1 was used as a reference.

Evaluation of EAE clinical findings:

• Measuring body weights

• Clinical EAE scoring of the tail and limbs (scales 0-5)

0 = Healthy

1 = Flaccid tail

2 = Ataxia or paralysis of the hind limbs

3 = Paralysis of the hind limbs and/or ataxia or paralysis of the fore limbs

4 = Ataxia or paralysis of all limbs

5 = Moribund

At days 15 or 40 after the immunization, mice were sacrificed with an overdose of Ketamin/Xylazine anesthesia and directly followed by cardiac perfusion. Their brain and spinal cord were isolated and stored in 4% paraformaldehyde (PFA) for 24 hours and prepared for immunofluorescence and immunohistochemistry studies.

2.2 PLP EAE Model

The EAE model produced by MOG injections mimics the PPMS, a chronic MS subtype. On the other hand, Relapsing Remitting MS (RRMS) is more frequent than PPMS (66). According to literature, the RRMS model manifests as a chronic model in C57Bl/6 mice strain, but mimics the RRMS model closer in SJL mice strain. This SJL mice strain has been commonly used in the literature for mimicking RRMS and is a better model for our hypothesis, however needs PLP immunization instead of MOG

The PLP EAE model was generated in SJL mice strain by immunizing with PLP. The first clinical EAE signs start to occur at days 6-8 post immunization (PI), increase and decrease respectively during the follow-up and mimics the RRMS form. 6 weeks old female SJL mice produced at Koç University Experimental Animal Production Center (Ethics approval number 2016-02, see Appendix II)

were used for both 40 days (SHAM n=9, PLP EAE n=9) and 15 days (SHAM n=7, PLP EAE n=7) experimental groups. PLP139-151 (Peptides International, Louisville KY, PLP-3812-PI) was dissolved in PBS with a stock concentration of 1 mg/mL. With a total volume of 200 µl, a dose of 100 µg of PLP139-151 peptide per mouse was emulsified with CFA (1:1) containing 533 µg inactivated Mycobacterium Tuberculosis, and divided into four areas which were s.c. injected to SJL mice under isoflurane anesthesia. In addition, 1 hour after immunization, 250 ng of PTX per mouse was administered i.p. as shown in Figure 2 and Table 2.

Evaluation of EAE Clinical Findings:

• Measuring body weights on a daily basis

• Daily clinical EAE scoring of the tail and limbs (scales 0-5)

0 = Healthy

1 = Flaccid tail

2 = Ataxia or paralysis of the hind limbs

3 = Paralysis of the hind limbs and/or ataxia or paralysis of the fore limbs

4 = Ataxia or paralysis of all limbs

5 = Moribund

In PLP EAE induced mice, body weight and clinical EAE scoring were monitored every day. Also, because of the more severe clinical EAE outcome, mice with EAE score above 3 received wet food in their cages and even i.p. 0.09% saline if dehydration was observed. At days 15 or 40 after the immunization, mice were sacrificed with an overdose Ketamin/Xylazine anesthesia and directly followed by cardiac perfusion. Their brain and spinal cord were isolated and stored in 4% PFA for 24 hours and prepared for immunofluorescence studies.

Since there are many EAE groups and SHAM groups and even between different mouse strains, in this thesis, hereafter it is classified as MOG EAE 40, MOG SHAM 40, MOG EAE 15, and MOG SHAM 15 for MOG and SHAM groups for late stage 40 days and early stage 15 days in C57Bl/6 mouse strain. Hereafter also, PLP

EAE 40, PLP SHAM 40, PLP EAE 15, and PLP SHAM 15 are classified for late stage 40 days and early stage 15 days in SJL mouse strain.

Table 2: Overview of compounds used in the PLP EAE model.

Compound	Stock Concentration	Injected Dose	Total Volume	Ratio, Administration
PLP	1 mg/mL	100 µg	100 µl	1:1, s.c.
CFA	5.33 mg/mL	533 µg	100 µl	
PTX	5 µg/mL	250 ng	50 µl	i.p.

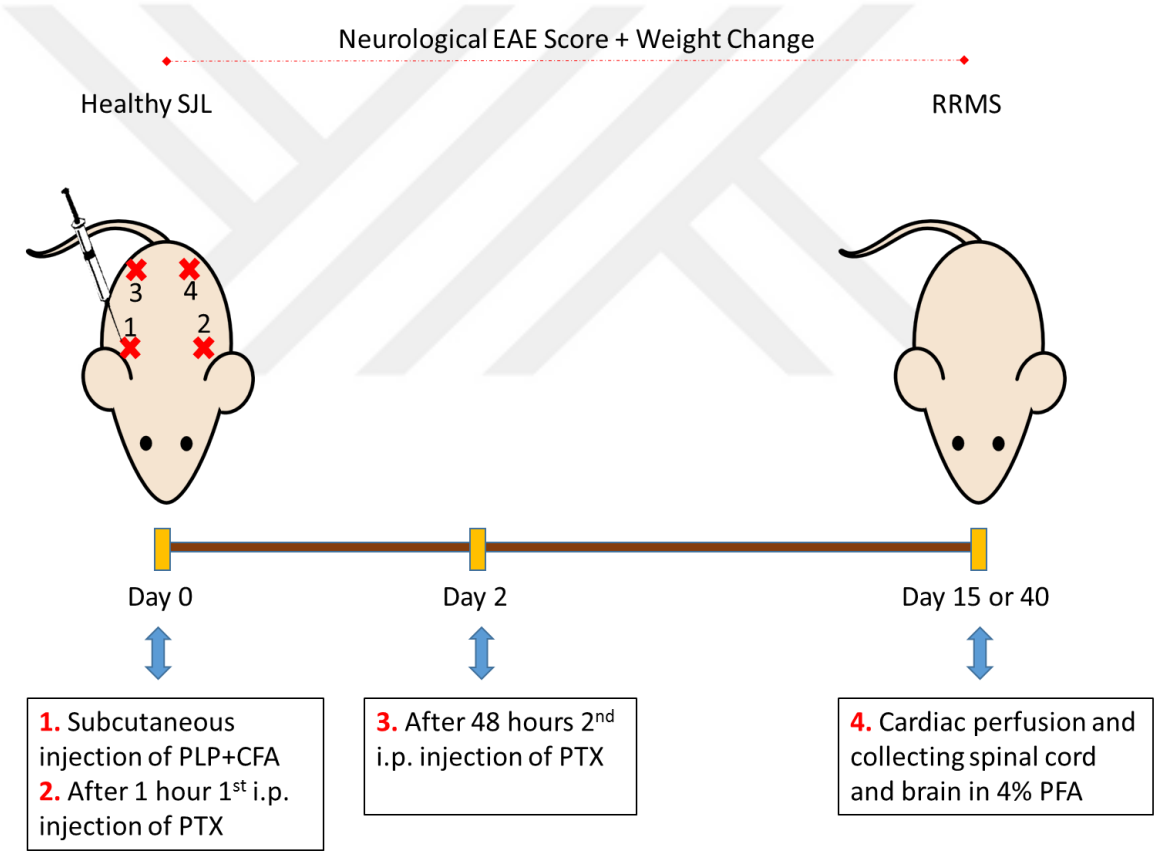

Figure 2: Scheme of PLP EAE model setup.

2.3 Immunofluorescence and Immunohistochemistry

2.3.1 Preparations of Cryosections

After cardiac perfusion brain and spinal cord tissues were left in 4% PFA for at least 24 hours at 4ºC and then respectively incubated in 10%, 20% and 30% sucrose solutions (in 0.1M phosphate buffer) for cryopreservation until the tissues dropped down to the bottom of the falcon tube for each sucrose concentration. Freezing of the tissues was carried out at -20 °C in optimal cutting temperature (OCT) compound. With the use of a Cryotome device, frozen brain sections of 10 µm thickness were taken on poly-lysine coated glass slides. Frozen brain and spinal cord sections of 10 µm thickness were obtained from the areas as shown in Figure 3.

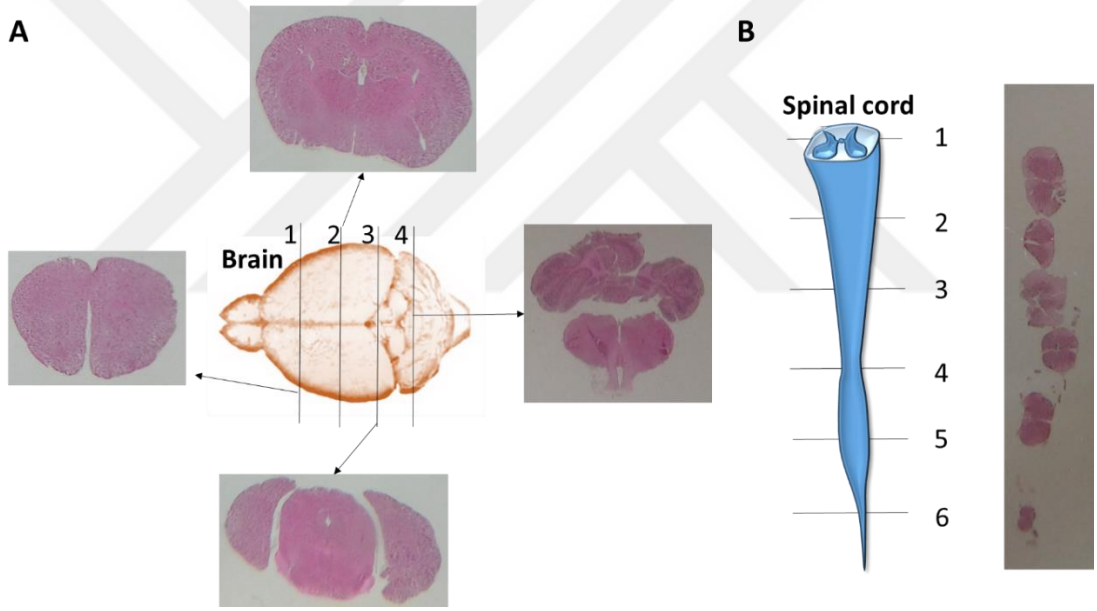

Figure 3: Schematic representation of sectioned areas of the brain and spinal cord. A) Mouse brain cross-sections. B) Mouse spinal cord cryosections. Sections were taken from the 6 levels as indicated in the spinal cord scheme. With one cryosection, we were able to collect 6 different areas of the spinal cord which increased the chance of encountering lesion areas.

2.3.2 Luxol Fast Blue Staining

Luxol Fast Blue (LFB) staining (Abcam, ab150675) is used to show myelin in both paraffin embedded and frozen tissues. Briefly, tissue slides were washed with distilled water to remove cryo material and other debris. For defatting, samples were incubated in a 1:1 alcohol-chloroform solution at room temperature overnight and subsequently hydrated in distilled water. Samples were then incubated in LFB Solution for 2-4 hours at 60ºC. Then, samples were washed in distilled water and transferred to lithium carbonate solution to differentiate the staining. Next, washing was carried out with alcohol reagent until the white matter remained blue and gray matter became colorless. The slides were washed with distilled water, dehydrated with respectively 96% and 100% alcohol and finally covered with Entellan. Images were captured with light microscopy.

2.3.3 Hematoxylin and Eosin Staining

The slides were left for 1 minute in distilled water to remove residues and cryo material. Then, incubated in the following solutions: Respectively, Mayer's Hemalum solution (Merck, 109249) for 3 minutes, running tap water to remove excess staining, PBS for 5 minutes, Eosin Y-alcohol solution (Shandon, 6766007) for 30 seconds, running tap water to remove excess staining, PBS for 5 minutes, two times 100% ethanol for 2 minutes, and two times Xylene for 5 minutes. Finally the tissues were covered with Entellan. Hematoxylin and Eosin (H&E) images were captured with light microscopy.

2.3.4 Immunofluorescence Staining

Slides were dipped in distilled water a few times until the residues and OCT were removed. Then, slides were incubated in methanol for 5 minutes at room temperature to permeabilize cell membranes. Slides were three times washed in Dulbecco's phosphate buffered saline (DPBS) and Super Block (Thermo Scientific™, PI37535) solution was added on top of each sample which was within a circle marked by a PAP pen liquid blocker and incubated for 1 hour at room temperature. The slides were kept humidified with the use of wet paper towels in their boxes at all times. Next, the super block solution was removed, and the first antibody of interest (diluted in Super Block solution) was added to

on top of the sample and incubated for 1.5 hours at 37ºC. The antibody solution was removed, and the slides were washed with DPBS by dipping three times for 1 minute. Then, the secondary antibody of interest (diluted in super block solution) was added on top of the sample and incubated for 1.5 hours at 37ºC in dark. Subsequently, the secondary antibody was removed, and was washed again in DPBS, three times for 1 minute. Next, either the cells were mounted with 4 ', 6-diamidino-2-phenylindole (DAPI, Abcam) containing mounting medium or stained for another primary antibody for dual or triple series. In the end, after mounting the samples, slides were covered by a cover glass and nail polish was used to stabilize the coverglass on the slide. Fluorescent images were taken with Leica DMi8 LCI microscope and processed with Leica LasX software. Used antibody dilution factors are listed in Table 3. Three types of antibodies have been used to track down pericytes, each having different pericyte marking properties. For example, αSMA refers to both pericytes and smooth muscle cells, while NG2 marks both pericytes and oligodendroglial cells. PDGFRβ is relatively the most specific within these antibodies. However, it will be important to evaluate each staining pattern separately to determine the role of the vascular bed in disease pathogenesis.

Table 3: Antibodies and their dilution factors used for immunofluorescent staining.

Target	Primary Antibody	Ratio	Secondary antibody	Ratio
T-lymphocyte	Rabbit anti-CD8	1:100	Goat anti-rabbit FITC	1:200
BBB Leakage	Goat anti-mouse Albumin	1:50	Donkey anti-goat FITC	1:200
Macrophage	Rat anti-F4/80	1:100	Goat anti-rat Alexa Fluor 594	1:200
Myelin	Mouse anti-MBP	1:100	Goat anti-mouse FITC or Goat anti-mouse CY3	1:200
Pericyte	Rabbit anti-PDGFRβ	1:100	Goat anti-rabbit CY3	1:200

Pericyte / Oligodendroglial Cell	Rabbit anti-NG2 Cy3 conjugated	1:100	-	-
Pericyte / Smooth Muscle Cell	Mouse anti-αSMA FITC conjugated	1:100	-	-
Endothelium	IB4 FITC conjugated	1:100	-	-
Astrocyte	Rabbit anti-GFAP	1:200	Goat anti-rabbit CY3	1:200
Neuron	Chicken anti-MAP2	1:100	Goat anti-Chicken FITC	1:200
Fibronectin	Rabbit anti-Fibronectin	1:100	Goat anti-rabbit CY3	1:200
Apoptosis	Rabbit anti-CC3	1:100	Goat anti-rabbit FITC	1:200
Collagen I	Rabbit anti-Collagen I	1:100	Goat anti-rabbit CY3	1:200
Collagen IV	Rabbit anti-Collagen IV	1:100	Goat anti-rabbit CY3	1:200
Laminin	Rabbit anti-Laminin	1:100	Goat anti-rabbit CY3	1:200
Microglia	Rabbit anti-IBA1	1:100	Goat anti-rabbit CY3	1:200
Pericytes? / Smooth Muscle Cell?	Phalloidin-FITC conjugated	1:100	-	-
Nestin	Rabbit anti-Nestin	1:100	Goat anti-rabbit CY3	1:200
TGFB1	Mouse anti-TGFB1	1:100	Goat anti-mouse FITC	1:200
Collagen Crosslinking	Rabbit anti-LOXL2	1:100	Goat anti-rabbit CY3	1:200
Collagen Crosslinking	Rabbit anti-LOXL3	1:100	Goat anti-rabbit CY3	1:200

Abbreviations: CD8, T-lymphocyte; F4/80, Macrophage; MBP, Myelin Basic Protein; PDGRβ, Platelet-derived Growth Factor Beta; NG2, Neuron-glial Antigen 2; αSMA, Alpha smooth Muscle Actin; IB4, Isolectin; GFAP, Glial Fibrillary Acidic Protein; MAP2, Microtubule-associated protein; CC3, Cleaved Caspase 3; IBA1, Ionized calcium binding adaptor molecule 1; TGFβ1, Transforming Growth Factor Beta 1; LOX, Lysyl Oxidase; FITC, Fluorescein Isothiocyanate;; CY3, Cyanine.

2.4 *In Vitro* Pericyte Studies

2.4.1 Pericyte Culture

Human brain vascular pericytes (HBVP) were obtained from ScienceCell (#1200).

This cell line was cultured with Dulbecco's modified eagle medium (DMEM)

containing L-glutamine and was further supplemented with 10% (v/v) fetal bovine serum (FBS), 1% (v/v) penicillin/streptomycin (P/S) and 1% (v/v) Amphotericin. The cells were seeded on poly-L-lysine (PLL) coated plates (For a T75 flask: 15 µl of stock 10 mg/mL PLL in 10 mL of dH_2O and incubate overnight in incubator) and incubated at 37°C and 5% CO_2 and grown until 80-90% confluency in either T25 or T75 culture flasks. Medium was changed every two-three days. Subculturing was performed by gently trypsinizing cells with 0.05% Trypsin/EDTA solution for 3-5 minutes at 37°C and 5% CO_2, and subsequently inhibited trypsin activity 1:1 (v/v) with 10% FBS containing culture medium. The obtained cell suspension was washed twice with 10% FBS containing culture medium by centrifuging the cell suspension at 1400 rpm for 3 minutes and throwing away the supernatant. The cell pellet was dissolved in culture medium and either subcultured in a new PLL coated flask or frozen for storage. For the latter, 10% DMSO was added to the culture medium and the cells were aliquoted as 500 000 cells/mL in cryovials. Cryovials were kept at least 48 hours in a Mr. Frosty box in -80°C before transporting to a nitrogen tank.

2.4.2 xCELLigence and Pericyte Proliferation

The xCELLigence RTCA SP system includes a computer, an electronic sensor analyzer, a workstation and a 96-well microtiter detection device (Figure 4). This xCELLigence system is able to measure the impedance of selected wells and analyzes the data with the RTCA software on the computer resulting in a parameter called cell index. This so-called cell-index is representing the cell status based on the detected cell electrode impedance. After seeding cells in the special E-plate wellplates designed for xCELLigence, the system can monitor cell attachment and proliferation.

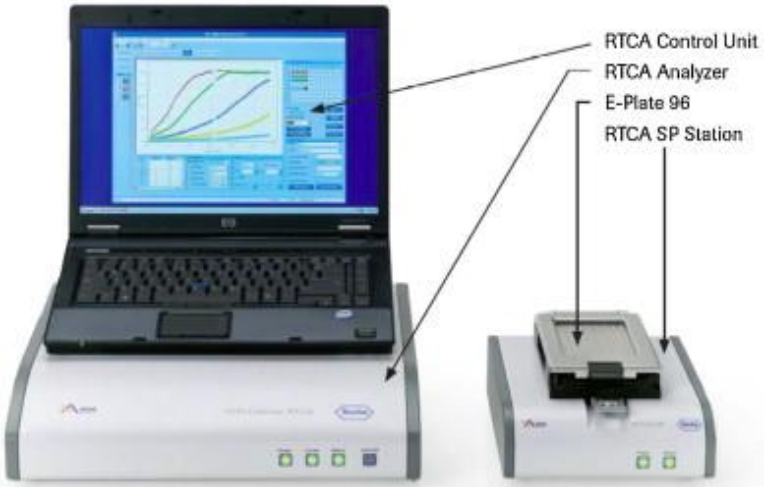

Figure 4: The xCELLigence system.

Firstly, for each experiment it is important to perform an equilibration measurement. For this, culture medium was added (50 µL) to the wells of an xCELLigence E-plate. After equilibration to 37 °C, plates were inserted into the xCELLigence station to measure the baseline impedance to ensure that all wells and connections were working within acceptable limits. If one or more of the wells/connections are not working, the system will give a warning, this will make it possible to check your system and connections before wasting experiments and/or expensive xCELLigence plates.

HBVP were seeded in E-plates in duplicates per sample and incubated in the xCELLigence system to monitor cell proliferation in real-time. First, the optimal cell density was measured for this cell line. HBVP cells were seeded in cell densities ranging from 2500-40000 cells per well in duplicates and incubated for 72 hours at 37°C and 5% CO_2 in the xCELLigence system. Then, in another experiment, serum working concentrations were assessed by exposing three different cell seeding densities to either 10% serum or 2% serum (v/v) in culture medium (with 1% FBS instead of 10%) (For ethical approval of patient material, see Appendix III). Briefly, the cells were seeded with either 40000, 20000 or 10000 cells per well and incubated for 24 hours thereafter healthy human serum (10% or 2%) or no serum (culture medium only) was added to the wells and

was further incubated for a total of 100 hours. The effects of serum on the susceptibility to either death or proliferation were to be observed. Finally, in a novel setting, 24 hours after seeding HBVP, cells were exposed to MS patient serum (n=3, in duplicates) and healthy human serum (n=3, in duplicates) with the selected optimum cell density (20000 cells/well) and serum concentration (10%). No serum but only culture medium was used as control. The impedance value of each well was automatically monitored by the xCELLigence system for 100 hours and expressed as the cell-index value. The proliferation rate between samples were calculated by their slopes between two time points after exposure. This experiment makes it possible to investigate the direct effect of inflammatory compounds, residing in the serum of MS patients, on the cleavage and proliferation ability of pericytes and indirectly to investigate the effect on pericyte survival ability. In the absence of living cells (only medium) or with a suspension of dead cells, the cell index values will be close to zero. After attachment of cells onto the electrode, the measured signal correlates linearly with cell number throughout the experiment.

2.4.3 Fibrotic Activity of Pericytes

The fibrotic response of pericytes upon exposure to MS serum was investigated in a cell culture study. 20000 HBVP cells/well were seeded in transparent flat-bottom 96-wellplates and incubated overnight at 37°C and 5% CO_2 for cell attachment. Culture medium was prepared as follows: DMEM (containing L-glutamine) was supplemented with 1% FBS, 1% P/S and 1% amphotericin. Then, after 24 hours, HBVP were exposed to 10% (v/v) MS (n=2, in triplicate) and healthy human (n=2, in triplicate) serum, or no serum/only culture medium (n=2, in triplicate) for 24 hours at 37°C and 5% CO_2. Subsequently, the medium was removed, and cells were washed twice with DPBS and fixed with 4%PFA for 30 min at room temperature respectively. Cells were stained for immunofluorescent markers αSMA, collagen I, collagen IV and laminin as described above.

TGFβ1 secretion is known to mediate fibrosis (68, 69). To assess how HBVP react upon this cytokine, HBVP pericytes were exposed to TGFβ1. Briefly, 5000 cells/well were seeded in transparent flat-bottom 96-wellplates and incubated overnight at 37°C and 5% CO_2 for cell attachment. Culture medium was prepared as follows: DMEM (containing L-glutamine) was supplemented with 1% FBS, 1% PS and 1% amphotericin. Then, after 24 hours, HBVP were exposed to 1 ng/mL TFGβ1 in culture medium (n=3) and culture medium only was used as control (n=3) for either 24 hours or 72 hours at 37°C and 5% CO_2. Subsequently, the medium was removed, and cells were washed twice with DPBS and fixed with 4%PFA for 30 min at room temperature respectively. Cells were stained for fibronectin, collagen I, collagen IV and Cleaved Caspase 3 (CC3). Fluorescent images were taken with Leica DMi8 LCI microscope and processed with Leica LasX software.

2.6 ImageJ Analysis

Fluorescence microscopy images exported as Tiff files from LAS X program (Leica, Germany) were imported and analyzed with ImageJ 1.52e (NIH, USA). For cell counting, DAPI positive cells were marked with "Find Maxima" where noise was adjusted to mark each cell as a single point. Fluorescent staining of images was represented in integrated density or area (%). Briefly, Image Split Channels > Take grayscale channel to be measured > Duplicate channel > Threshold the duplicated channel (red on dark background) > Set Measurement on the grayscale channel, Integrated Density and/or Area (%), Limit to Threshold, Redirect to threshold image > Measure > Transfer data to Excel.

2.7 Statistical Analysis

Statistical analysis was performed with GraphPad Prism 5.02 (La Jolla, USA) by using unpaired two-tailed students T-test with ***=P< 0.001, **=P< 0.01, *=P< 0.05 and ns= non-significant.

3 Results and Discussion

3.1 Weight Change and EAE Scores

Clinical EAE scores and weight change follow-up were monitored every day or every two days. The results were statistically analyzed by two-tailed unpaired t test and $p<0.05$ was considered statistically significant.

Figure 5 and 6, show the weight change and EAE score graphs for MOG EAE 40 and MOG EAE 15 with their corresponding SHAM groups, representing a progressive MS type. Figure 7 and 8, are the results of PLP EAE 40 and PLP EAE 15 with their corresponding SHAM groups, representing RRMS. Compared to their corresponding SHAM groups, a significant weight loss was found for MOG EAE 40, PLP EAE 40, and PLP EAE 15 groups, for P-values see Table 4-7. Only MOG EAE 15 did not show a statistically significant weight change compared to its SHAM group. This was however expected, since in our lab, the MOG EAE model was a slowly progressing model with a peak around 24 days post 1st immunization (17 days post 2nd boost immunization) see Figure 5B.

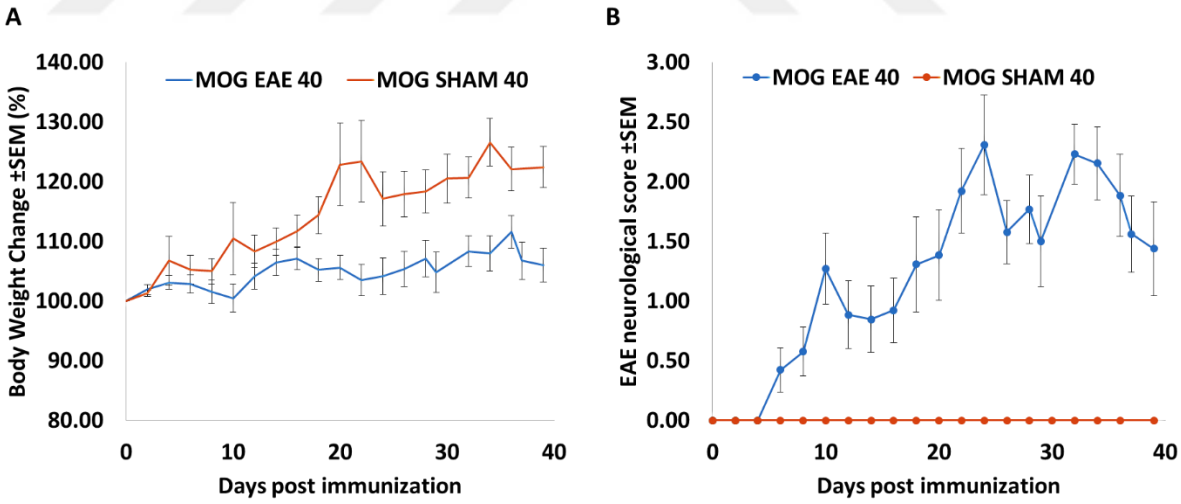

Figure 5: A) The body weight change (%) of late stage 40 days MOG EAE and SHAM groups. Compared to SHAM, statistical significance was reached after 18 days PI. Data is shown as mean±SEM for MOG EAE 40 n=13 and MOG SHAM 40 n=11. B) EAE neurological scores (0-5) of late stage 40 days MOG EAE and SHAM

groups. Compared to SHAM, statistical significance was reached after 6 days PI. Data is shown as mean±SEM for MOG EAE 40 n=13 and MOG SHAM 40 n=11.

Table 4: Statistical p-values and corresponding symbols for weight change (%) and EAE scores in MOG EAE 40 and MOG SHAM 40 groups.

	Group Size (n)	Group Size (n)	Weight Change (%)		EAE Score	
Days PI	MOG EAE 40	MOG SHAM 40	T-test MOG vs. SHAM 40 (P-Value)	Statistical Symbol	T-test MOG vs. SHAM 40 (P-Value)	Statistical Symbol
0	13	11	na	na	na	na
2	13	11	0.50775	ns	na	na
4	13	4	0.25033	ns	na	na
6	13	11	0.39231	ns	0.04938	*
8	13	11	0.25029	ns	0.01612	*
10	13	4	0.08068	ns	0.03528	*
12	13	11	0.24118	ns	0.00919	**
14	13	11	0.28568	ns	0.01106	*
16	13	11	0.16444	ns	0.00491	**
18	13	11	0.01642	*	0.00647	**
20	13	4	0.00427	**	0.06711	ns
22	13	4	0.00459	**	0.01059	*
24	13	9	0.02211	*	0.00019	***
26	13	11	0.01447	*	0.00002	***
28	13	11	0.02603	*	0.00001	***
30	8	11	0.01303	*	0.00020	***
32	13	11	0.00758	**	0.00000	***
34	13	4	0.00590	**	0.00172	**
36	13	11	0.03244	*	0.00005	***
39	8	11	0.00271	**	0.00046	***

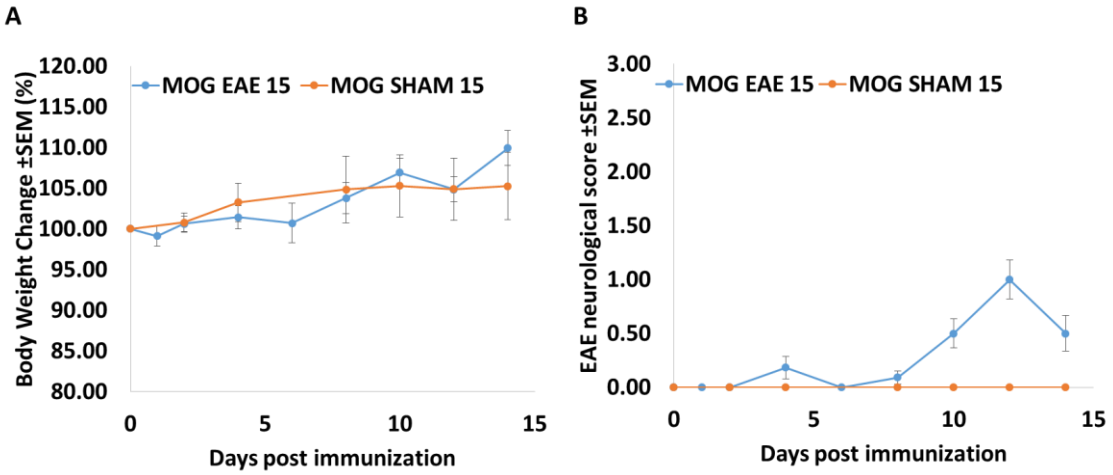

Figure 6: A) The body weight change (%) of early stage 15 days MOG EAE and SHAM groups. Compared to SHAM, there was no statistical significance reached within the given 15 days. Data is shown as mean±SEM for MOG EAE 15 n=11 and MOG SHAM 15 n=4. B) EAE neurological scores (0-5) of early stage 15 days MOG EAE and SHAM groups. Compared to SHAM, statistical significance was reached after 10 days PI. Data is shown as mean±SEM for MOG EAE 15 n=11 and MOG SHAM 15 n=4.

Table 5: Statistical p-values and corresponding symbols for weight change (%) and EAE scores in MOG EAE 15 and MOG SHAM 15 groups.

	Group Size (n)	Group Size (n)	Weight Change (%)		EAE Score	
Days PI	MOG EAE 15	MOG SHAM 15	T-test MOG vs. SHAM 15 (P-Value)	Statistical Symbol	T-test MOG vs. SHAM 15 (P-Value)	Statistical Symbol
0	11	4	na	na	na	na
2	11	4	0.91904	ns	na	na
4	11	4	0.23314	ns	0.31141	ns
6	5	na	na	na	na	na
8	11	4	0.79333	ns	0.39603	ns
10	11	4	0.66185	ns	0.04794	*
12	11	4	0.99880	ns	0.00573	**
14	11	4	0.30306	ns	0.09800	ns

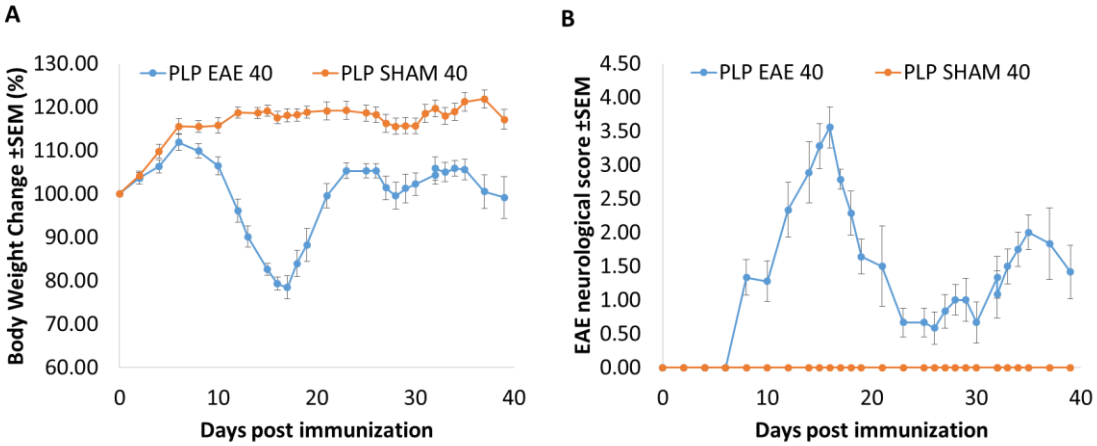

Figure 7: A) The body weight change (%) of late stage 40 days PLP EAE and SHAM groups. Compared to SHAM, statistical significance was reached after 8 days PI. Data is shown as mean±SEM for PLP EAE 40 n=9 and PLP SHAM 40 n=9. B) EAE neurological scores (0-5) of late stage 40 days PLP EAE and SHAM groups. Compared to SHAM, statistical significance was reached after 8 days PI. Data is shown as mean±SEM for PLP EAE 40 n=9 and PLP SHAM 40 n=9.

Table 6: Statistical p-values and corresponding symbols for weight change (%) and EAE scores in PLP EAE 40 and PLP SHAM 40 groups.

	Group Size (n)	Group Size (n)	Weight Change (%)		EAE Score	
Days PI	PLP EAE 40	PLP SHAM 40	T-test PLP vs. SHAM 40 (P-Value)	Statistical Symbol	T-test PLP vs. SHAM 40 (P-Value)	Statistical Symbol
0	9	9	na	na	na	na
2	9	9	0.74351	ns	na	na
4	9	9	0.12129	ns	na	na
6	9	9	0.18214	ns	na	na
8	9	9	0.01793	*	0.00012	***
10	9	9	0.00371	**	0.00063	***
12	9	9	0.00000	***	0.00003	***
14	9	9	0.00000	***	0.00001	***
15	9	9	0.00000	***	0.00000	***

16	7	9	0.00000	***	0.00000	***
17	7	9	0.00000	***	0.00000	***
18	7	9	0.00000	***	0.00000	***
19	7	9	0.00000	***	0.00000	***
21	6	9	0.00007	***	0.01222	*
23	6	9	0.00038	***	0.00166	**
25	6	9	0.00023	***	0.00166	**
26	6	9	0.00025	***	0.00924	**
27	6	9	0.00076	***	0.00102	**
28	6	9	0.00038	***	0.00009	***
29	6	9	0.00111	**	0.00166	**
30	6	9	0.00080	***	0.01787	*
32	6	9	0.00043	***	0.00012	***
32	6	9	0.00083	***	0.00201	**
33	6	9	0.00087	***	0.00001	***
34	6	9	0.00064	***	0.00000	***
35	6	9	0.00039	***	0.00000	***
37	6	9	0.00016	***	0.00079	***
39	6	9	0.00253	**	0.00064	***

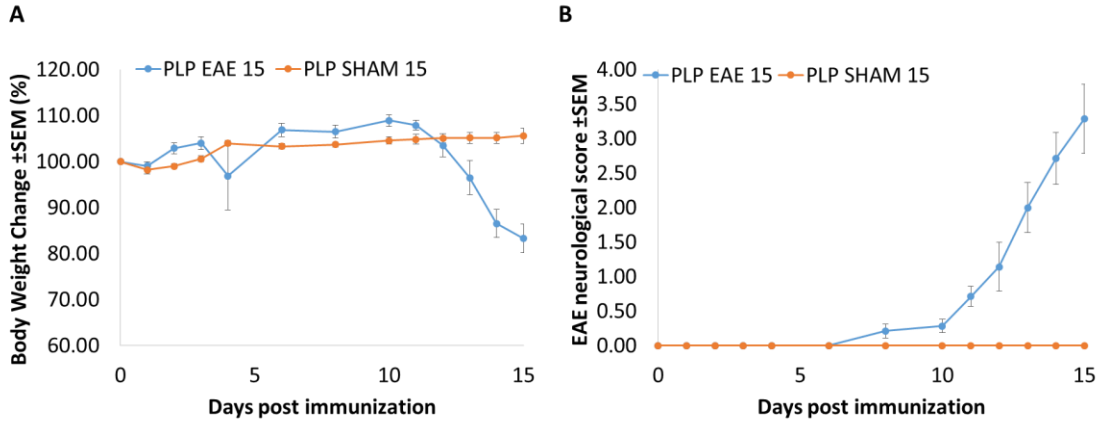

Figure 8: A) The body weight change (%) of early stage 15 days PLP EAE and SHAM groups. Compared to SHAM, statistical significance was stable after 13 days PI. Data is shown as mean±SEM for PLP EAE 15 n=7 and PLP SHAM 15 n=7. B) EAE neurological scores (0-5) of early stage 15 days PLP EAE and SHAM groups. Compared to SHAM, statistical significance was reached after 10 days PI. Data is shown as mean±SEM for PLP EAE 15 n=7 and PLP SHAM 15 n=7.

Table 7: Statistical p-values and corresponding symbols for weight change (%) and EAE scores in PLP EAE 15 and PLP SHAM 15 groups.

	Group Size (n)	Group Size (n)	Weight Change (%)		EAE Score	
Days PI	PLP EAE 15	PLP SHAM 15	T-test PLP vs. SHAM 15 (P-Value)	Statistical Symbol	T-test PLP vs. SHAM 15 (P-Value)	Statistical Symbol
0	7	7	na	na	na	na
1	7	7	0.48102	ns	na	na
2	7	7	0.01211	*	na	na
3	7	7	0.05006	ns	na	na
4	7	7	0.35583	ns	na	na
6	7	7	0.04709	*	na	na
8	7	7	0.08652	ns	0.05540	ns
10	7	7	0.01263	*	0.01522	*
11	7	7	0.06847	*	0.00043	***

12	7	7	0.57026	ns	0.00763	**
13	7	7	0.04592	*	0.00013	***
14	7	7	0.00009	***	0.00001	***
15	7	7	0.00003	***	0.00002	***

3.2 EAE Pathology

H&E and LFB staining were performed to assess demyelination and cell infiltrates/accumulation at lesion sites. However, detailed investigations for lesion sites were identified by immunofluorescence staining which allowed double/triple marking and co-localizations. Figure 9 shows a schematic view of the spinal cord and the expected findings. From both Figure 10 and Figure 11, it is clearly shown that inflammation and infiltrated cells are accumulated in the white matter areas particularly close to the pia mater site. Also, multiple lesion spots are observed in the same brain or spinal cord section, indicating heterogeneous BBB leakage. At the exact spots of cell infiltrations, decreased LFB staining is observed, indicating loss of myelin at these areas.

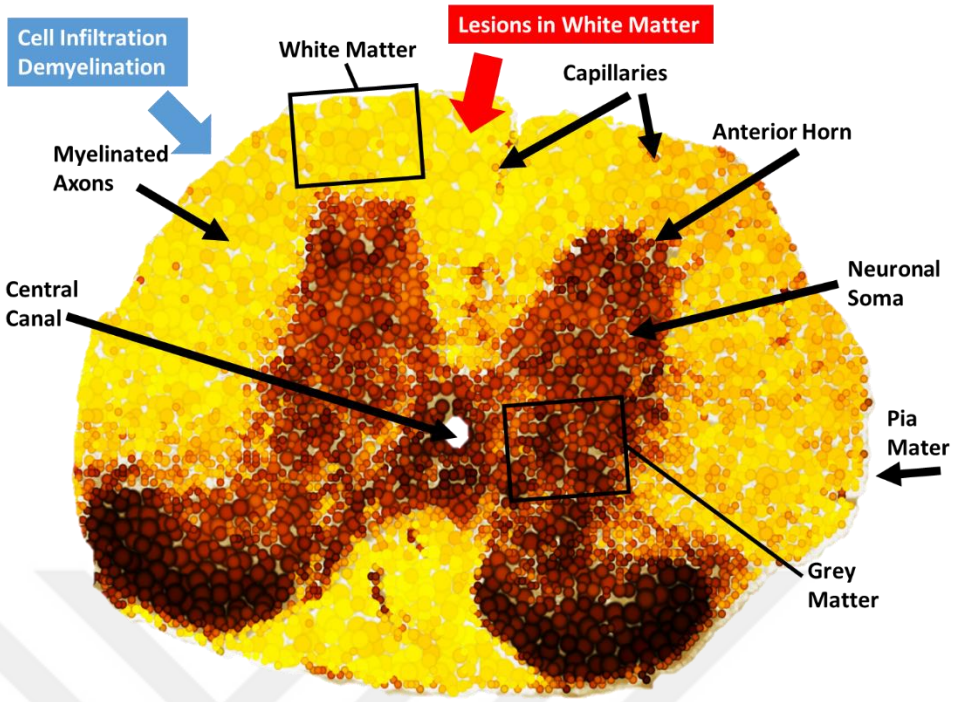

Figure 9: Schematic representation of the spinal cord and expected results in the EAE model.

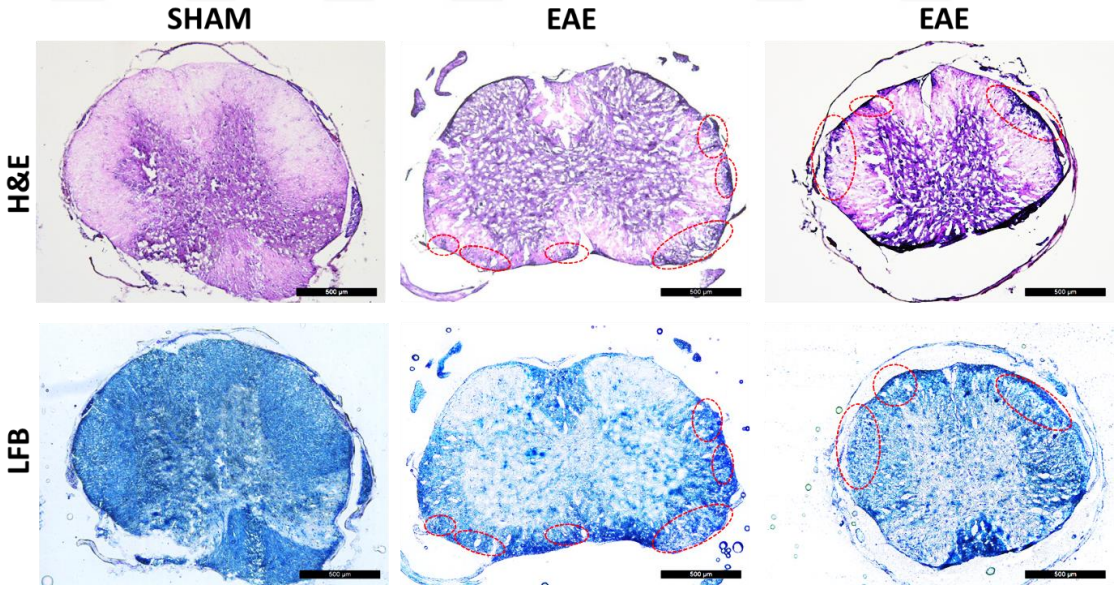

Figure 10: Spinal cord samples. Upper panel - H&E staining: Compared with the SHAM group there is clearly accumulation of inflammatory cells in the lesion regions (areas marked with red circles). Lower panel - LFB staining: Generally, there is lost tissue integrity especially in the white matter. Reduced LFB staining

in lesions in the white matter region indicate lost and/or non-intact myelin. The representative sections in the figure are taken from the 4th level (see materials and methods section) of the spinal cord (lumbar area). Lesions were mainly found in sections 1 and 4 in all EAE models. Scale bars represent 500 µm.

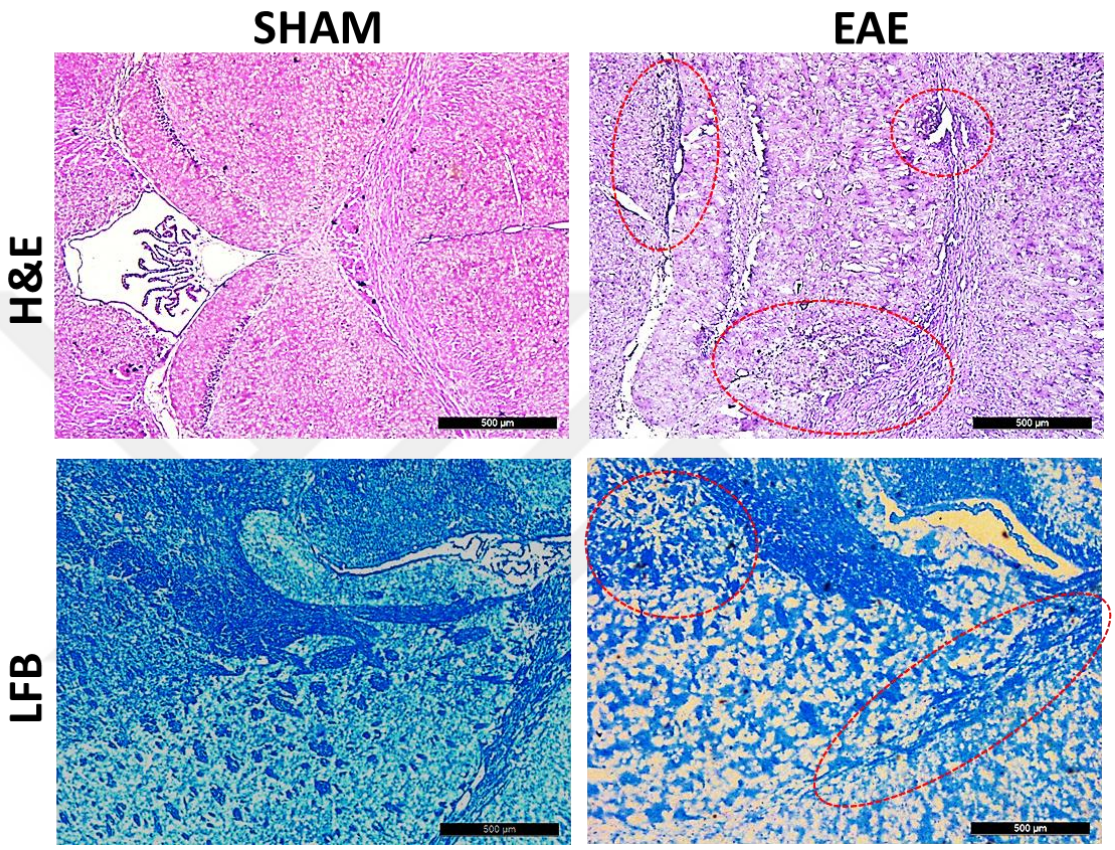

Figure 11: Brain samples. Upper panel - H&E staining: Compared with the SHAM group there are several small spots with accumulation of inflammatory cells in the lesion regions (areas marked with red circles). Of note is that these spots in the brain are often close to ventricles. However in the cerebellum (no data shown), these lesion spots are mainly in the white matter. Lower panel - LFB: Overall integrity loss is present in the brain tissue, especially in the white matter. Compared to SHAM, LFB staining is not dense or continuous in the EAE white matter (red circles). This indicates lost myelin. Scale bars represent 500 µm.

3.3 BBB Leakage

As mentioned in our hypothesis, we compared early stage (15days) and late stage (40 days) EAE to assess the progression of the disease in terms of vascular pathology and the role of pericytes. To this end, to show the time-dependent effects and changes in the BBB and its subsequent leakage, albumin staining was performed. Albumin staining showed BBB disrupted areas where albumin is leaked into the perivascular area. As can be seen from Figure 12-14, SHAM groups showed no leakage except the staining of the vascular bed. All EAE groups showed either small spots (MOG EAE) or larger leakage spots (PLP EAE) in the spinal cord and brain. Exceptionally in one mice, having a clinical score of 4 in the MOG EAE 40 group, there was much larger BBB leaked area, see Figure 14. This albumin leaked area contained also multiple large infiltrated cell clusters.

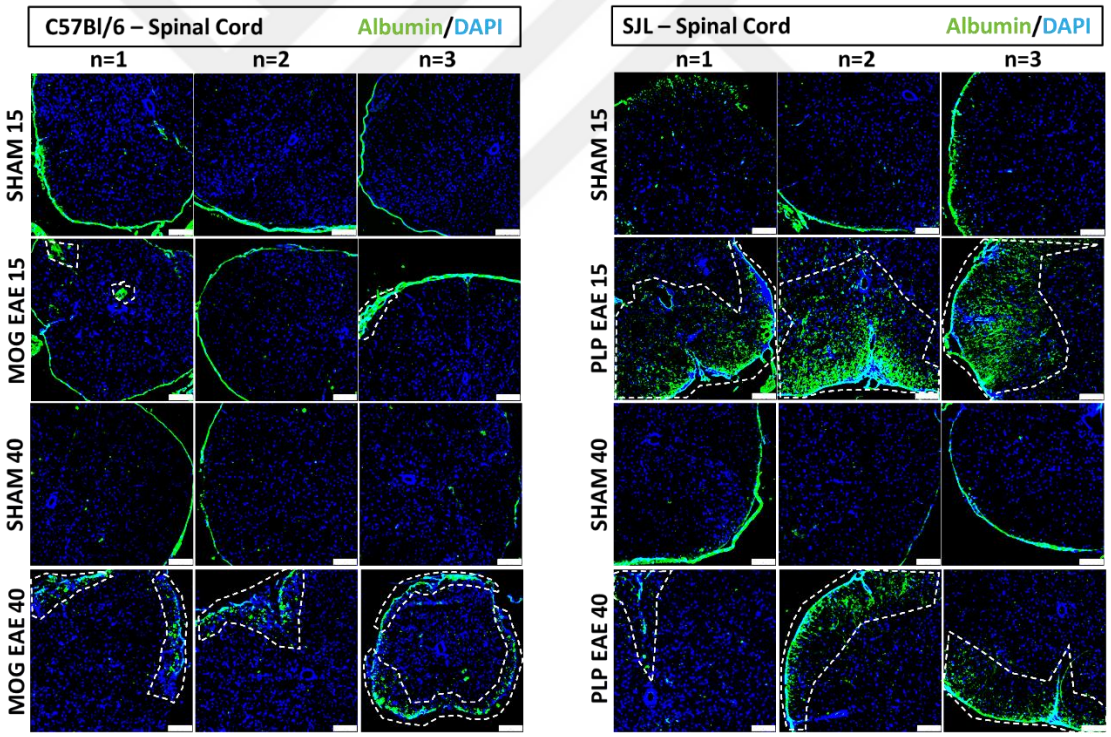

Figure 12: Albumin staining in spinal cord sections of MOG and PLP groups. Three different spinal cord sections are shown for each group. Albumin (green) stains BBB leakage and DAPI (blue) stains cell nucleus. Dashed areas show albumin leakage. The scale bars represent 250 µm.

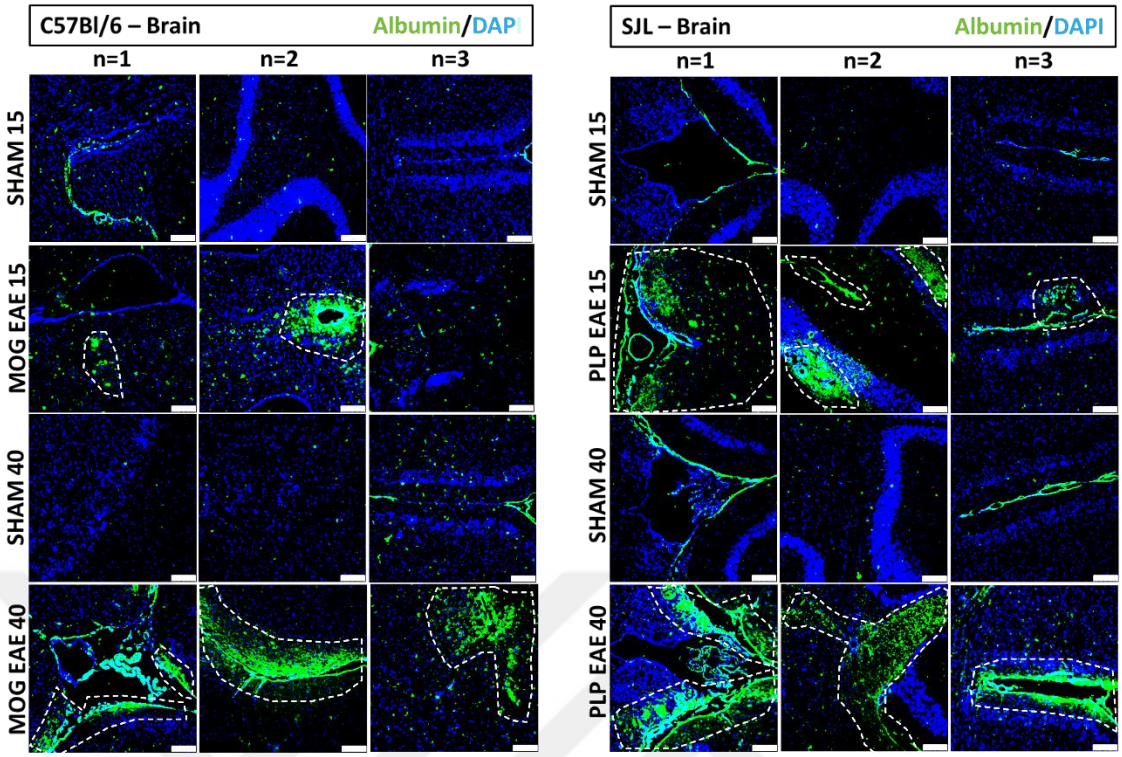

Figure 13: Albumin staining in brain/cerebellum sections of MOG and PLP groups. Three different brain/cerebellum sections are shown for each group. Albumin (green) stains BBB leakage and DAPI (blue) stains cell nucleus. Dashed areas show albumin leakage. The scale bars represent 250 µm.

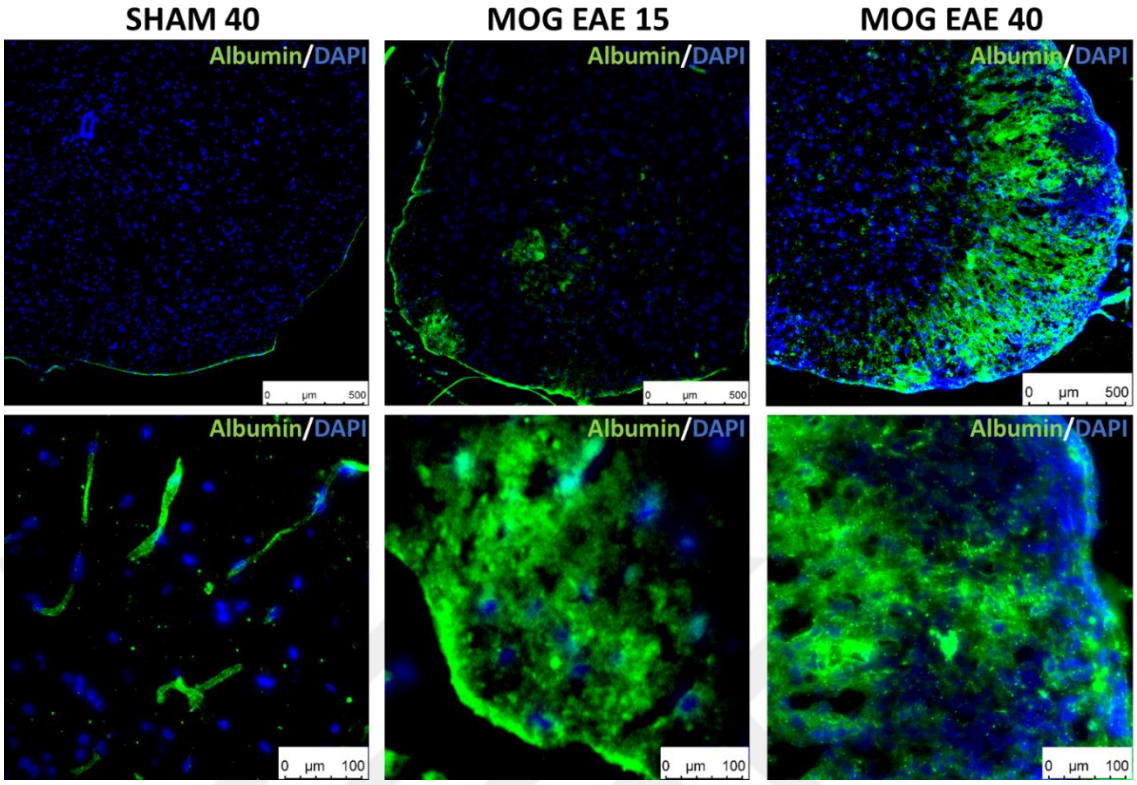

Figure 14: Fluorescent images of spinal cord sections obtained by staining of the BBB leakage with albumin in SHAM, MOG EAE 15 and MOG EAE 40 models. In the SHAM group, albumin does not show any leakage in the tissue except intact endothelial staining. On the other hand, in EAE models, albumin leaking into the tissue is observed. It is especially noteworthy that leakage around infiltrated cell clusters is observed. Over time, between early and late stage EAE, the BBB leakage worsened and covered a larger area in the white matter. Upper panel scale bars represent 500 µm. Lower panel represent corresponding zoomed images with scale bars of 100 µm.

3.4 Inflammation

We next examined inflammatory cells, T lymphocytes marked with CD8 and macrophages with F480, in order to see the time-dependent changes of immunological cell infiltration in EAE versus SHAM groups. In the spinal cord sections of MOG models, inflammatory cell infiltration started mild in MOG EAE 15 (Figure 15) and then increased in MOG EAE 40 (one mice with large lesion (Figure 17). Due to the lack of images for the spinal cord sections of PLP EAE

40, no comparison could be made for the early and late stage PLP EAE model. However, the inflammatory cell infiltration in PLP EAE 15 is in line with the results for albumin leakage (Figure 12-14). The increased inflammation in MOG EAE 40 (Figure 17) is showing a progressive process which is line with cell infiltration and BBB deterioration.

Inflammation in the brain was mainly located around ventricles and in the cerebellum (Figure 16).

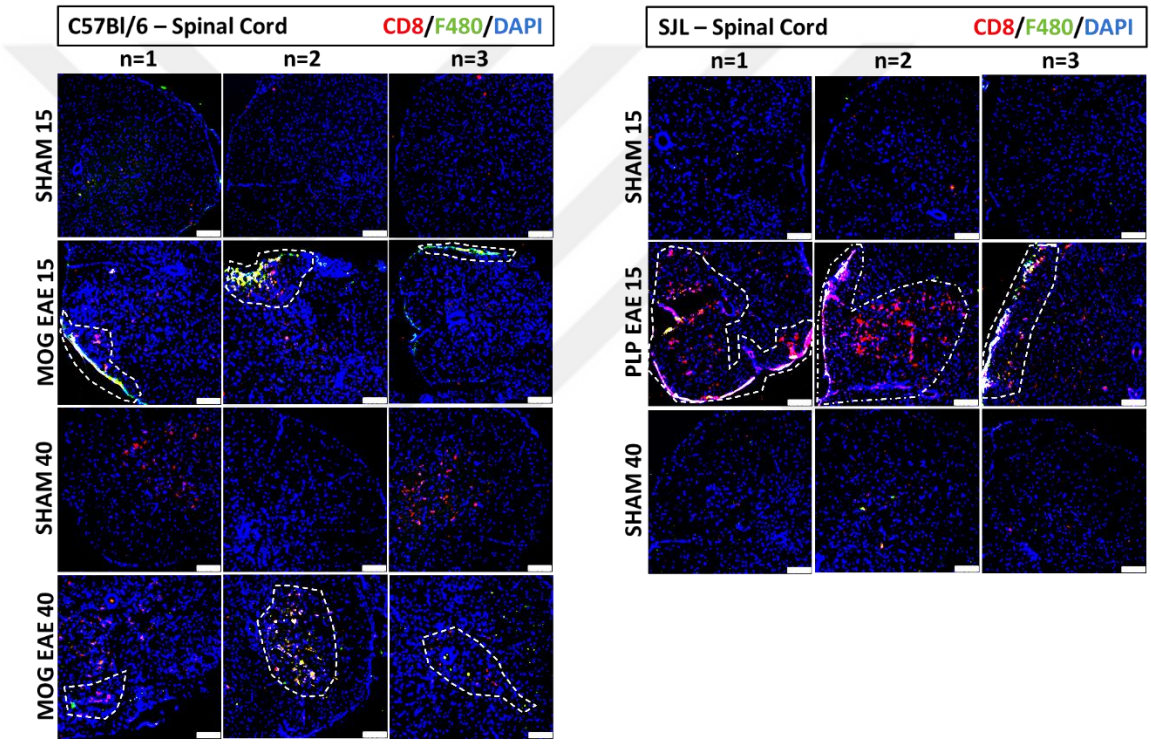

Figure 15: T-lymphocyte marker CD8 (red) and macrophage marker F4/80 (green) staining merged with DAPI (blue) in spinal cord sections of MOG and PLP groups. Dashed areas show inflammation. Three different spinal cord sections are shown for each group. The scale bars represent 250 µm.

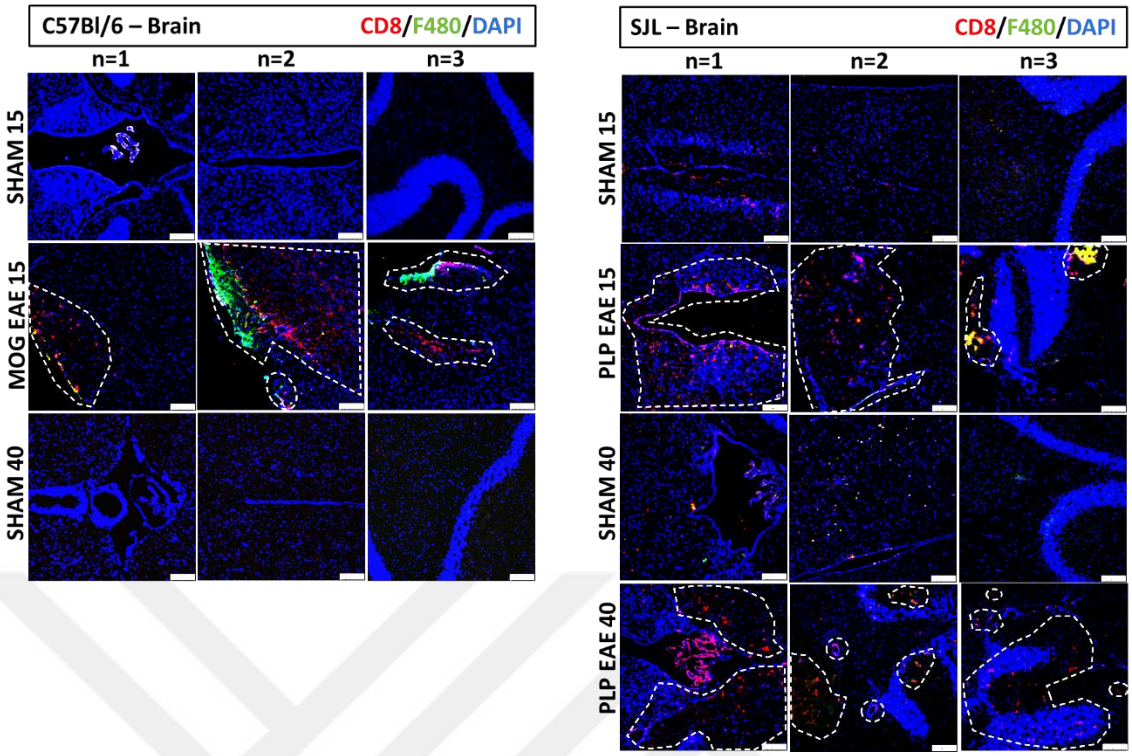

Figure 16: T-lymphocyte marker CD8 (red) and macrophage marker F4/80 (green) staining merged with DAPI (blue) in brain/cerebellum sections of MOG and PLP groups. Dashed areas show inflammation. Three different brain/cerebellum sections are shown for each group. The scale bars represent 250 µm.

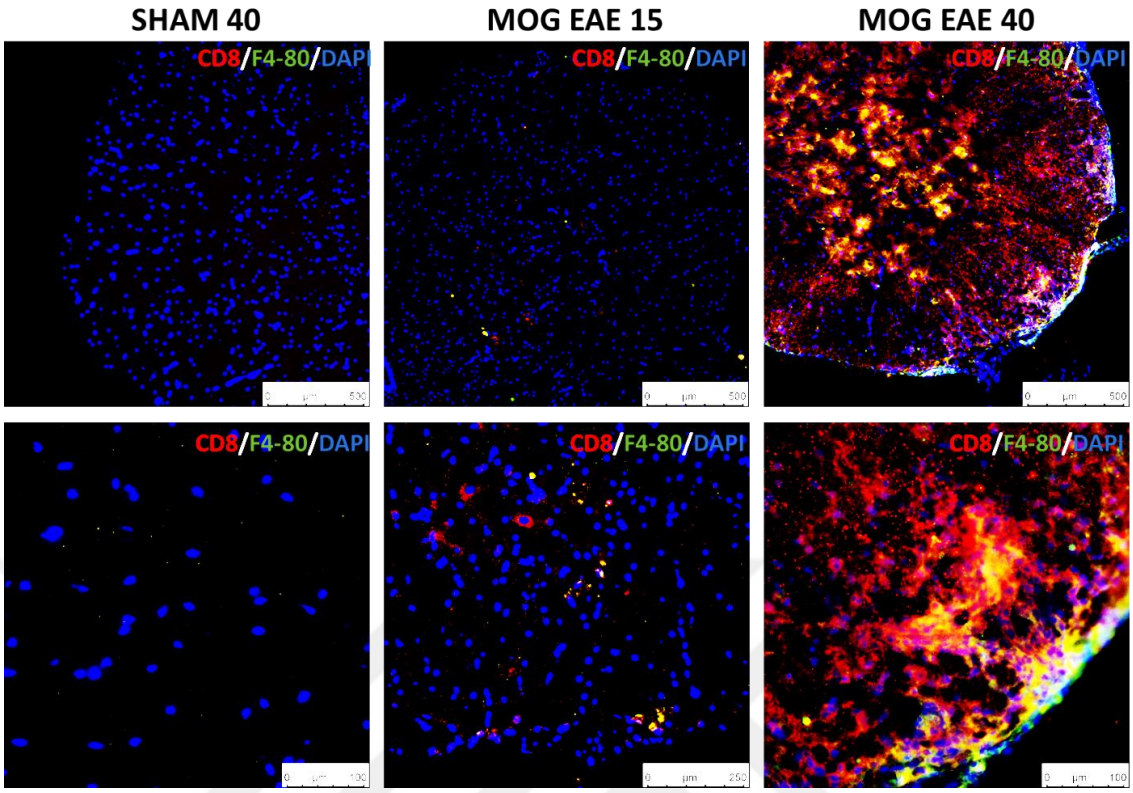

Figure 17: Fluorescent images obtained from spinal cord sections of SHAM 15, MOG EAE 15 and MOG EAE 40 models with inflammatory cell infiltration, CD8 (T-lymphocyte) and F4-80 (macrophage). While no inflammatory cells were seen in the SHAM group, a few number of T-lymphocytes and macrophages were observed in the MOG EAE 15 group. In the MOG 40 EAE group, both increased and clustered T-lymphocytes and increased and clustered macrophages were detected in the lesion regions. In particular, an infiltration pathway from the outer part of the tissue to the inner areas is noteworthy. Upper panel scale bars represent 500 µm. Lower panel represent corresponding zoomed images with scale bars of 100 µm (except the image in the middle which is 250 µm).

3.5 Demyelination

The validation for disease occurrence in EAE modeling is the detection of demyelination areas in the tissue with MBP staining. BBB leakage and inflammatory cells lead to invasion of lymphocytes, leukocytes and macrophages into the brain and spinal cord. Myelin sheaths are degenerated and myelin is removed from the environment by microglia. Demyelination progression leads to the impedance of axonal signals.

Demyelination areas were assessed in both MOG and PLP models. In Figure 18 and Figure 19 it is shown that both EAE groups showed myelin loss compared to their corresponding SHAM groups. Spinal cord sections from MOG EAE 15 showed multiple spots of complete demyelination, however in MOG EAE 40 myelin lost its compact density when compared to SHAM 15 and 40. This indicates a chronic demyelination. On the other hand, in PLP EAE 15 and PLP EAE 40, demyelination started at the border of the white matter with the gray matter in PLP EAE 15 and progressed towards the edges of the tissue in the PLP EAE 40 model. Moreover, in PLP EAE 40, there was also accumulation at the edges of the white matter indicating possible remyelination which is not unexpected given the fact that PLP models a RRMS type (Figure 20).

Demyelination areas were detected in the brain and cerebellum sections from day 15 onwards (Figure 19). Multiple spots of demyelination were observed in the white matter areas the cerebellum and around ventricles.

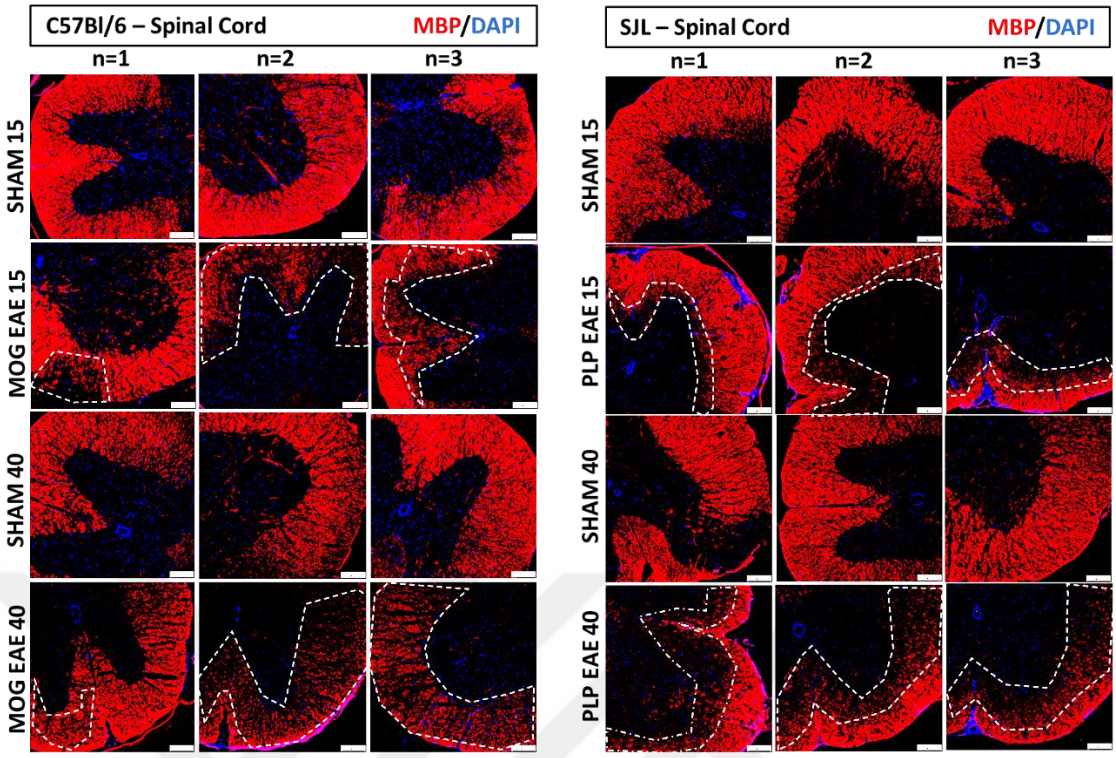

Figure 18: Myelin marker MBP (red) merged with DAPI (blue) in spinal cord sections of MOG and PLP groups. Dashed areas represent loss of myelin. Note that in PLP EAE models, demyelination starts at the border of gray matter and white matter in PLP EAE 15 and extends towards white matter over time in PLP EAE 40. Three different spinal cord sections are shown for each group. The scale bars represent 250 µm.

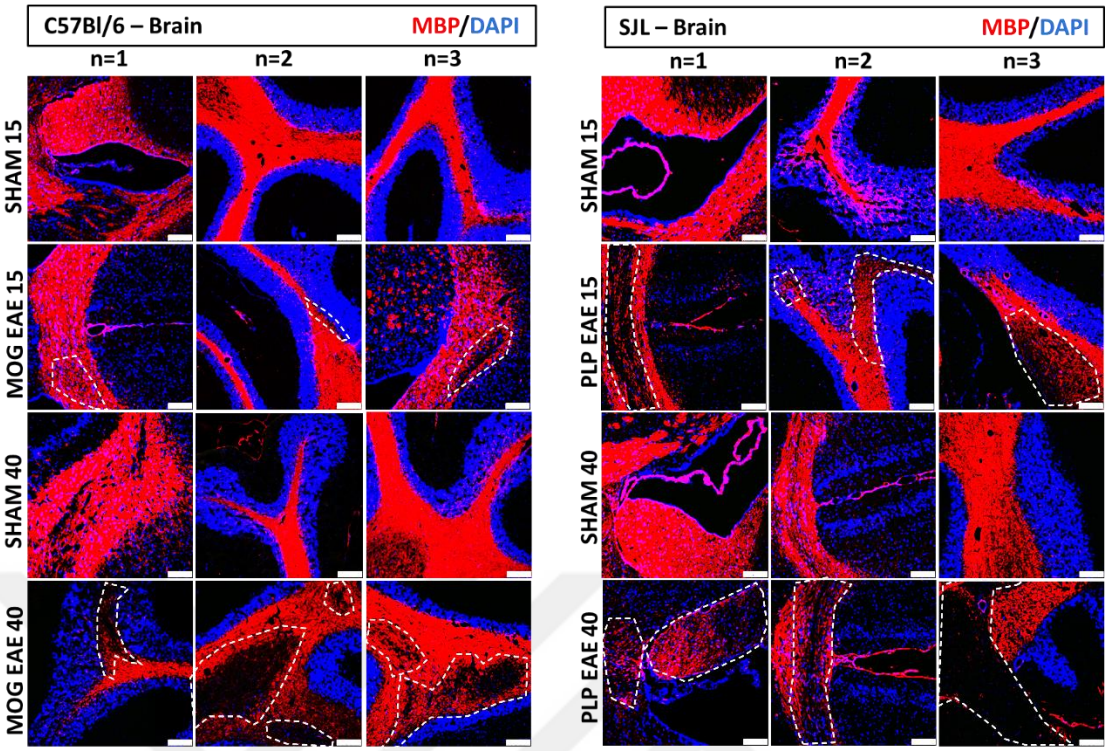

Figure 19: Myelin marker MBP (red) merged with DAPI (blue) in brain/cerebellum sections of MOG and PLP groups. Dashed areas represent loss of myelin. Three different brain/cerebellum sections are shown for each group. The scale bars represent 250 µm.

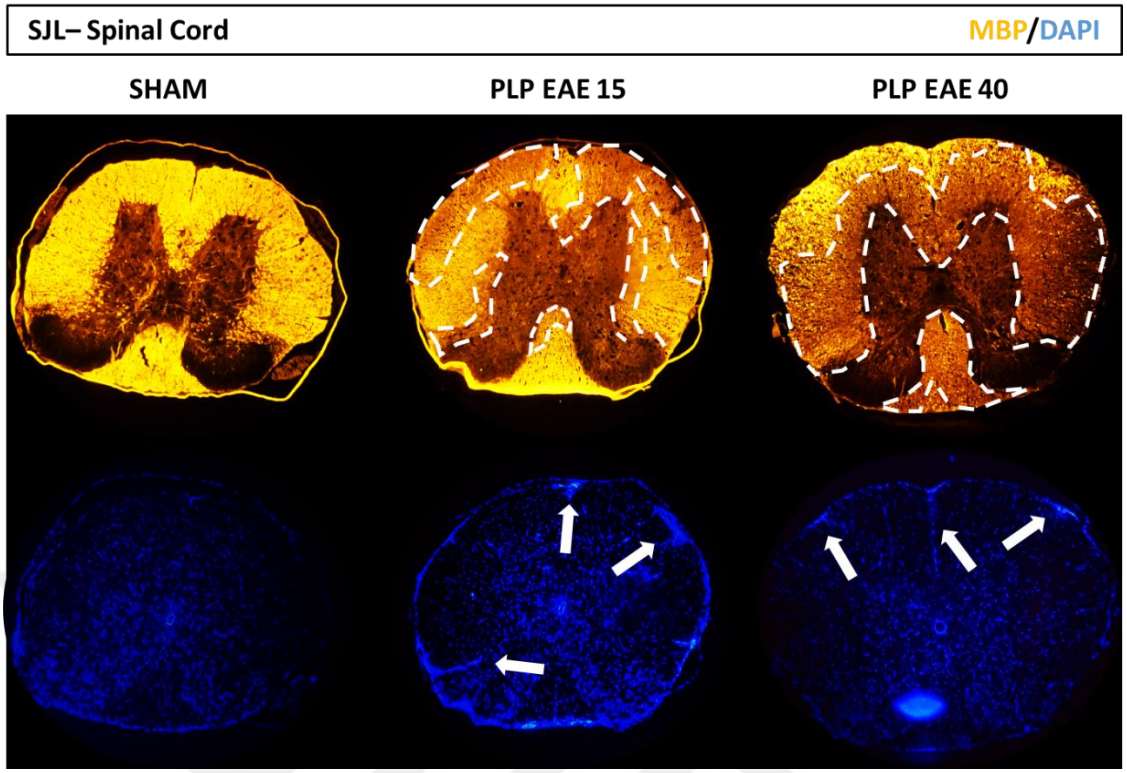

Figure 20: Myelin marker MBP (Yellow) and DAPI (blue) in spinal cord sections of PLP groups. Pictures are obtained with a regular photo camera capturing from the ocular lens while the sample was illuminated with fluorescent light. Dashed areas (upper panel) indicate demyelinated white matter areas with corresponding spots (lower panel) with cell infiltrations/accumulations (white arrows) in the white matter close to the pia mater. Note that, even areas without cell accumulations show decreased myelin (orange/red, dashed areas upper panel) compared to SHAM. Another observation is that myelin loss is increased over time. PLP EAE 40 has relatively less myelin compared to PLP EAE 15. Also, due to the RRMS type of PLP model, myelin debris and/or accumulations are localized around lesion sites in the white matter of PLP EAE 40 model, possibly indicating remyelination.

3.6 Axonal Loss and Gliosis

One of the features of MS is axonal loss and gliosis (caused by GFAP positive activated astrocytes). To this end, we examined astrocytes stained with GFAP and neurons with Microtubule-associated Protein 2 (MAP2) to determine the status of these cells in both EAE models.

When the spinal cord sections were examined (Figure 21-24), it was observed that the density of GFAP positive astrocytes increased in PLP EAE model over time (day 15 versus day 40) and the number of astrocytes increased significantly in gray matter in PLP EAE 15. In PLP EAE 40, these astrocytes were still present in high numbers but relatively lower compared to PLP EAE 15 (Figure 21 and Figure 23). Of note is that these astrocyte were not increased gray matter in any of the MOG models (Figure 22).

In brain sections (Figure 25), GFAP positive astrocytes were slightly increased around ventricles but more importantly also increased in the white matter areas of the brain and especially highly increased in the cerebellum of both MOG and PLP EAE models. These astrocytes in the cerebellum were even more increased in the white matter over time when MOG and PLP EAE 15 models were compared to MOG and PLP EAE 40.

Neuronal marker MAP2 was overall decreased in density in all EAE models. Also the border between gray matter and white matter was indistinct (Figure 22-24). This may be due to either damaged and/or reduced stable axons. The border between gray matter and white matter was the most affected area with loss of both MAP2 and GFAP positive staining.

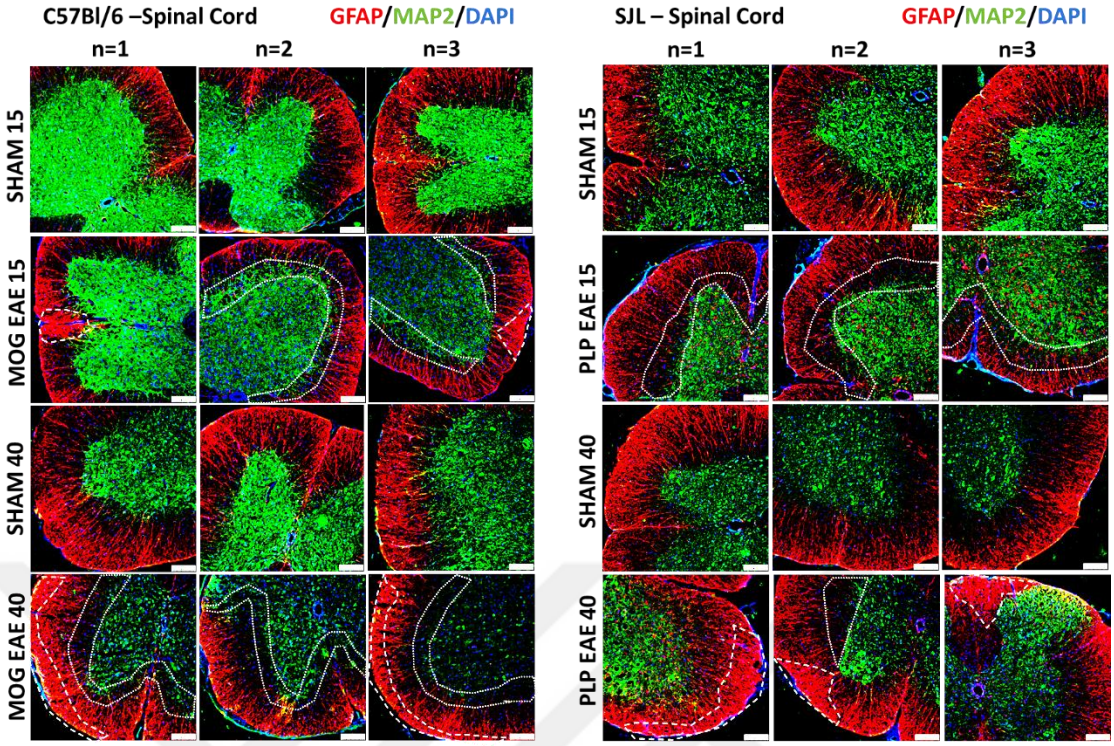

Figure 21: Spinal cord sections of MOG and PLP groups marked for activated astrocytes with GFAP (red) and mature neurons with MAP2 (green), merged with DAPI (blue). Dashed areas show increased GFAP+. Dotted areas show indistinctive border between gray matter and white matter. It is unknown whether MAP2 or GFAP is decreasing and/or shortening in these areas. Three different spinal cord sections are shown for each group. The scale bars represent 250 µm.

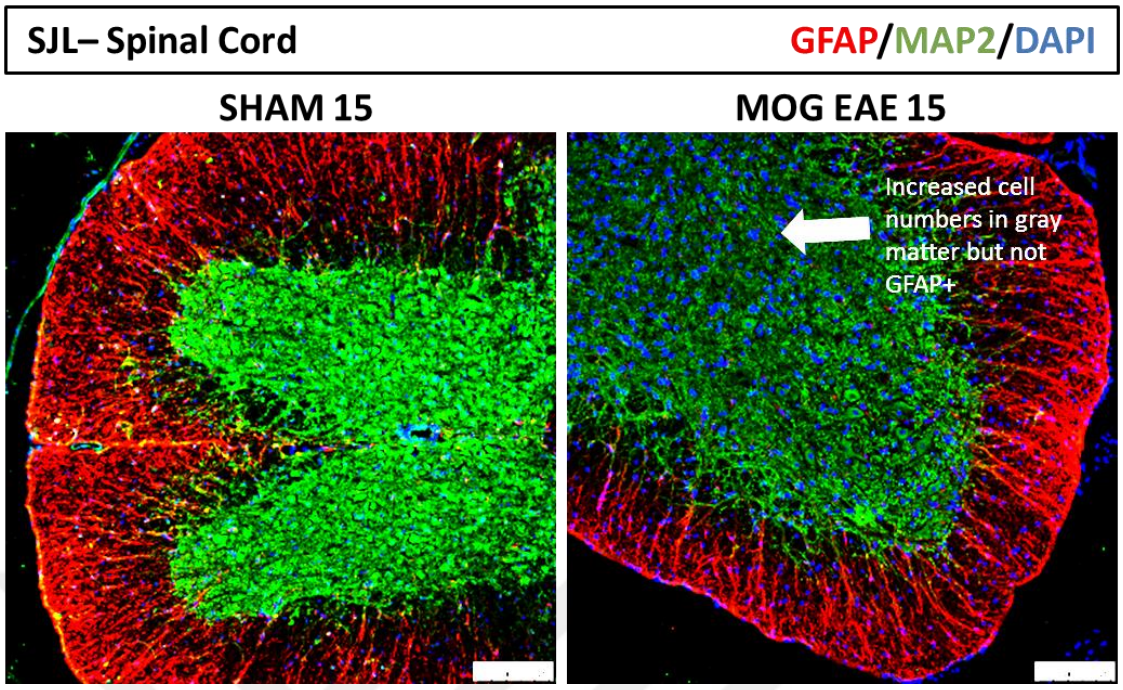

Figure 22: Spinal cord sections of SHAM 15 and MOG EAE 15 stained for activated astrocytes with GFAP (red) and mature neurons with MAP2 (green), merged with DAPI (blue). Note the increased cell numbers (DAPI) in MOG EAE 15 group. Also, overall decreased MAP2 density is present at the border between gray matter and white matter. No intensive astrocyte numbers are present in grey matter (arrow). The scale bars represent 250 µm.

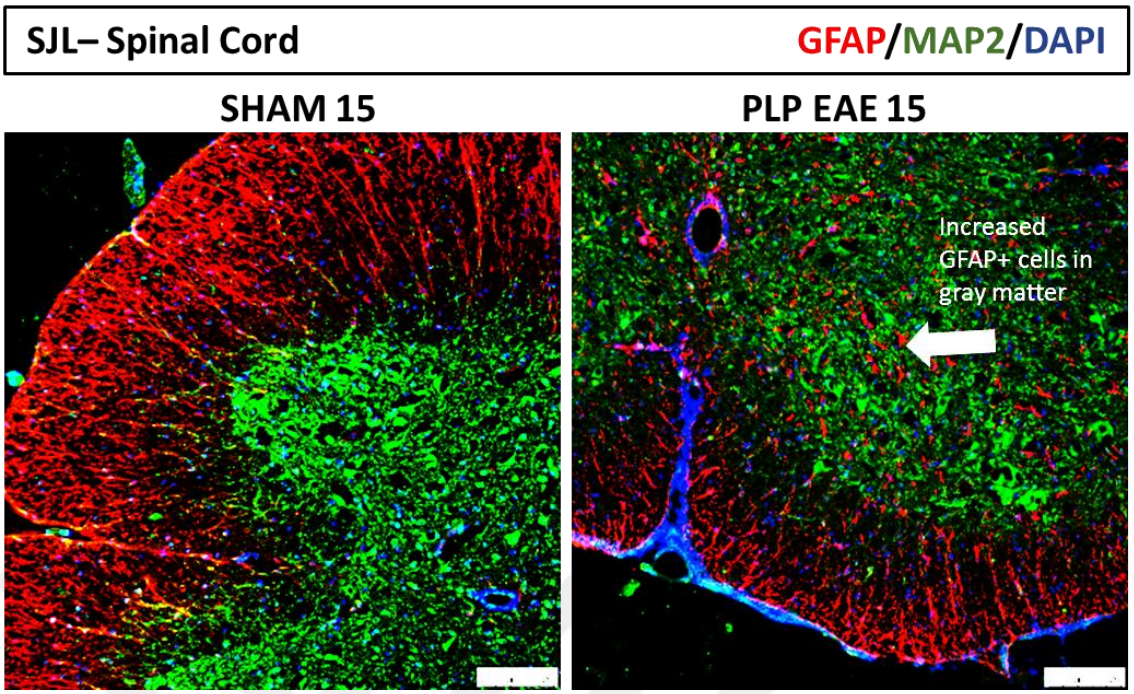

Figure 23: Spinal cord sections of SHAM 15 and PLP EAE 15 stained for activated astrocytes with GFAP (red) and mature neurons with MAP2 (green), merged with DAPI (blue). Note the increased cell accumulations (DAPI) in the white matter aligning the pia mater in MOG EAE 15 group. Also, a decreased GFAP and MAP2 density is present at the border between white matter and grey matter. Interestingly, highly increased GFAP+ astrocyte numbers (arrow) were present in grey matter. The scale bars represent 250 µm.

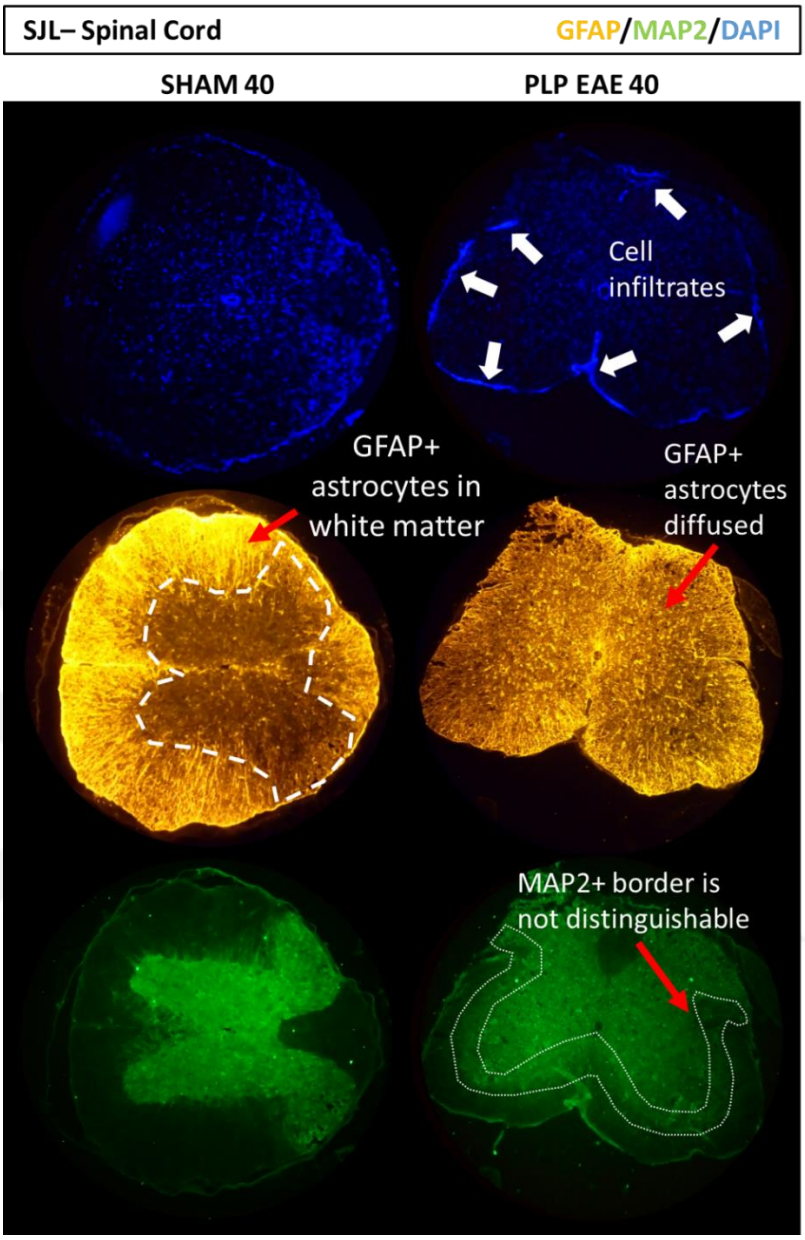

Figure 24: DAPI (blue), GFAP (Yellow) and MAP2 (green) staining in spinal cord sections of SHAM 40 and PLP EAE 40 groups. Pictures are obtained with a regular photo camera capturing from the ocular lens while the sample was illuminated with fluorescent light. Arrows show infiltration of cells. Dashed area represents gray matter where a minimal amount of GFAP+ astrocytes are present, however this is increased in the PLP EAE model. Doted area represents neuronal soma in the gray matter, from which the border between gray matter and white matter is not distinguishable. Note the diffused GFAP and MAP2 staining throughout the spinal cord tissue in the PLP EAE model.

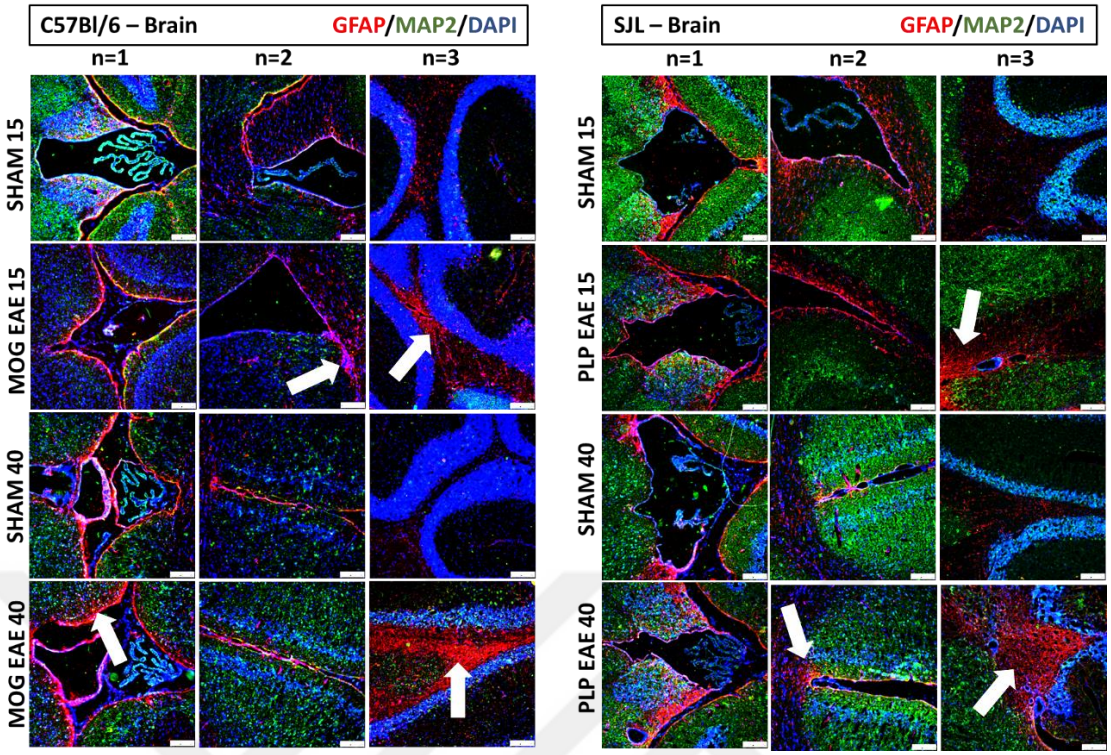

Figure 25: Brain and cerebellum sections of MOG and PLP groups stained for activated astrocytes with GFAP (red) and mature neurons with MAP2 (green), merged with DAPI (blue). Arrows show increased GFAP+ areas. Three different brain/cerebellum sections are shown for each group. The scale bars represent 250 µm.

3.7 Pericytes in EAE

In order to investigate our main hypothesis, we used double/triple stainings with DAPI for cell nucleus to track down pericytes. For this purpose, we used PDGFRβ, NG2, and αSMA which were expressed by pericytes and co-localized these with endothelium markers Isolectin (IB4) or albumin (BBB leakage).

In the spinal cord sections (Figure 26), PDGFRβ+ pericytes were increased heterogeneously all over the tissue in MOG EAE 15 compared to SHAM 15. On the other hand PDGFRβ+ pericytes accumulated at lesion sites in MOG EAE 40 (Figure 26, 28 and 29). IB4 (either marking endothelium or activated microglia) was increased in the gray matter of MOG EAE 40.

In PLP EAE 15, compared to SHAM 15, there were increased lesion sites in the outer white matter area with tightly accumulated PDGFRβ+ pericytes (Figure 26, 27 and 31). The appearance shows almost a band aid for the leaking endothelium by wrapping up the infiltrates. These areas also showed increased IB4 staining, even in the perimeter of the lesions. In PLP EAE 40, the same scenario was present as PLP EAE 15.

In brain sections of MOG EAE 15 (Figure 27), PDGFRβ+ pericytes are mainly accumulated around ventricle zones but their appearance increases in MOG EAE 40 where they are closer to the pia mater and mainly also present in the white matter of the cerebellum. Increase in IB4 was seen in larger lesions only. In PLP EAE 15, PDGFRβ+ pericytes were mainly accumulated around the ventricle zones and in the white matter of the cerebellum as well. These were representing enlarged vessels with cellular infiltrates, tightly wrapped up by increased PDGFRβ+ pericytes. The infiltration seems engulfed and controlled by pericytes. IB4 staining also increased mainly in the cerebellum in PLP EAE model.

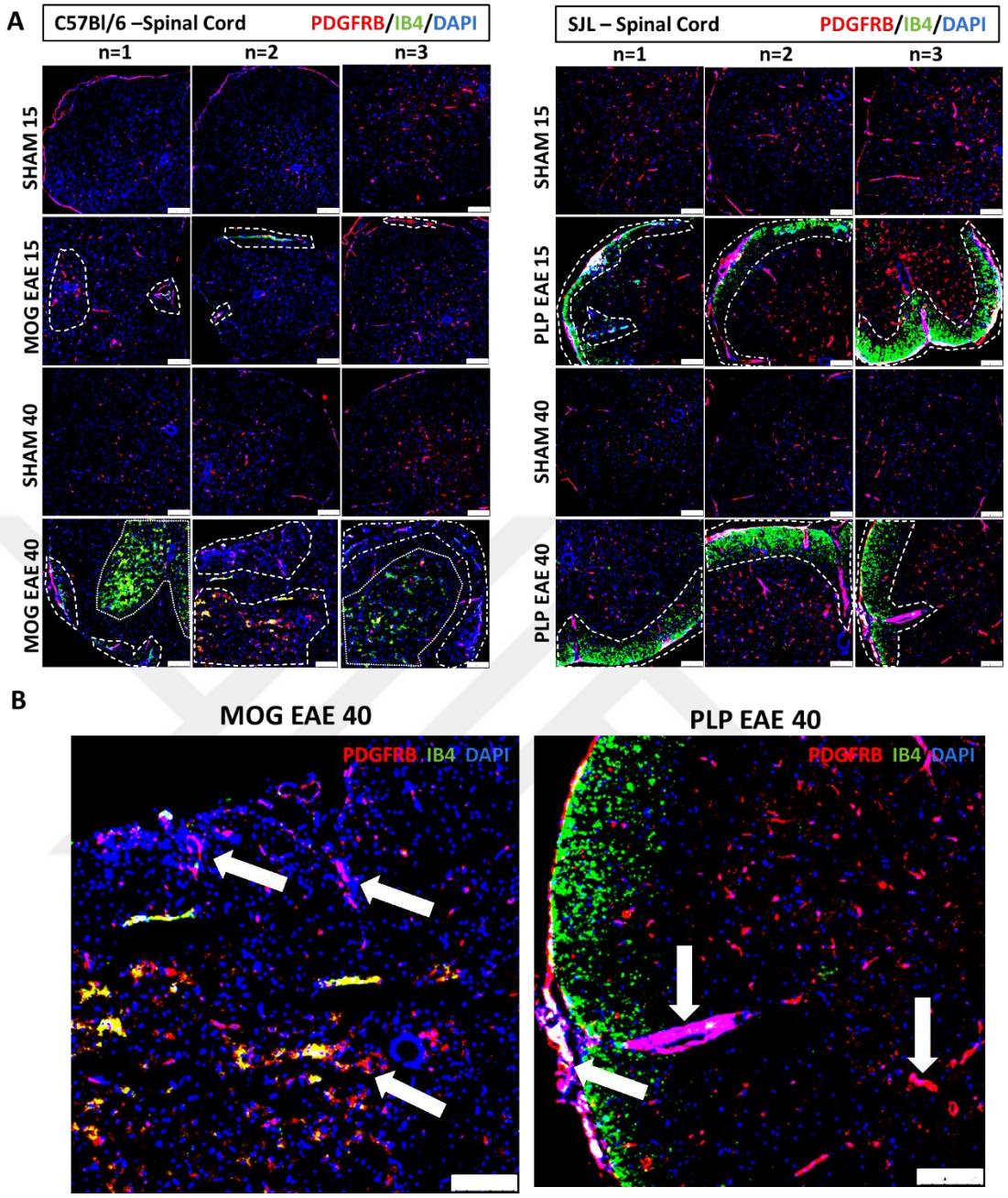

Figure 26: Spinal cord sections of MOG and PLP groups stained for pericytes with PDFRGβ (red) and endothelium with IB4 (green), merged with DAPI (blue). A) Dashed areas represent affected (increased in PDFRGβ and IB4) regions. B) Arrows show pericytes at affected areas. Note that in PLP EAE, PDFRGβ+ pericytes are tightly wrapping up the endothelium and thereby constraining the infiltrating cells. Three different spinal cord sections are shown for each group. The scale bars represent 250 µm.

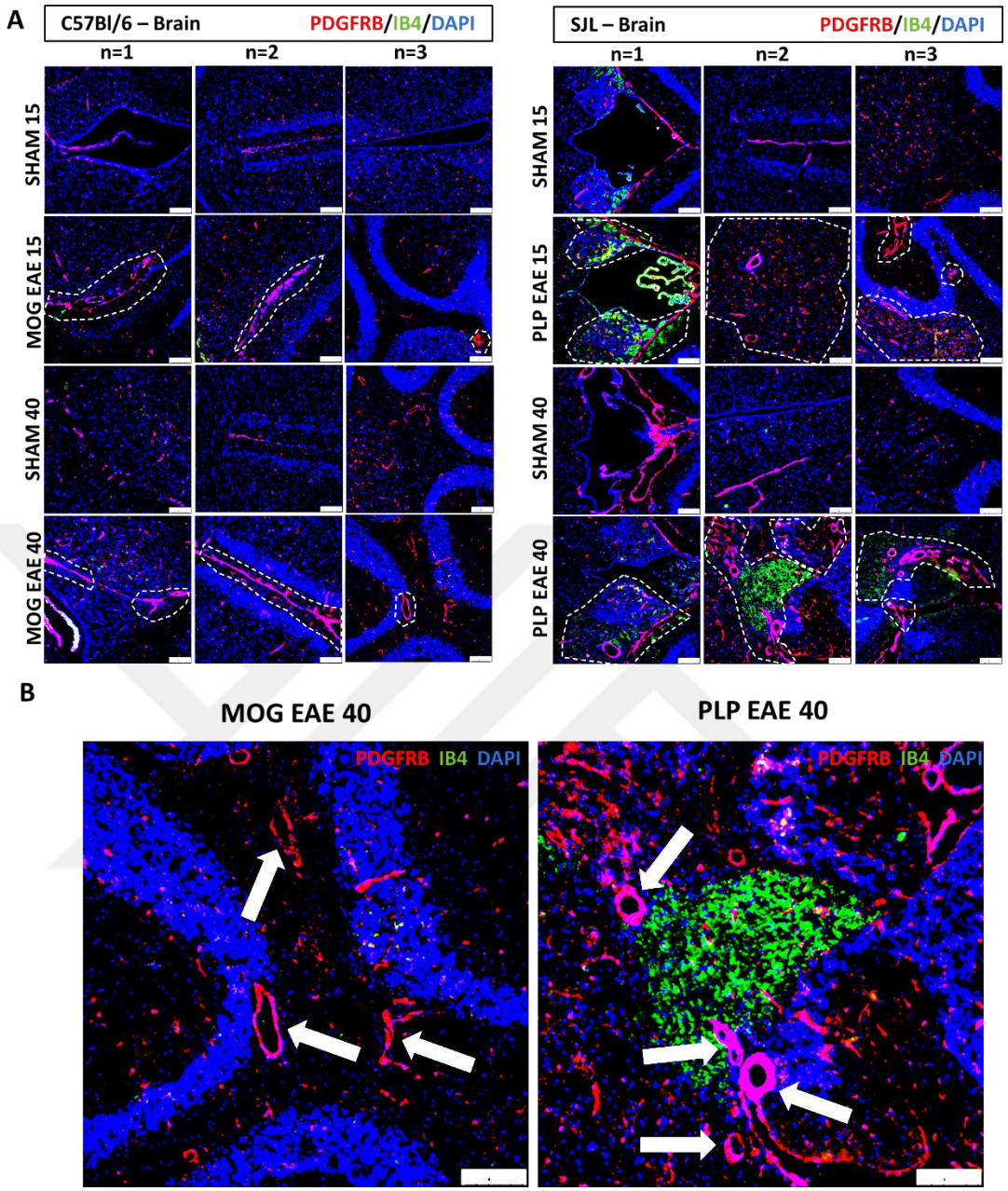

Figure 27: Brain/cerebellum sections of MOG and PLP groups stained for pericytes with PDFRGβ (red) and endothelium with IB4 (green), merged with DAPI (blue). A) Dashed areas represent affected (increased in PDFRGβ and IB4) regions. B) Arrows show pericytes at affected areas, note the increased PDFRGβ+ pericytes around the endothelium. Three different brain/cerebellum sections are shown for each group. The scale bars represent 250 μm.

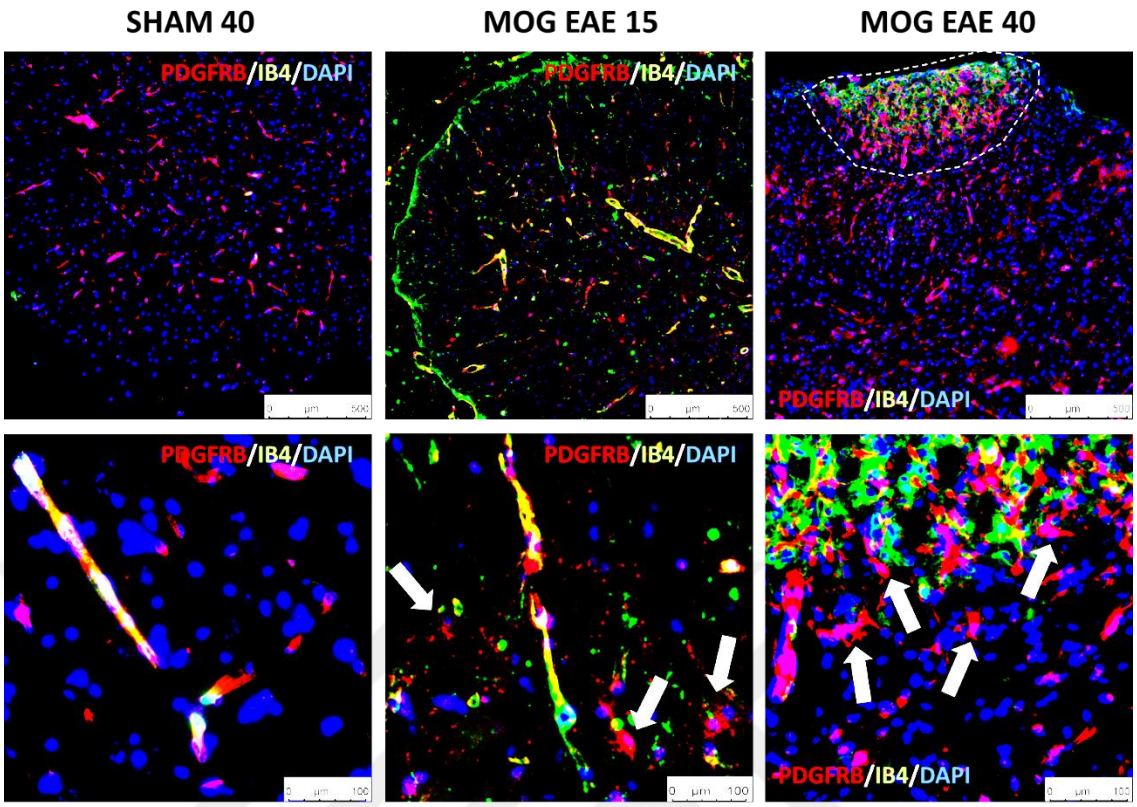

Figure 28: Fluorescence images of spinal cord sections obtained with PDGFRβ and IB4 staining of SHAM 40, MOG EAE 15 and MOG EAE 40 groups. Dashed area represents lesion area with increased PDGFRβ and IB4 staining. White arrows represent pericytes leaving endothelium. The scale bars represent: upper panel 500 µm, lower panel 100 µm.

The smooth muscle cell marker αSMA is also expressed by pericytes, co-localized with PDGFRβ it mainly marks larger vessels (Figure 30). In MOG EAE 40 model it is shown that PDGFRβ+ pericytes leave the endothelial wall and accumulate at lesion sites (Figure 29). αSMA+ cells decrease around vessels either, but these cells are mainly found as solely αSMA positive (when not attached to endothelial wall) throughout the spinal cord tissue, accumulating in lesion sites only in MOG EAE 40 model. In PLP EAE models, only PDGFRβ+ pericytes are found in lesion sites, no evidence is found for αSMA+ cells without attachment to endothelial wall. Adjacent to enlarged vessels with engulfed cell infiltrates, in PLP EAE models there was an accumulation of PDGFRβ+ pericytes shown (Figure 32). Albumin leakage is observed in the perimeter of these enlarged vessels.

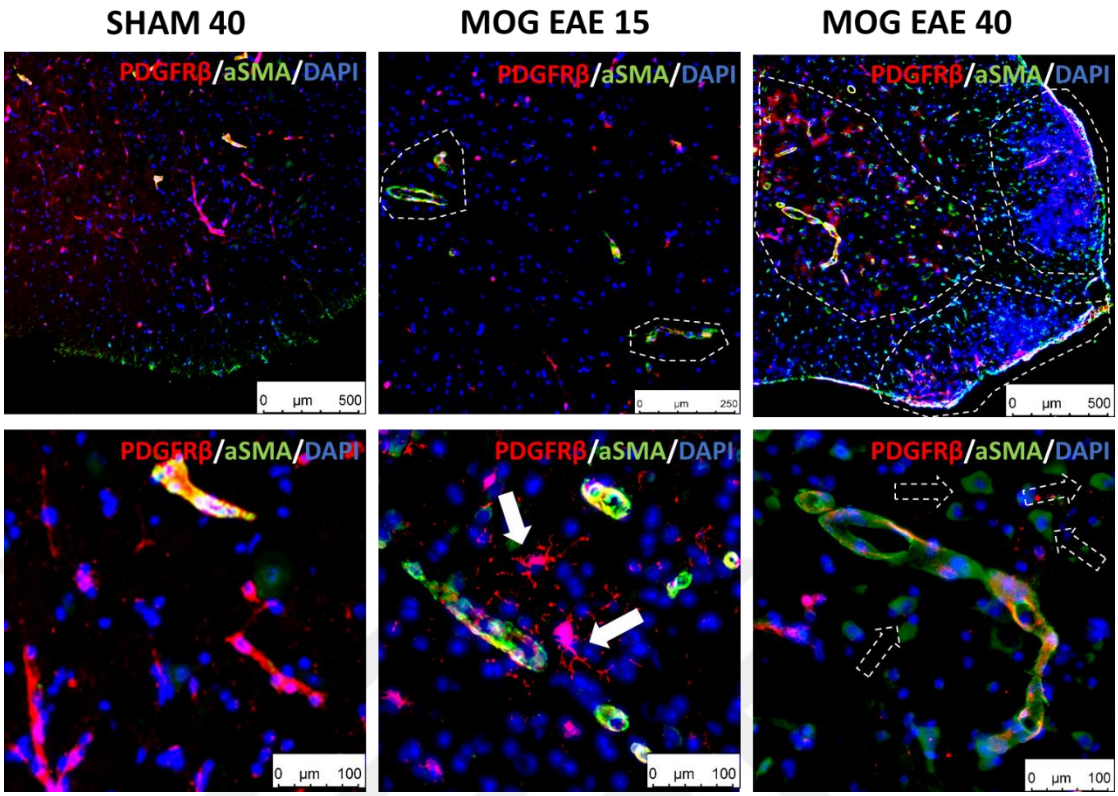

Figure 29: Fluorescence images of spinal cord sections obtained as a result of PDGFRβ and αSMA staining of SHAM 40, MOG EAE 15 and MOG EAE 40 groups. Dashed areas represent affected areas with lesions. White arrows show PDGFRβ+ pericytes detached from the endothelium, dashed arrows show αSMA+ cells detached from the endothelium. While PDGFRβ+/αSMA+ cells were detected in the SHAM group, this decreased in the MOG EAE 15 group. It is noteworthy that PDGFRβ+ pericytes moved away from the vessel enclosed by αSMA+ pericytes (white arrows). In the MOG EAE 40 group, PDGFRβ+αSMA+ cells, are decreased at the endothelium, however solely expressing PDGFRβ+ (white arrows) and αSMA+ (dotted arrows) cells were found scattered throughout the tissue but mostly found concentrated in the lesion regions. The scale bars represent: upper panel 500 µm (image in the middle 250 µm), lower panel 100 µm.

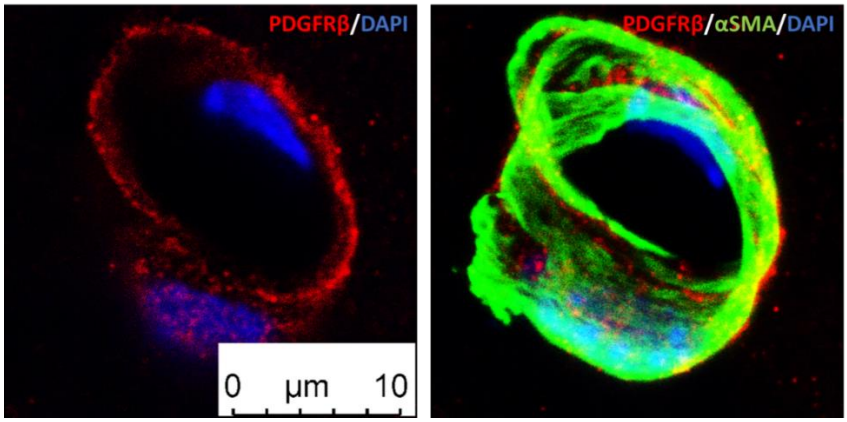

Figure 30: Confocal image of PDGFRβ+/αSMA+ pericyte wrapping around a capillary of 10 μm (endothelium is not shown).

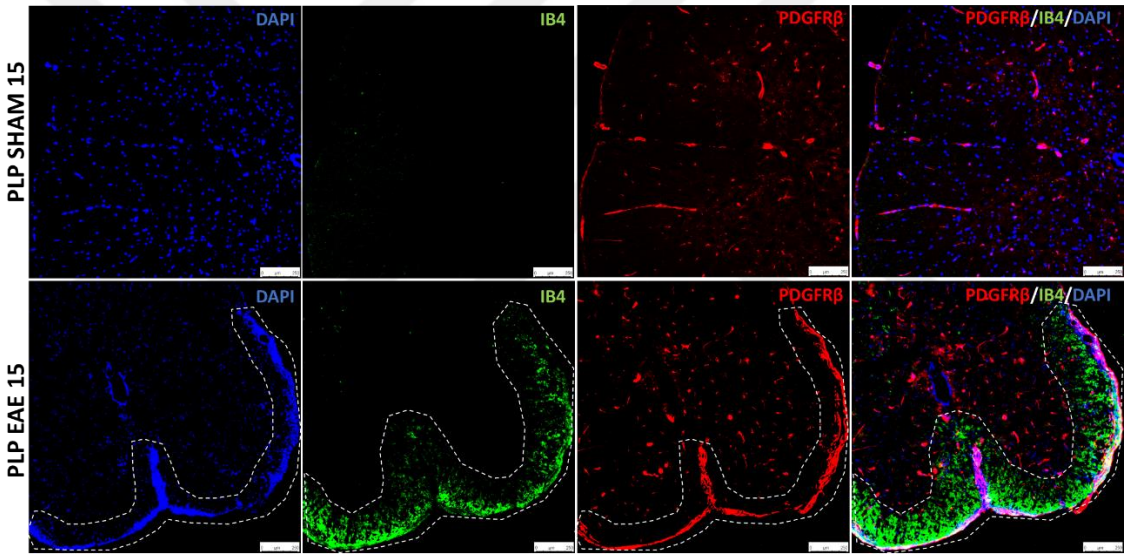

Figure 31: Fluorescence images of spinal cord sections obtained with PDGFRβ and IB4 staining of SHAM 15 and PLP EAE 15 groups. Dashed areas show most affected regions. Compared to SHAM, PDGFRβ+ pericytes were increased and accumulated around endothelium within the core of the lesion sites. It is unknown whether local pericytes were proliferated at these sites, or whether pericytes from the neighborhood migrated towards the lesion sites. Note also the increased and scattered IB4 staining at these lesion sites. The scale bars represent 250 μm.

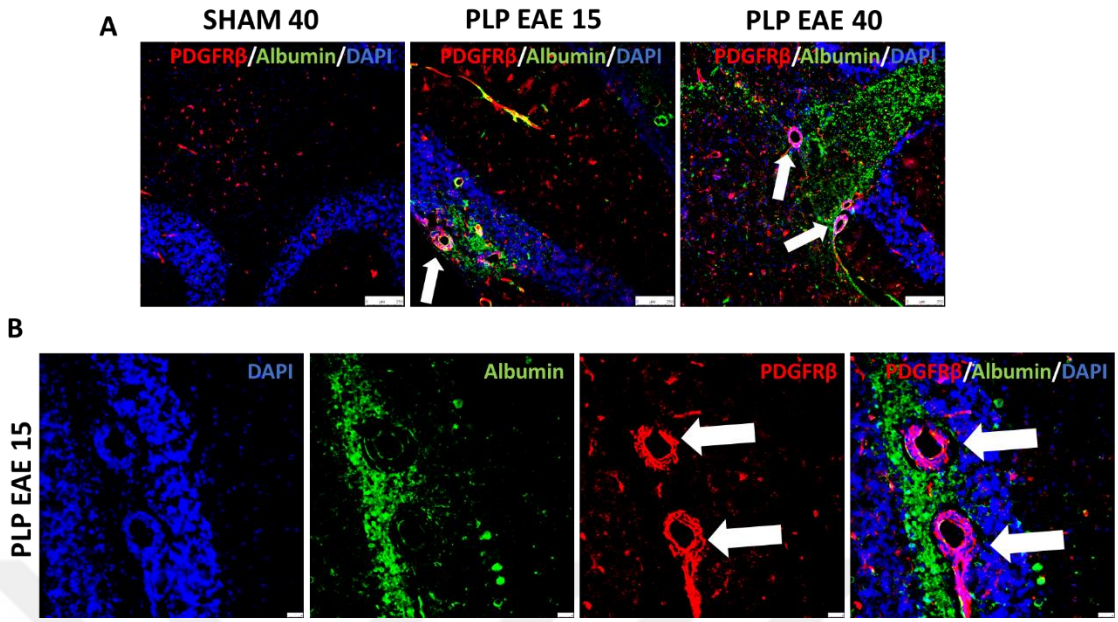

Figure 32: Fluorescence images of cerebellum sections obtained with PDGFRβ and Albumin staining of SHAM 40 and PLP EAE 15 and PLP EAE 40 groups. A) Compared to SHAM, PDGFRβ+ pericytes were increased and accumulated (white arrows) around endothelium within the core of the lesion sites. B) These lesion sites (white arrows) were prominently in the white matter areas in the cerebellum, or adjacent to ventricular zones in the brain. Note the leaked BBB areas by albumin staining around these enlarged vascular lesion sites. The scale bars represent: upper panel 250 μm, lower panel 50 μm.

Compared to SHAM 40 (Figure 33), and likewise PDGFRβ+ pericytes, NG2+ pericytes/oligodendroglial cells were also found scattered through the white matter but nearby the lesion sites in MOG EAE 40 model. In PLP EAE 15 model (Figure 34), NG2+ pericytes/oligodendroglial cells are also scattered around the lesion and its perimeter. However, in PLP EAE 40 model NG2+ scattering is decreased to only the endothelial wall along the pia mater.

Furthermore, IBA1 is a microglia marker but recent evidence showed that activated pericytes leave the endothelial wall (Figure 35C), proliferate and may change in a microglia phenotype (70-72). According to the obtained IBA1 staining results in this study (Figure 35), it is obvious that there are two areas

with IBA1+ cells. One part of this is in the grey matter, and the other part within the lesion cores. Also, the lesion cores show decreased myelin and accumulated cell infiltration. However, the question remains whether these IBA1+ cells are pericyte derived cells or solely activated microglia or both simultaneously.

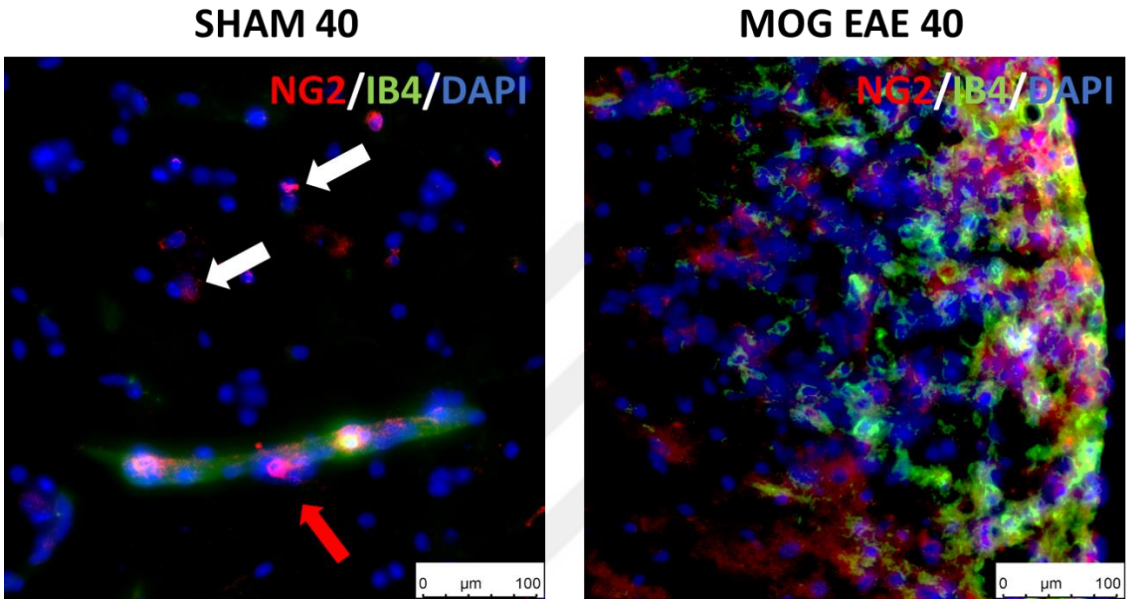

Figure 33: Fluorescence images of spinal cord sections of SHAM 40 and MOG EAE 40 obtained by staining with NG2 and IB4. In the SHAM group, NG2+ pericytes were found localized stable around the vessel (red arrow). Since NG2 antibody also stained oligodendroglial cells, it is understood that the free circulating NG2+ cells are oligodendroglial cells in the perivascular regions (white arrows). On the other hand, the scattered appearance of IB4 in the MOG EAE 40 group indicates that the endothelial wall is scattered and has lost its integrity. NG2 positive pericyte/oligodendroglial cells were detected near the disrupted endothelial structures which were in the core region of the lesions located especially in the white matter near the pia mater. The scale bars represent 100 µm.

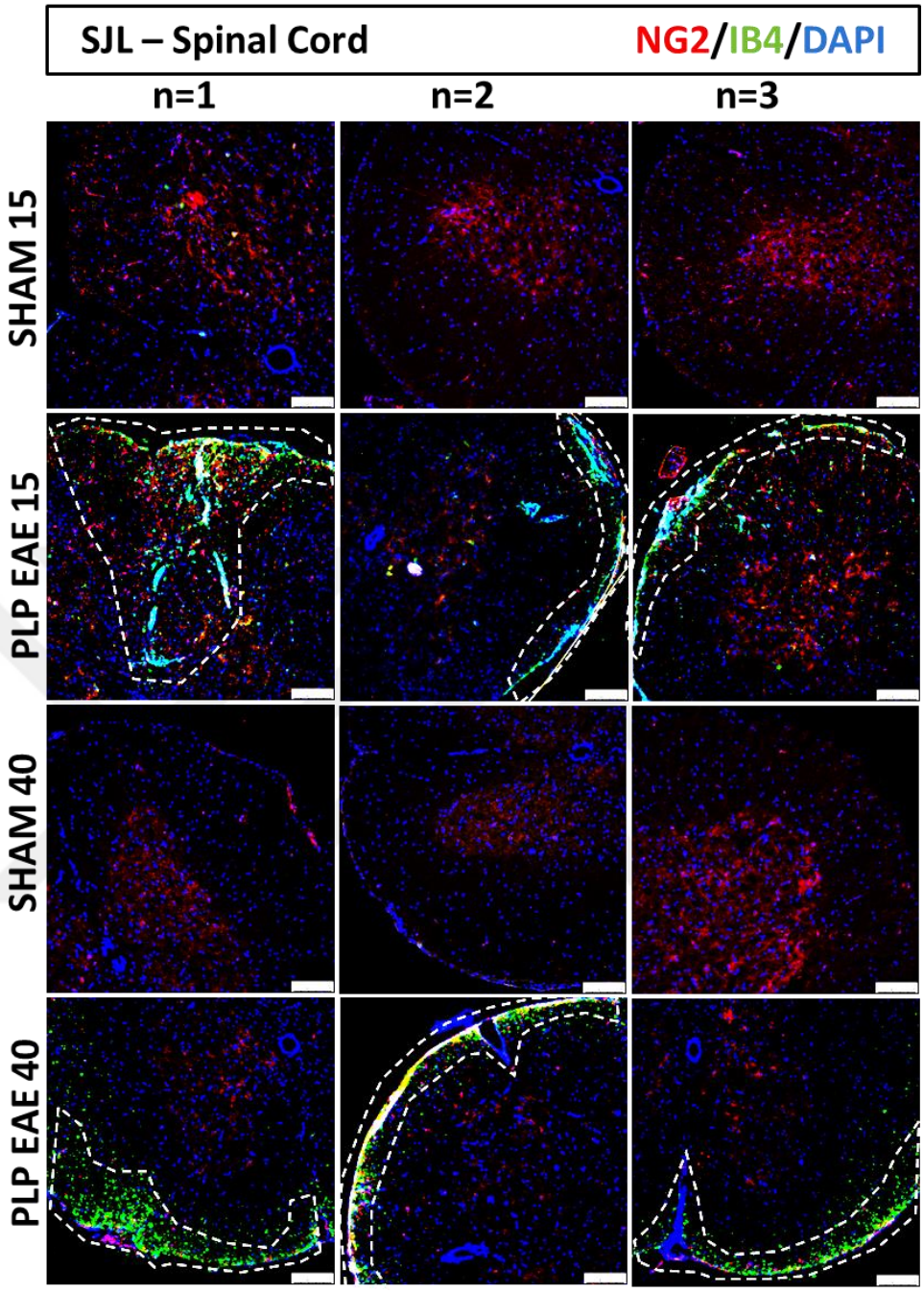

Figure 34: Fluorescence images of spinal cord sections of SHAM and PLP EAE models obtained by staining with NG2 and IB4. Dashed areas represent affected areas with lesions. There is a scattered appearance of both NG2 and IB4 in PLP EAE 15 group, which decreases for NG2 but slightly increases for IB4 in PLP EAE 40. The scale bars represent 250 μm.

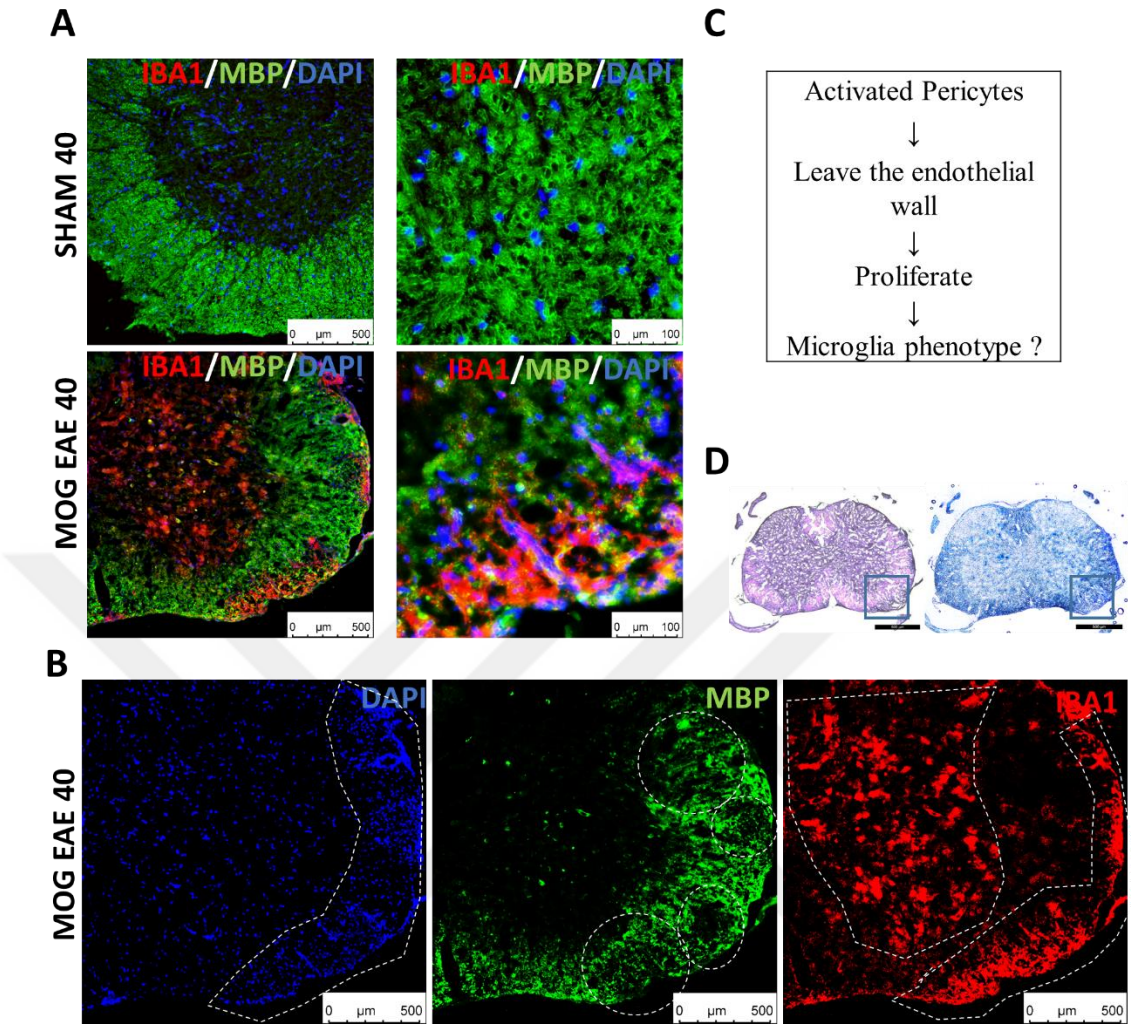

Figure 35: A) Fluorescence images of spinal cord sections obtained with IBA1 and MBP staining of SHAM 40 and MOG EAE 40 groups. B) Unmerged DAPI, MBP and IBA1 staining for MOG EAE 40 group is shown. Dashed areas represent affected areas with lesions, respectively, cell infiltration in DAPI image, demyelination in MBP image and microglia activation and accumulation in IBA1 image. Compared to SHAM, IBA1+ microglia and/or activated pericytes (C) were increased and accumulated around the core of the lesion sites (accumulated DAPI+ cells). Note also the increased IBA1+ cells in the grey matter (B). Furthermore, the areas with myelin loss were increased in IBA1+ cells. D) Corresponding H&E and LFB sections of the images in A&B. The scale bars represent 100 µm.

The fluorescence images obtained for PDGFRβ staining were analyzed for PDGFRβ+ pericyte integrated density (Figure 36A&D), the covered area (Figure B&E) and the total cells present in the spinal cord tissues (Figure 36C&F). The integrated density was measured as a unit for the intensity of PDGFRβ+, while the area (%) was measured as a unit of PDGFRβ+ fraction from the total measured area. The total amount of DAPI+ cells were measured to assess cell infiltration between groups p-values of t test measurements are shown in Table 8 and 9.

Results showed a non-significant change in PDGFRβ+ integrated density between SHAM 15 and MOG EAE 15 (Figure 36A), whereas in MOG EAE 40 this change became significantly increased (*=$p<0.05$). This is in line with the progressive MS type of MOG EAE model. In PLP EAE 15 and PLP EAE 40 (Figure 36D), both models showed significant increase in PDGFRβ+ pericytes in the spinal cord. In PLP EAE 40 model, pericytes were decreased compared to PLP EAE 15. This could be due to the RRMS form of PLP EAE model. Hence, this indicates that pericytes are very crucial in the progression of MS and RRMS. Of note, in both MOG and PLP SHAM 15 groups, there has been an increase in PDGFRβ+ pericytes but these decreased over time on both MOG and PLP EAE 40 models. This results is in line with the increased cell count number for these groups, indicating that upon exposure to CFA+PTX in the SHAM groups, cell infiltration is present and pericytes are increased, however at the late stage this phenomenon is recovered.

In relationship with the total DAPI+ cell numbers which show a significant reduction between early and late stage SHAM groups (Figure 36C&F), it can be concluded that in SHAM models, there is a slight response by pericytes or indirect by pericytes via other infiltrated and/or proliferated cells which is in the first place increased in the early stage models, but then decreased in the late stage models of both MOG and PLP groups. A reason for the different cell numbers in SHAM groups may be because the SHAM groups received CFA and PTX, which most

possible triggered a mild inflammatory response in the initial stage but then recovered after 40 days.

PDGFRβ+ area (Figure 36B) was not changed between SHAM 15 and MOG 15, however was significantly changed in MOG EAE 40. The latter indicates either pericytes proliferated and covered a relatively larger area or activated pericytes changed their morphology from finger shaped to a more protoplasmic cell structure such as a myofibroblasts, increasing in cell area.

On the other hand, in PLP EAE 15 model (Figure 36E), pericytes significantly covered a larger area compared to SHAM 15. However, this area decreased in PLP EAE 40 and became nonsignificant compared to SHAM 40, indicating a relapse phase.

Because of the differences between SHAM groups, the early and late EAE groups could not be analyzed against each other, but could be analyzed only indirect via its corresponding SHAM group.

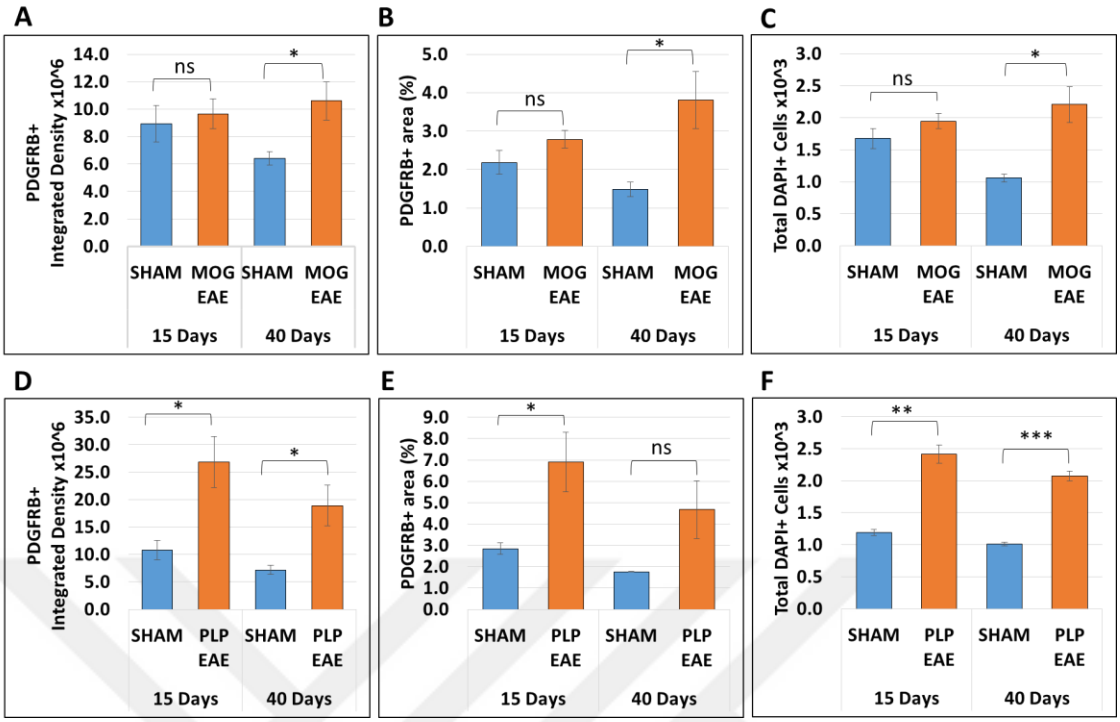

Figure 36: Analysis of fluorescent images measured by the ImageJ program on spinal cord sections of early (15 days) and late stage (40 days) MOG and PLP groups. PDGFRβ+ areas were presented in integrated density values, and the covered area in percentage. Also, the corresponding number of DAPI positive cells were analyzed for all groups. Graphs are expressed as mean ± SEM for n = 3. Statistical data $p < 0.05$ was considered significant: * = $p < 0.05$; ** = $p < 0.01$; *** = $p < 0.001$ and ns = non-significant.

Table 8: P-values of unpaired two-tailed T-test for PDGFRβ+ pericytes within each group of EAE model. Statistical p-values were calculated according to the data measured by ImageJ program from fluorescent images of spinal cord sections.

T-Test: P-value		PDGFRB+ Pericyte					
		Integrated Density	Symbol	Area	Symbol	DAPI+ Cell	Symbol
C57Bl/6	SHAM 15 vs. MOG EAE 15	0.69458	ns	0.19001	ns	0.24107	ns
C57Bl/6	SHAM 40 vs. MOG EAE 40	0.04731	*	0.03862	*	0.01622	*
SJL	SHAM 15 vs. PLP EAE 15	0.03174	*	0.04690	*	0.00113	**
SJL	SHAM 40 vs. PLP EAE 40	0.03355	*	0.09710	ns	0.00022	***

Table 9: P-values of unpaired two-tailed T-test for PDGFRβ+ pericytes between early and late stage models of each SHAM model. Statistical p-values were calculated according to the data measured by ImageJ program from fluorescent images of spinal cord sections.

T-Test: P-value		PDGFRB+ Pericyte					
		Integrated Density	Symbol	Area	Symbol	DAPI+ cells	Symbol
C57Bl/6	SHAM 15 vs. SHAM 40	0.14832	ns	0.12264	ns	0.02163	*
SJL	SHAM 15 vs. SHAM 40	0.11356	ns	0.01790	*	0.03170	*

3.8 Fibrosis in EAE

Fibrosis is the condition when the balance between deposition and degradation of collagen is disrupted leading to irreversible tissue dysfunction (73). Fibrotic remodeling of ECM can be caused by fibroblasts, myofibroblasts and endothelial cells or adipocytes, chondrocytes and osteocytes. Collagen is one of the major strength and recoil components of ECM (73).

Fibronectin and laminin are examples of adhesive glycoproteins. Fibronectin can increase by both leaking from the BBB and/or being produced by CNS resident cells. According to literature fibronectin expresses in the form of aggregates in chronic and relapsing remitting EAE lesions (74, 75).

In this study we aimed to investigate whether EAE/MS also shows signs of fibrosis and in particular whether pericytes are contributing to fibrosis in EAE *in vivo* models.

Results showed that in both MOG and PLP EAE models (Figure 37 and Figure 38), fibronectin was increased at the lesion sites (infiltrated cell clusters). Fibronectin was progressively increased in MOG EAE models over time, where MOG EAE 40 showed the highest fibronectin accumulation (Figure 37). In PLP EAE models, fibronectin was highly increased in both PLP EAE 15 and PLP EAE 40, and showed no difference over time (Figure 38).

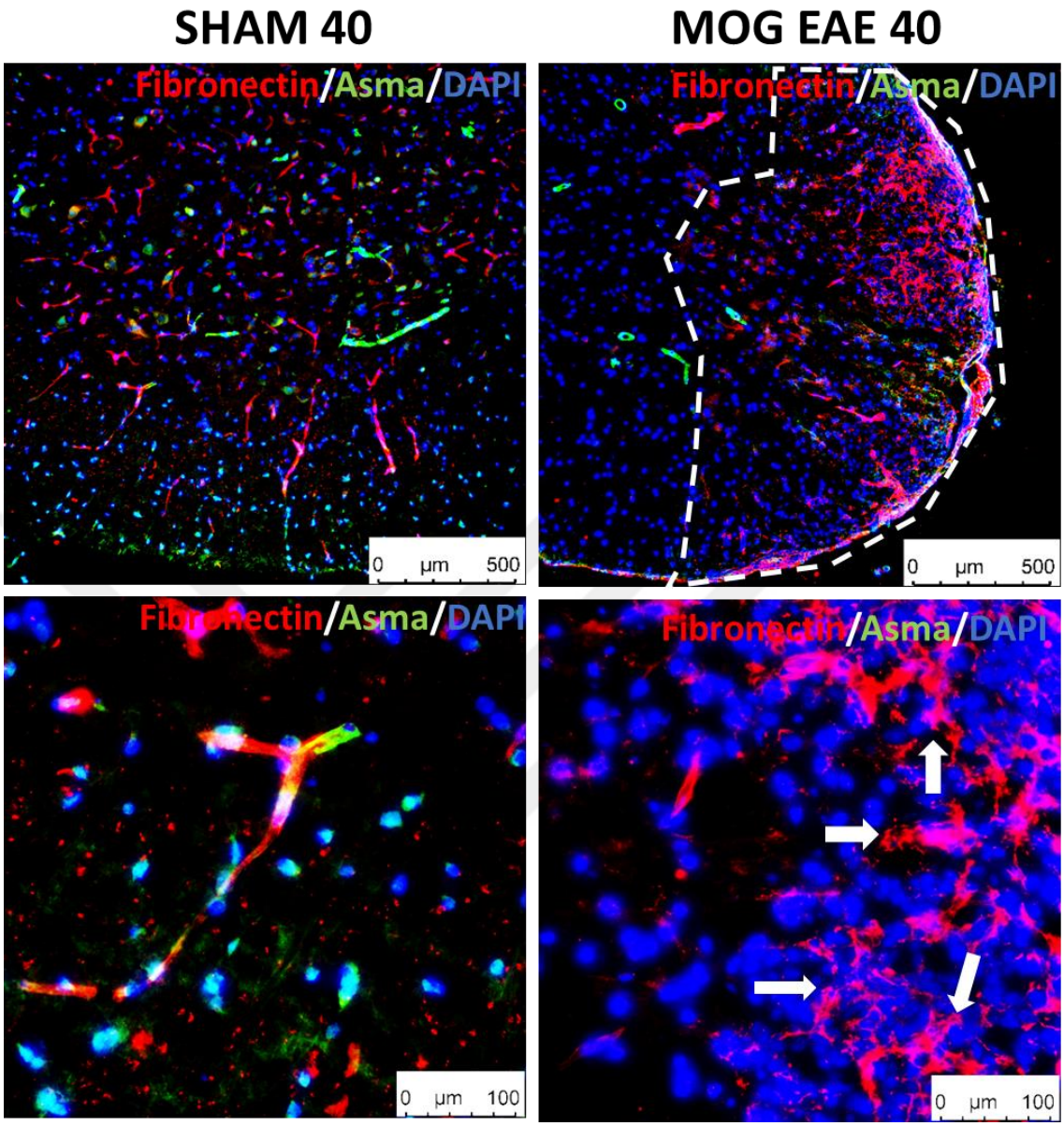

Figure 37: Fluorescence images of spinal cord sections obtained as a result of fibronectin and αSMA staining of SHAM 40 and MOG EAE 40 groups. Dashed areas represent affected areas with lesions. Fibronectin is found concentrated in the lesion regions, however also shows ruptured endothelium (white arrows). The scale bars represent: upper panel 500 µm and lower panel 100 µm.

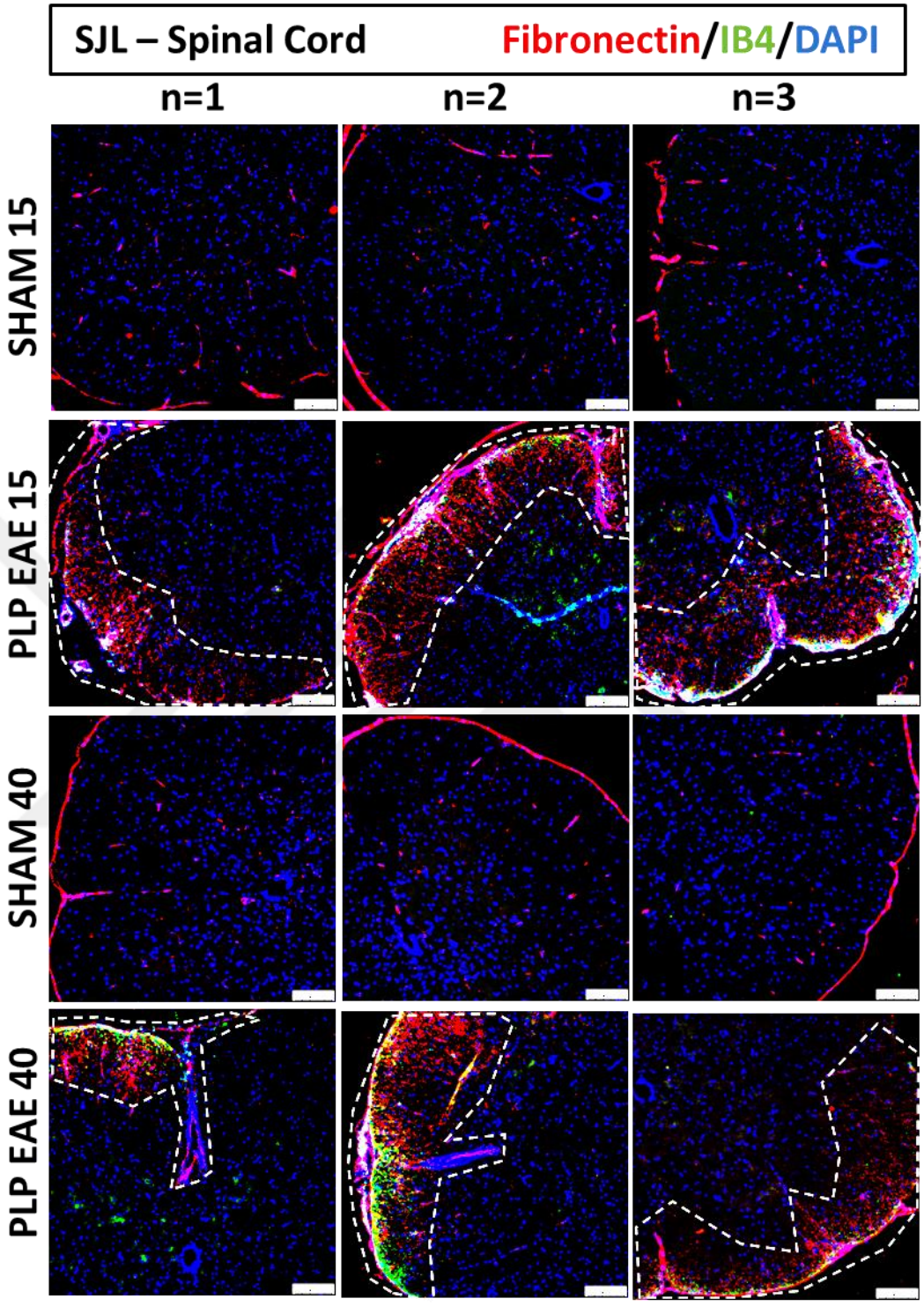

Figure 38: Spinal cord sections of PLP groups stained for fibronectin (red) and merged with IB4 (green) and DAPI (blue). Dashed areas represent affected areas with lesions. Three different spinal cord sections are shown for each group. The scale bars represent 250 µm.

Collagen I staining showed increase in both EAE models (Figure 39 and Figure 40). Compared to the corresponding SHAM groups (Figure 39), in MOG EAE, Collagen I increase was seen progressive over time, whereas the PLP EAE model first occurred with higher Collagen I in the early stage and decreased at the later stage. When MOG EAE 40 was assessed from a closer look (Figure 40), it was observed that Collagen I was appearing throughout the lesion site as ruptured vessels and most possibly ECM in the perimeter.

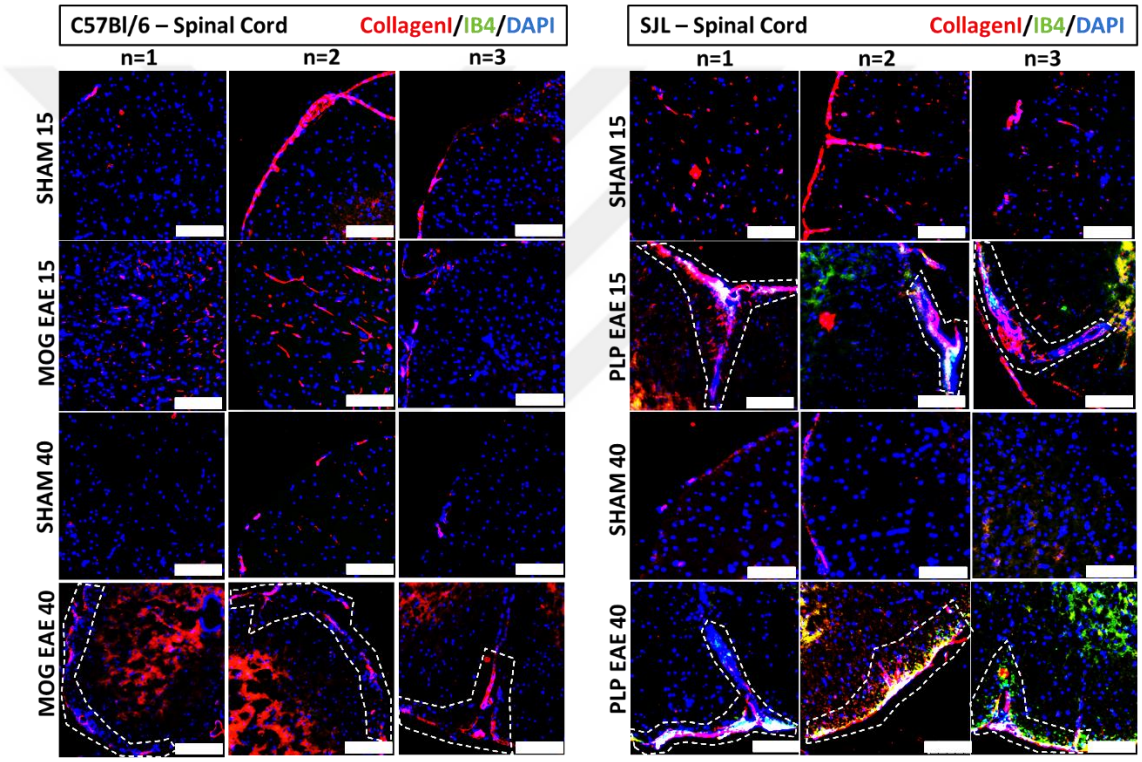

Figure 39: Spinal cord sections of MOG and PLP groups stained for Collagen I (red) and merged with IB4 (green) and DAPI (blue). Dashed areas represent affected areas with increased Collagen I. Three different spinal cord sections are shown for each group. The scale bars represent 250 µm.

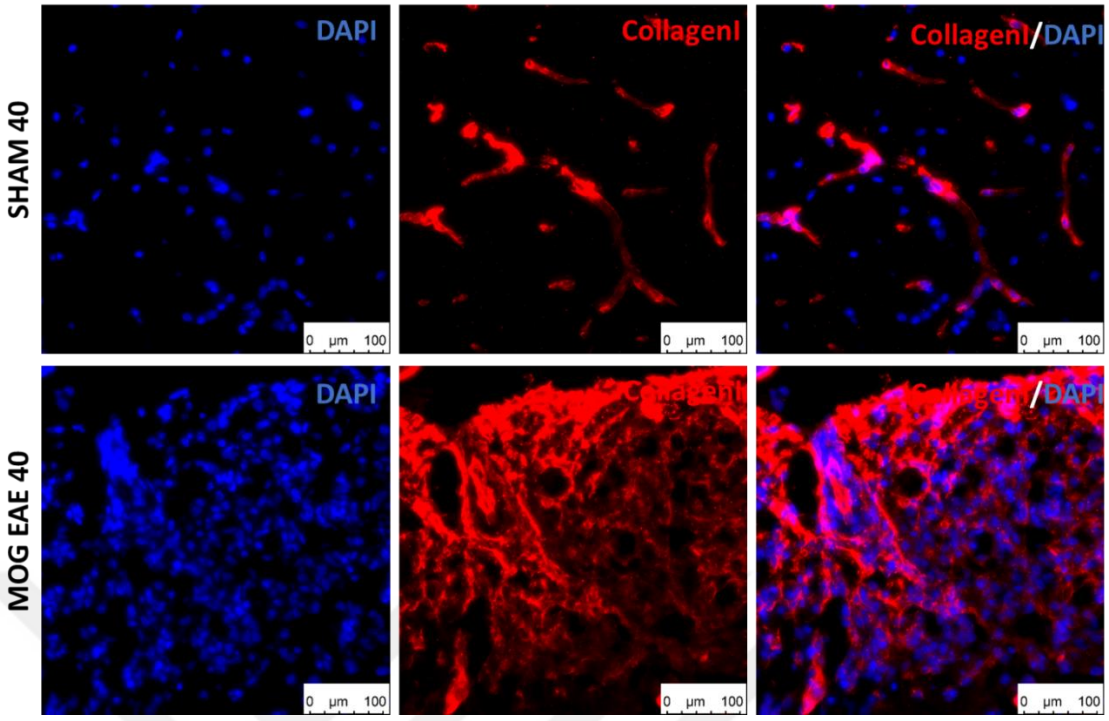

Figure 40: Fluorescence images of spinal cord sections obtained as a result of Collagen I and DAPI staining of SHAM 40 and MOG EAE 40 groups. Collagen I is found concentrated in the lesion regions. Note that the vascular bed is no longer intact in the MOG EAE 40 group and that Collagen I is found both in the ruptured vascular structures as well as throughout the lesion. The scale bars represent 100 µm.

Type IV collagen is required for the fibrotic response occurring in brain injury (76). We further assessed Collagen IV in both EAE models, and it was revealed that compared to Collagen I, Collagen IV is more present in the spinal cord tissue of SHAM groups (Figure 41-44). When EAE models were investigated, MOG EAE 15 showed small ruptured vessels along the pia mater in the white matter (Figure 41 and Figure 42). This appearance increased over time and in the late stage Collagen IV was also found scattered throughout the white matter within and around the lesions.

PLP EAE models showed both (early and late stage) similar increased Collagen IV throughout the spinal cord tissue and most intense accumulated in the vasculature structures at the lesion sites (Figure 41 and Figure 43). In particular, compared to SHAM groups, the increased vascular structures (Collagen IV+) and their increased thickness were noteworthy in PLP EAE model (Figure 43 and Figure 44). This was in line with the appearance of PDGFRβ+ pericytes, which may indicate that these PDGFRβ+ pericytes may be the Collagen IV producing cells at the vascular lesion regions. Furthermore, increased IB4 was observed in the perimeter of both Collagen I and IV in both PLP EAE models (Figure 41).

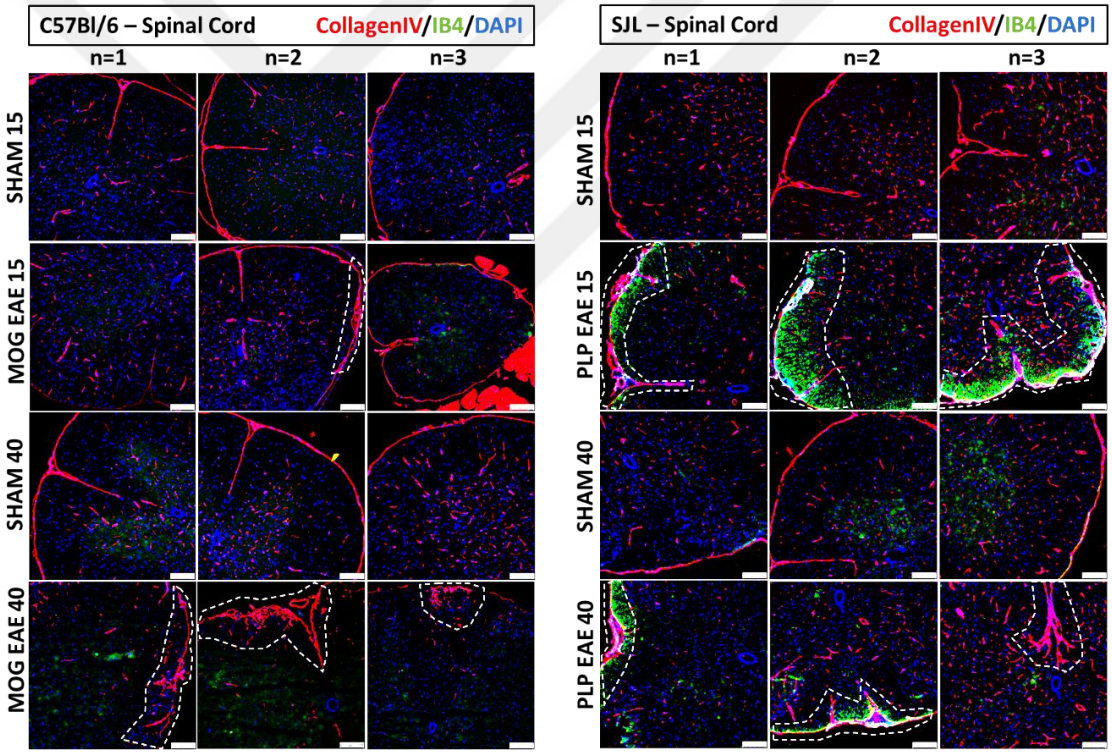

Figure 41: Spinal cord sections of MOG and PLP groups stained for Collagen IV (red) and merged with IB4 (green) and DAPI (blue). Dashed areas represent affected areas with increased Collagen IV. Three different spinal cord sections are shown for each group. The scale bars represent 250 µm.

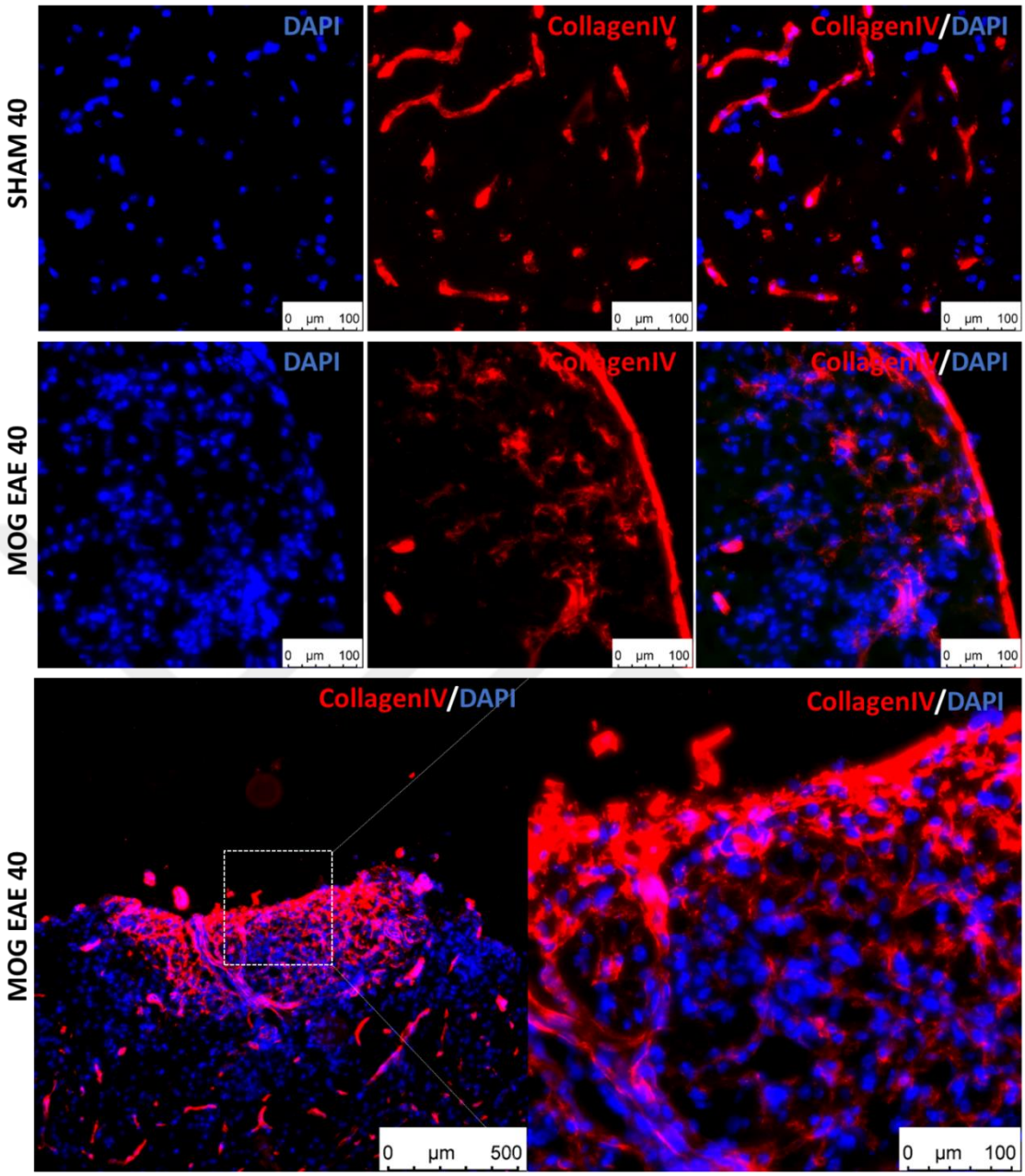

Figure 42: Fluorescence images of spinal cord sections obtained as a result of Collagen IV and DAPI staining of SHAM 40 and MOG EAE 40 groups. Collagen IV is found concentrated in the lesion regions. Note that the vascular bed is no longer intact in the MOG EAE 40 group and that Collagen IV is found both in the ruptured vascular structures as well as throughout the lesion. The scale bars represent: upper and middle panel 100 µm, lower panel 500 µm.

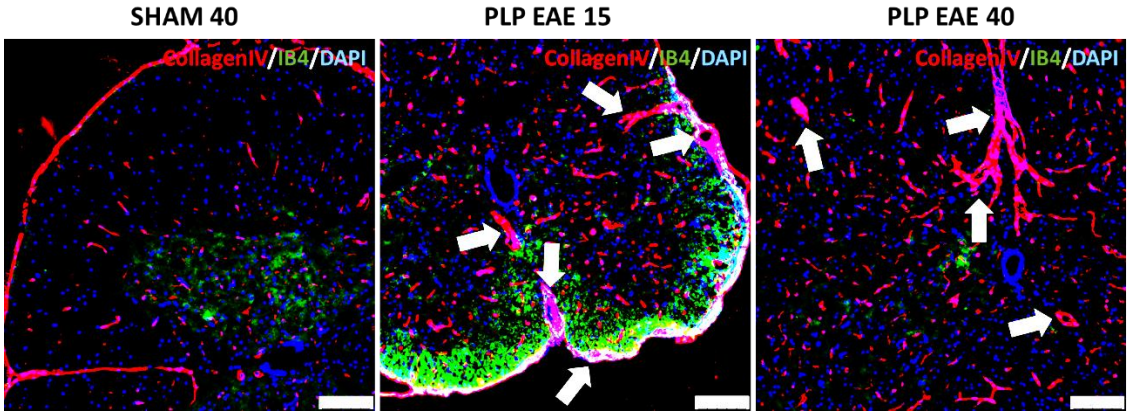

Figure 43: Fluorescence images of spinal cord sections obtained as a result of Collagen IV and DAPI staining of SHAM 40 and PLP EAE 14 and PLP EAE 40 groups. Collagen IV is found concentrated in the vascular structures. Note that the collagen is increased around the vasculature throughout the whole spinal cord tissue in PLP EAE 15 and 40 with especially being accumulated at cell infiltrating areas (white arrows). The scale bars represent 250 μm.

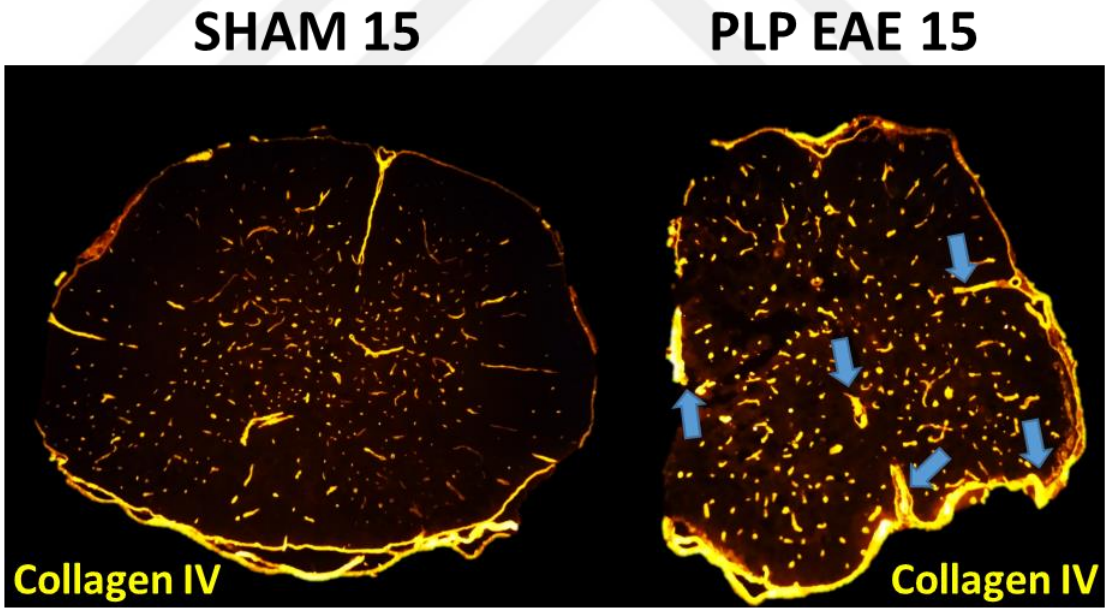

Figure 44: Collagen IV (Yellow) staining in spinal cord sections of SHAM 15 and PLP EAE 15 groups. Pictures are obtained with a regular photo camera capturing from the ocular lens while the sample was illuminated with fluorescent light. Of note is that the vasculature throughout the tissue in PLP EAE 15 shows thicker Collagen IV staining compared to SHAM (blue arrows).

Lysyl oxidase (LOX) family members are responsible for enzymatic enhancement of collagen crosslinking and therefore cause ECM stiffness (77). Mesenchymal cells dominantly express LOXL1 subtype, and LOXL2 is mainly produced by endothelial cells and fibroblasts. Pericytes express all LOX family members, but most dominantly they express LOXL3 (78).

In a spinal cord section of PLP EAE 40, LOXL2 and 3 were stained and the results showed that both LOXL2 and LOXL3 are present at the lesion sites (Figure 45). Especially LOXL3 was highly increased around the cell clusters infiltrated in the vessel structure along the pia mater. Note that LOXL2 showed overlapping with IB4 indicating endothelial cells, while LOXL3 did not show overlapping with IB4 and showed a similar trend as PDGFRβ+ pericytes.

Nestin is a marker that marks newly formed cells. According to literature, PDGFRβ+ cells also positive for Nestin+ are involved in fibrosis (79, 80). However their role in CNS injury remains controversial. We analyzed in this study whether Nestin+ cells are involved in EAE and correlated its presence with PDGFRβ and NG2 location in the spinal cord sections.

Both MOG and PLP-induced EAE models showed an increase in the number of Nestin+ cells over time (Figure 46). This increase is especially present close to the pia mater where inflammation is intense. In both MOG and PLP model Nestin increases progressively between early and late stage EAE disease. In PLP EAE 15, it was remarkable that Nestin+ around the endothelial walls was in line with PDGFRβ staining. In the late stage, PLP EAE 40, Nestin+ areas extended to a larger part in the white matter.

Nestin+ cells could include newly formed pericytes, activated pericytes and/or derived cells, and/or newly formed endothelium (neovascularization) or neural progenitor cells.

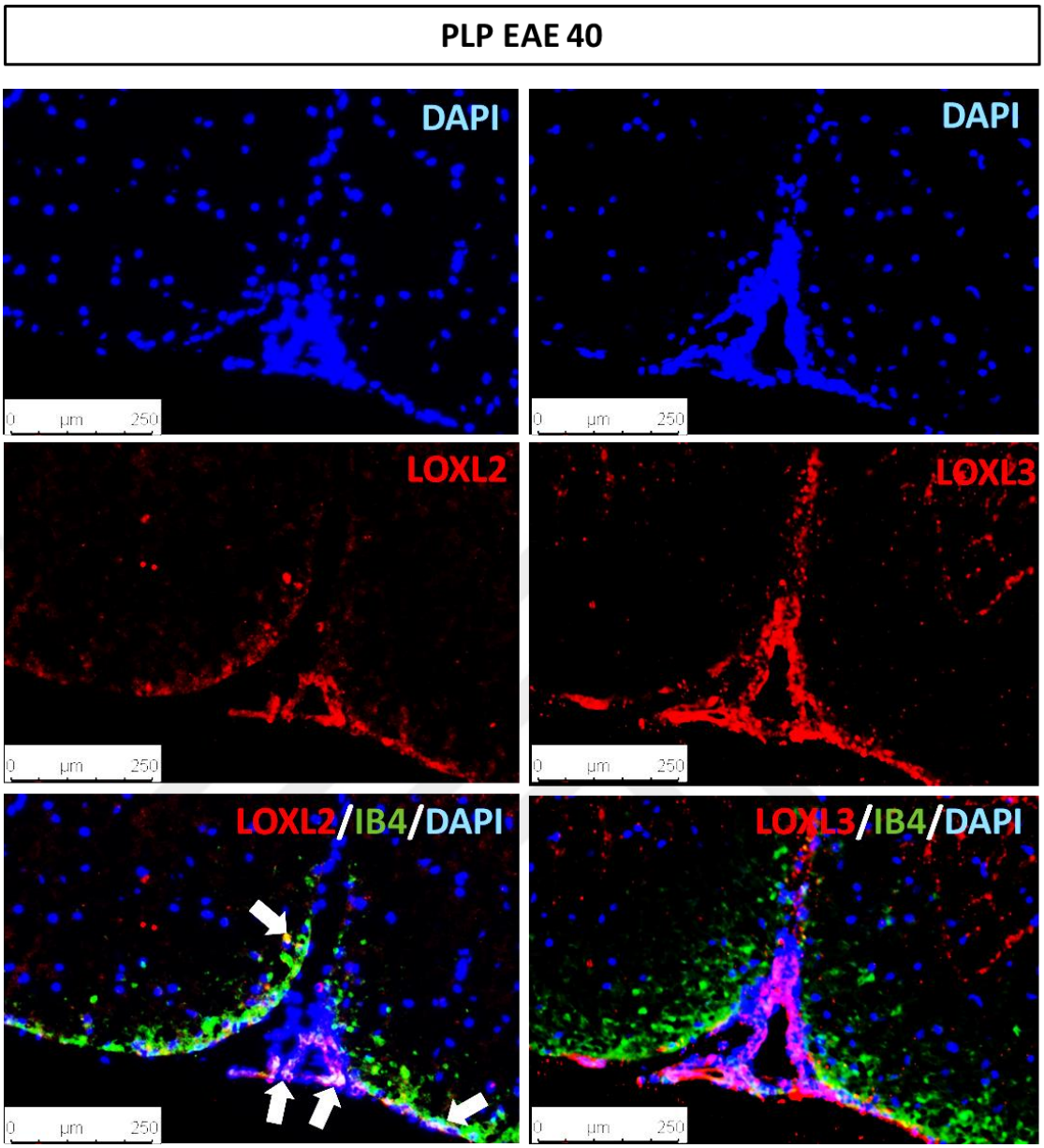

Figure 45: Fluorescence images of spinal cord sections of PLP EAE 40 group stained with LOXL2 or LOXL3 and merged with IB4 and DAPI. White arrows show overlapping between LOXL2 and IB4, indicating endothelial cells. The scale bars represent 250 µm.

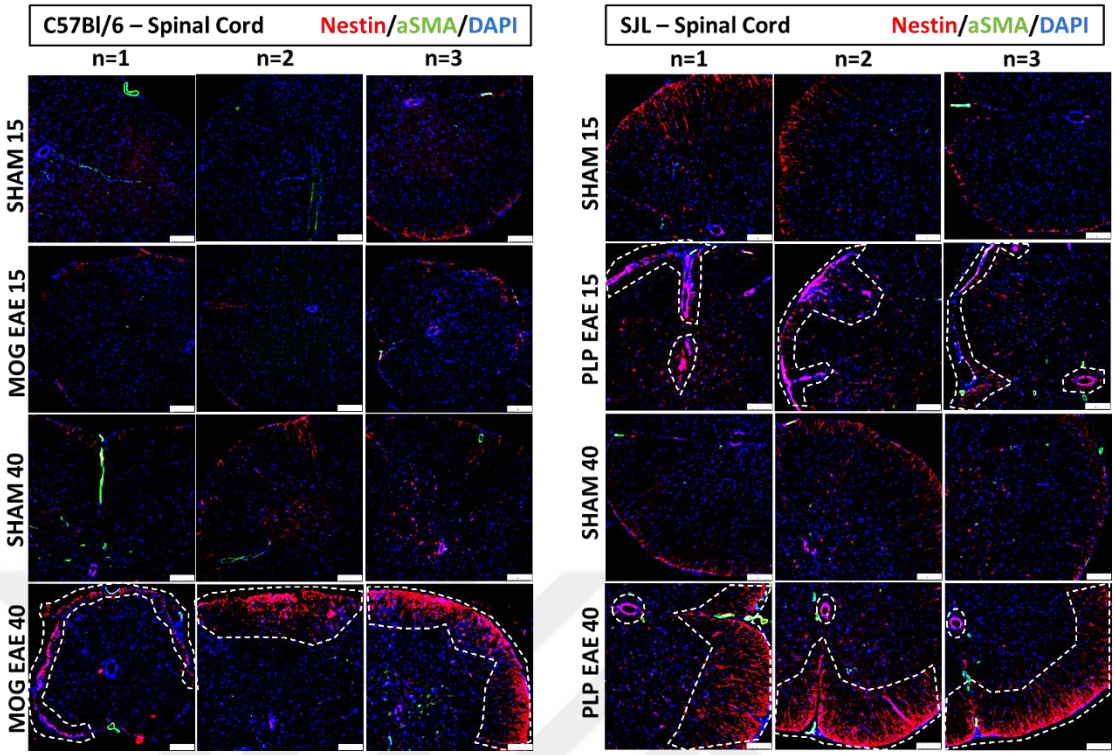

Figure 46: Spinal cord sections of MOG and PLP groups stained for newly formed cells with Nestin (red) and merged with αSMA (green) and DAPI (blue). Dashed areas show increased Nestin. Three different spinal cord sections are shown for each group. The scale bars represent 250 µm.

TGFB is a growth hormone that is chemotactic for white blood cells and fibroblasts, Normally, TGFB inhibits the proliferation of epithelial cells but can be a promoter of fibroplasia and angiogenesis as well. TGFB can promote differentiation of fibroblasts into myofibrolasts leading to increased collagen production and therefore presents a profibrotic function.

Assessment of TGFB1 staining (Figure 47) in MOG EAE model revealed that TGFB1 was present at both early and late stage MOG EAE. Moreover, the expression of TGFB1 was primarily found along the pia mater and in the perimeter of the lesion sites.

PLP EAE 15 showed an intense increase in TGFB1 compared to its corresponding SHAM group. The overall TGFB1+ areas decreased over time in PLP EAE 40 compared to PLP EAE 15, but still remarkably increased compared to SHAM 40. The TGFB1+ areas included mostly the perimeter of the lesion sites, along the pia mater, and in the grey matter. In PLP EAE 40, TGFB1 in the gray matter was decreased. It was also observed that there was minimal overlapping between PDGFRβ and TGFB1 throughout the spinal cord tissue. The latter suggests that pericytes are most possibly not the main source of increased TGFB1 in EAE. With regard to IB4, GFAP and IBA1 staining it is most possible that TGFB1 is produced by endothelial cells, activated astrocytes and microglia.

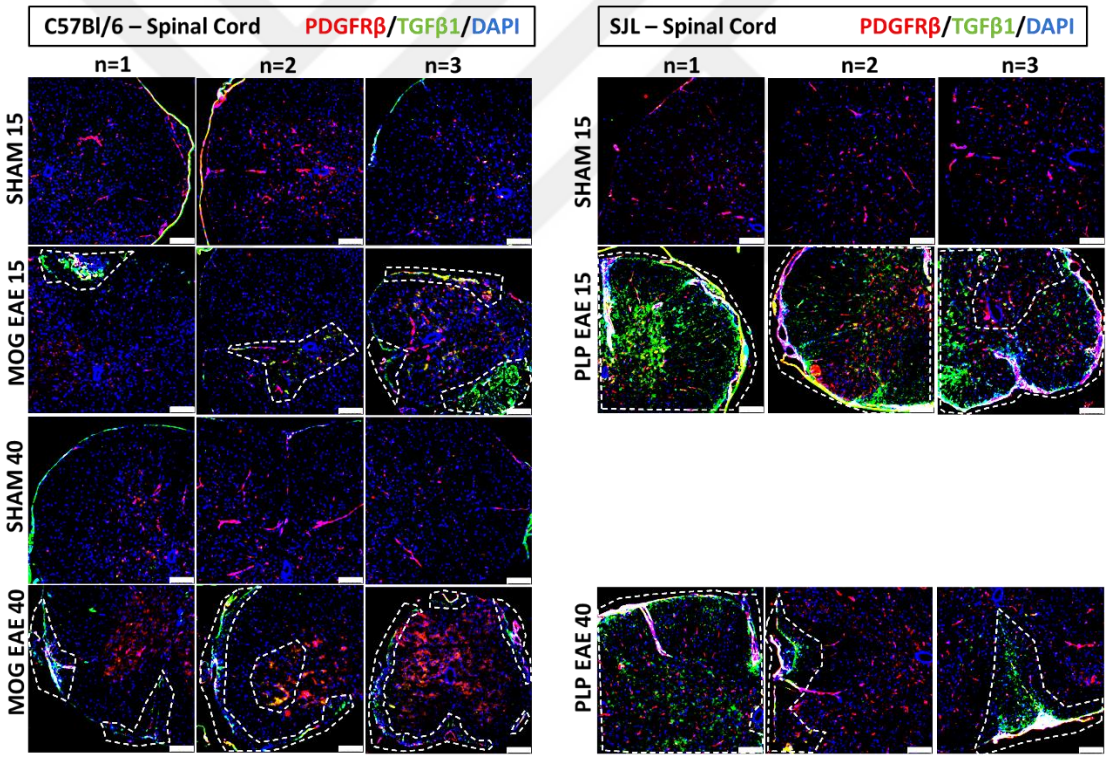

Figure 47: Spinal cord sections of MOG and PLP groups stained for PDGFRβ (red) and merged with TGFβ1 (green) and DAPI (blue). Dashed areas show increased TGFβ1. Three different spinal cord sections are shown for each group. The scale bars represent 250 µm.

3.9 Increased Pericyte Proliferation upon Exposure to MS Serum

In this essay, we first optimized the cell seeding densities (20000 cells/well) (Figure 48) for the special designed xCELLigence E-plates and choose an optimal serum concentration (10%) based on healthy human serum (Figure 49). Next we incubated HBVP with healthy human serum and MS patient serum, and used culture medium as control (Figure 50).

Both healthy and MS serum were remarkably increasing the proliferation rate of pericytes compared to culture medium only, which is expected due to many growth factors in serum (Figure 50). We quantified the proliferation rate by calculating the slope between 40 and 80 hours which was 0.022±0.002 per hour (mean±SD for n=2) for MS serum and 0.014±0.001 per hour (mean±SD for n=2) for healthy serum. According to the data, it was revealed that pericytes when exposed to MS serum had a tendency to significantly (t-test p value: 0.032) proliferate faster compared to healthy serum.

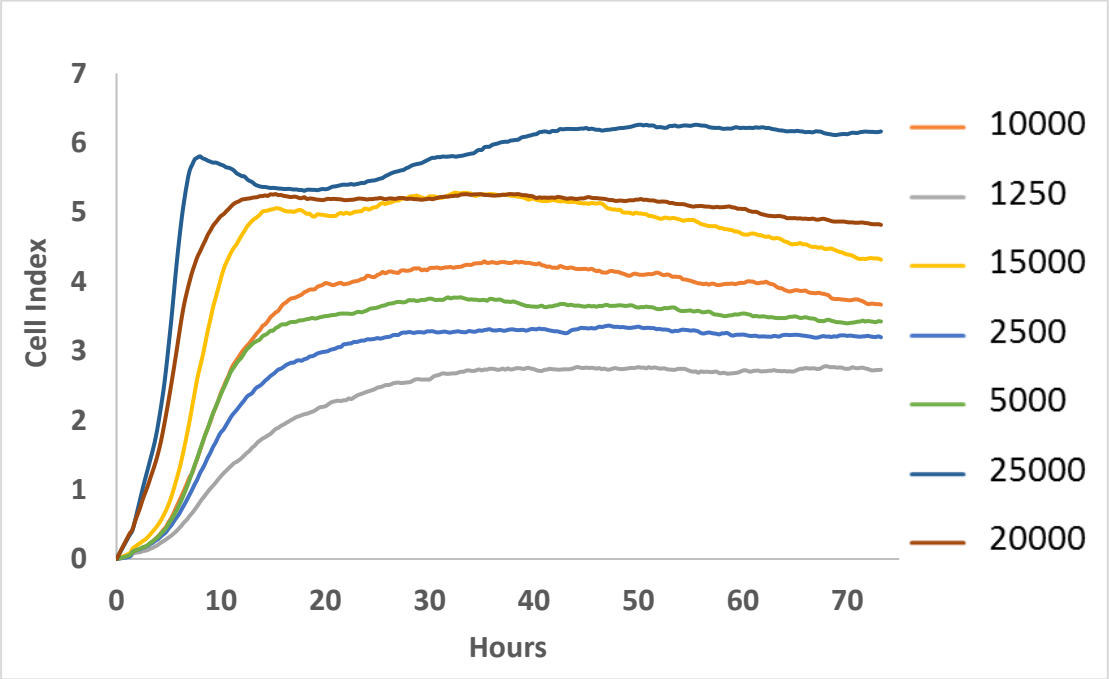

Figure 48: Cell proliferation of HBVP cell culture was measured by xCELLigence device by seeding at different cell densities (ranging between 1250-25000 cells/well). Each line was determined by the average of duplicate wells.

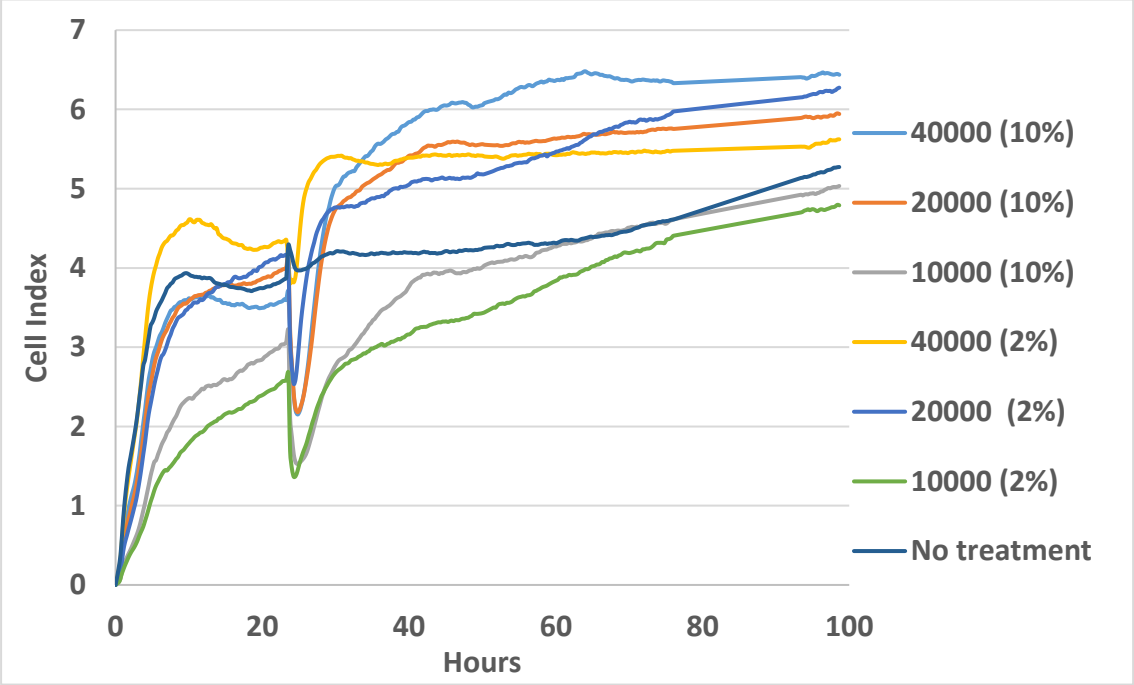

Figure 49: Cell proliferation of three different cell densities (40000, 20000 or 10000 cells/well) of HBVPs treated with two different serum concentrations (10% or 2%) was measured by xCELLligence device. Each line was determined by the average of duplicate wells.

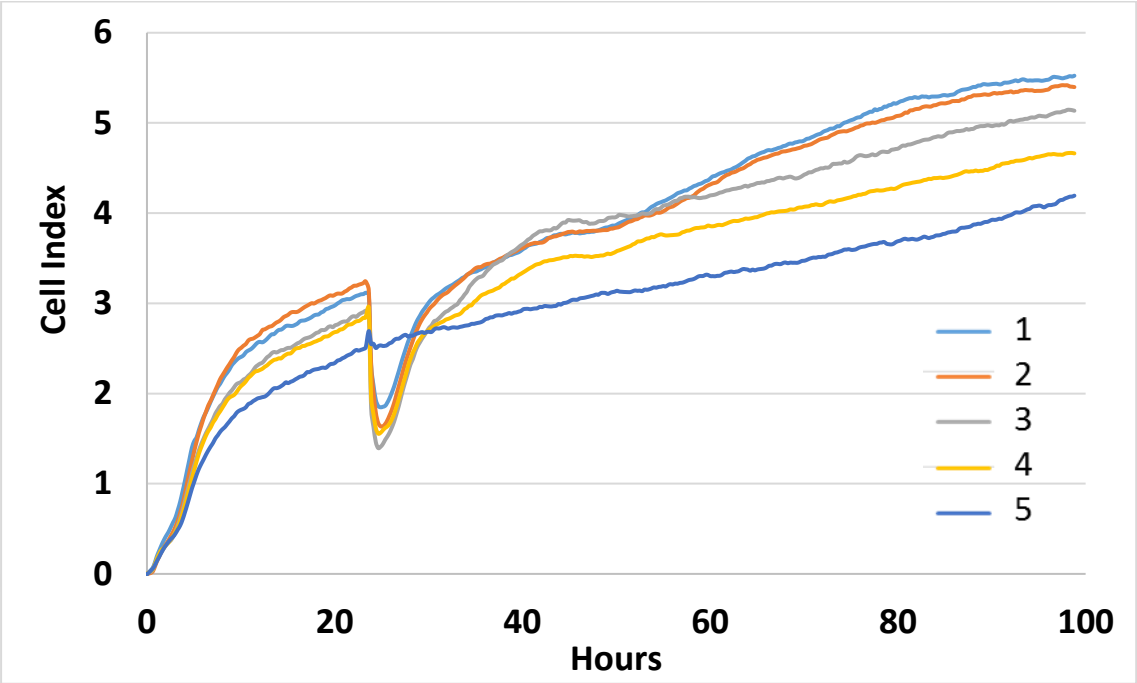

Figure 50: Cell proliferation was measured by xCELLigence device after exposure to 10% healthy human serum or MS patient serum. Each line was determined as the average of triplicate wells. Line 1-2 represent MS serum from two patients, line 3-4 present serum from 2 healthy individuals and line 5 is only culture medium.

3.10 Fibrogenic Pericytes

From our EAE *in vivo* data we hypothesized that PDGFRβ pericytes might be involved in fibrosis producing collagen. Hereupon, *in vitro* pericytes were exposed to MS patient serum and healthy human serum in order to assess collagen production. Results (Figure 51) indicated that compared to normal culture conditions pericytes produce increased collagen I and IV upon exposure to any serum (healthy or MS), however there was an intense difference between healthy and MS serum, Collagen I and IV were highly increased. Laminin on the other hand (Figure 52) did not show any increase upon MS serum exposure (there is an equal presence of intracellular laminin in all groups).

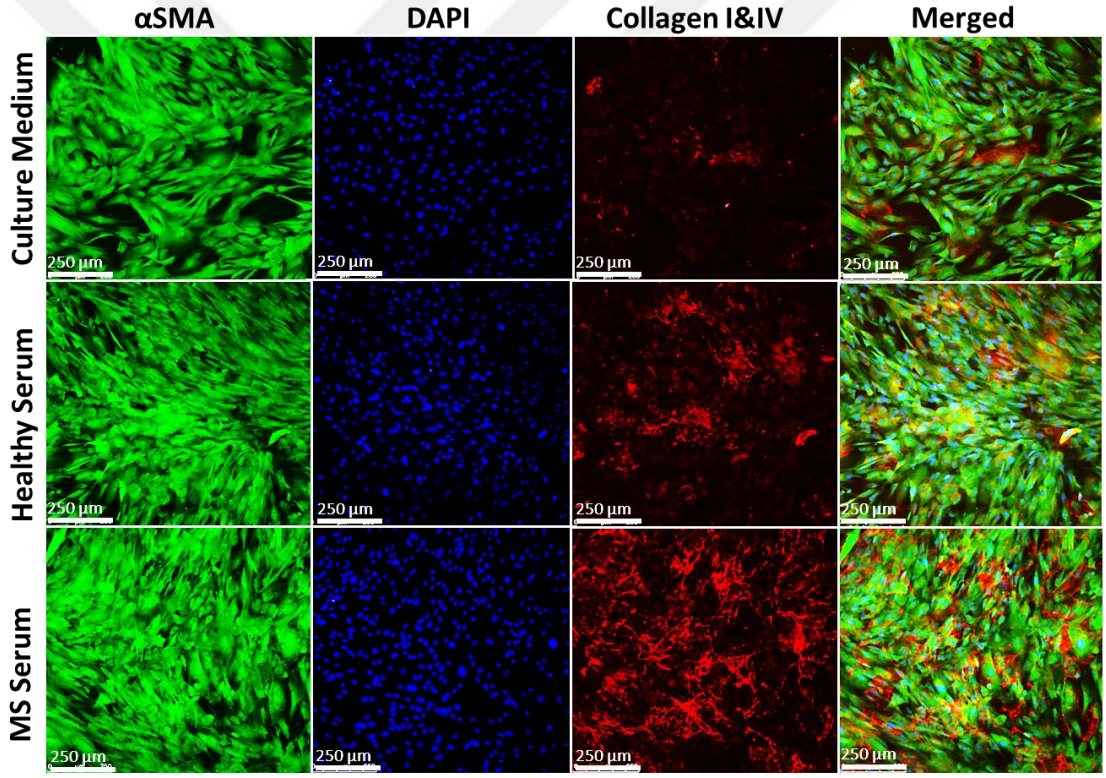

Figure 51: *In vitro* cultured HBVP cells exposed to either culture medium (control), healthy human serum or MS patient serum (10%, v/v) in triplicate for 24 hours. Cells were stained for Collagen I & IV and merged with DAPI for cell nucleus. Increased Collagen deposits by pericytes were observed after exposure to MS serum. Scale bars represent 250 µm.

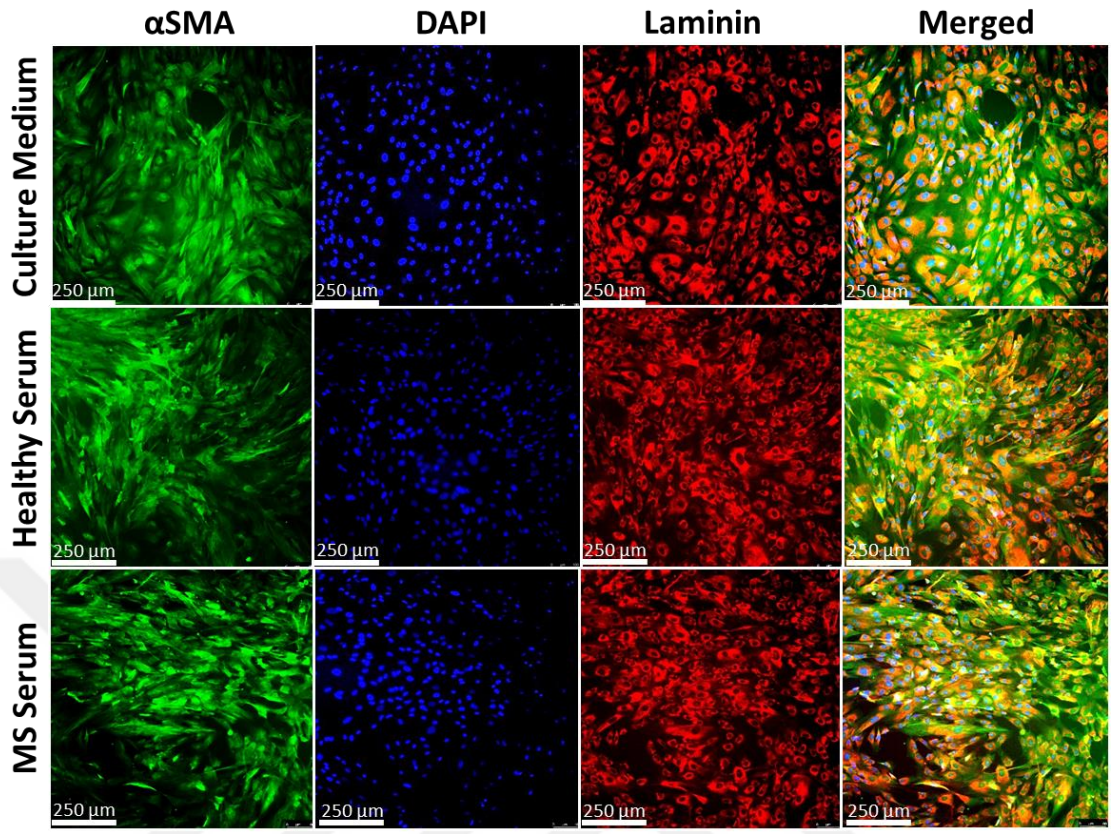

Figure 52: *In vitro* cultured HBVP cells exposed to either culture medium (control), healthy human serum or MS patient serum (10%, v/v) in triplicate for 24 hours. Cells were stained for Laminin and merged with DAPI for cell nucleus. No change in Laminin expression by pericytes were observed after exposure to MS serum. Scale bars represent 250 µm.

Pericytes *in vitro* are generally believed to be activated pericytes and therefore profibrogenic. Although expressing intrinsic TGFB1 in culture (Figure 53), pericytes produced fibronectin deposit after exposure to external TFGB1 (Figure 54). The latter increased over time, where compared to control cells an intense amount of fibronectin was produced.

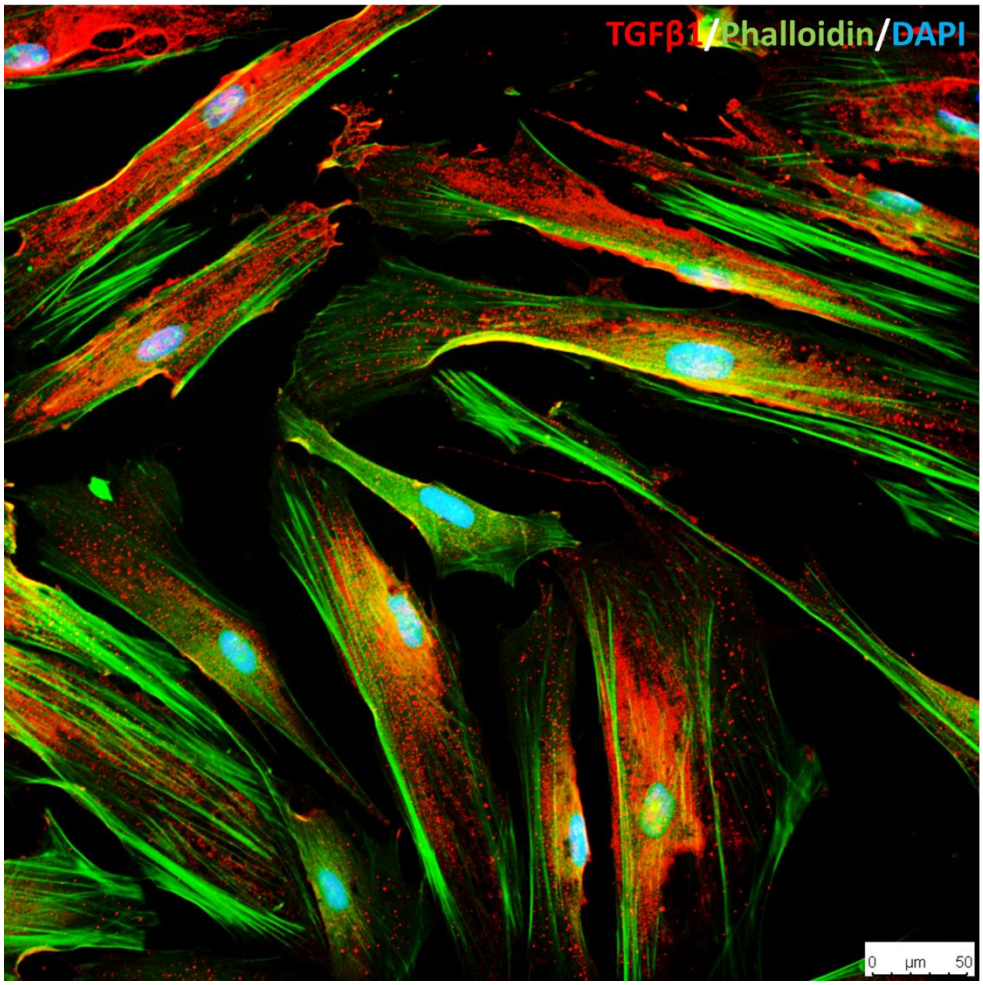

Figure 53: *In vitro* cultured HBVP in normal medium conditions stained for TGFB1 and Phalloidin and merged with DAPI. Scale bar represents 50 µm.

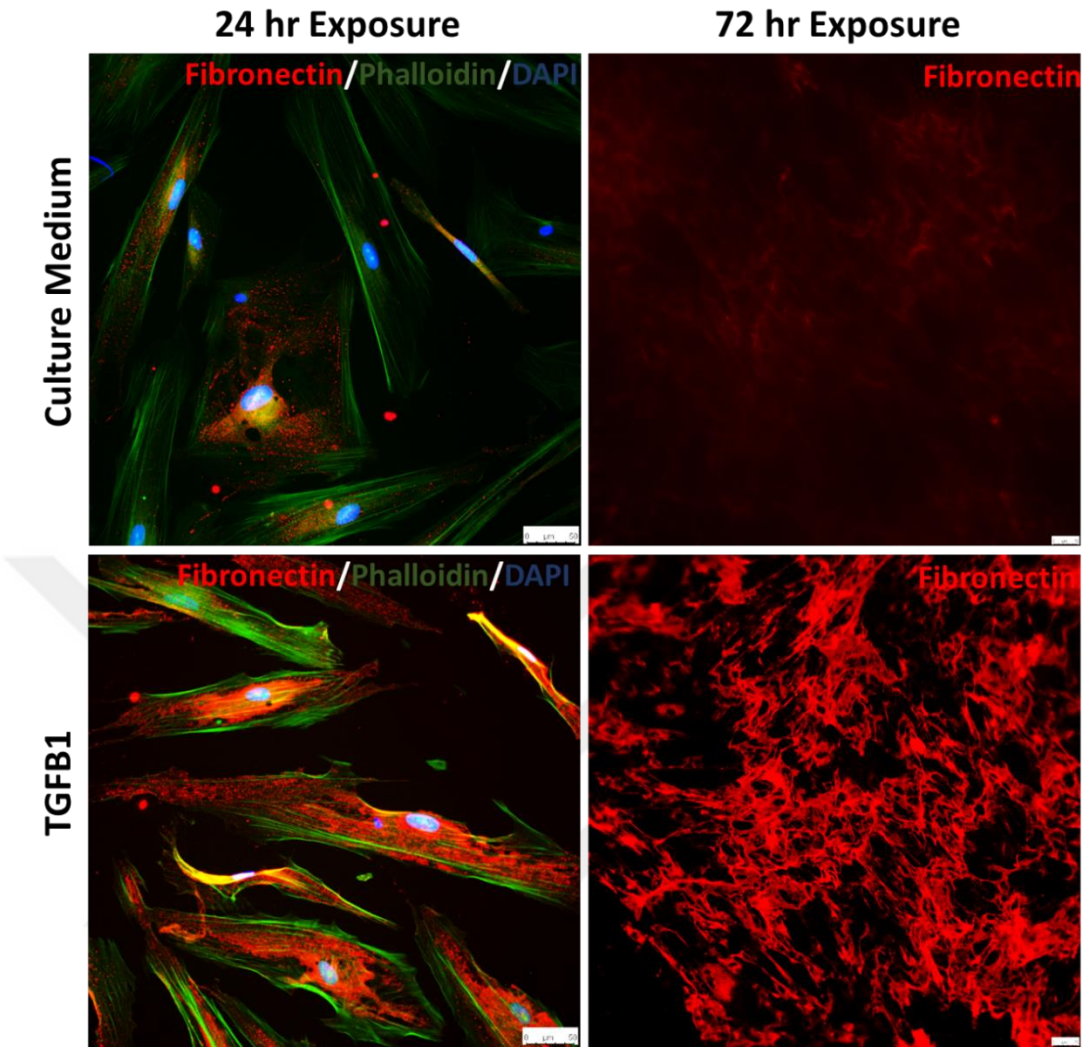

Figure 54: *In vitro* cultured HBVP cells exposed to TGFβ1 for 24 hours and 72 hours. Culture medium was used as control. Pericytes were stained with Phalloidin and Fibronectin and merged with DAPI for cell nucleus. A remarkable increase over time was seen for Fibronectin production in pericytes exposed to TGFβ1. Scale bars represent 50 µm.

Collagen I and IV were also produced upon TGFB1 exposure (Figure 55). Collagen IV was interestingly more produced in the same time window compared to Collagen I. This results was in line with our *in vivo* EAE models, were Collagen IV was more abundant in the CNS vasculature structures as well as in the EAE lesions. It is assumed that pericytes in EAE are producing mainly collagen IV due

to either exposure to EAE serum (leaking from the BBB) or to TGFB1 produced by surrounding endothelial cells, activated astrocytes of activated microglia. OF note, there were a few cells CC3 positive hence were activated for cell death after TGFB1 exposure.

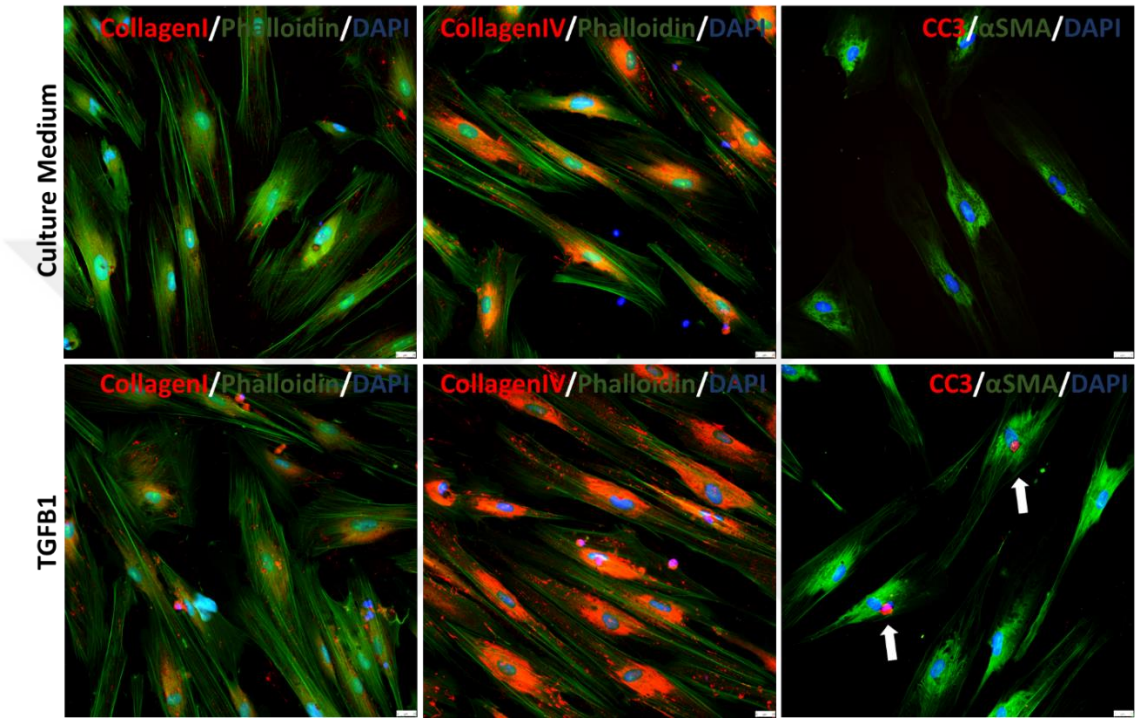

Figure 55: *In vitro* cultured HBVP cells exposed to TGFβ1 for 24 hours. Culture medium was used as control. Left and middle panel: Pericytes were stained with Phalloidin and Collagen I or Collagen IV and merged with DAPI for cell nucleus. Right panel: Pericytes were stained with αSMA and CC3 (apoptosis marker) and merged with DAPI for cell nucleus. Left and middle panel: TGFB1 exposure led to a lightly increase in Collagen I and a higher increase in Collagen IV by pericytes. Right panel: TGFB1 exposure was also inducing apoptosis (white arrows) in pericytes. Scale bars represent 25 µm.

4 Discussion

In this project we aimed at investigating pericytes in the pathophysiology of MS indirectly in two EAE *in vivo* models and compared results with *in vitro* pericyte data. For this purpose, all features of MS/EAE (*in vivo* paralysis, BBB leakage, inflammation, demyelination, axonal loss and gliosis) have been analyzed in brain and spinal cord sections in order to integrate and interpret pericyte data as correctly as possible.

First of all, clinical EAE score and weight change have been monitored to assess clinical EAE outcome in both MOG and PLP EAE models. Achieving statistical significance in terms of weight change and EAE scores in EAE 40 groups, and even a tendency to increase and decrease in the PLP EAE group (a clinical representation of relapsing), all indicated successful model development for both MOG EAE model and the PLP EAE model. According to our results, the first change in the observation studies was seen in neurological EAE scoring. This suggests that the neurological examination score is the most sensitive clinical tracking system in the EAE model. The clinical observations started at the 6th day in MOG EAE 40 model and on the 8th day in PLP EAE 40 model, which is consistent with the literature (81, 82). On the other hand, based on clinical data the success rate of MOG EAE induction in our laboratory was 60%, PLP EAE induction was recorded as 100%.

Next we assessed BBB leakage and found that BBB leakage patterns between MOG EAE and PLP EAE were in line with the clinical EAE scores and weight changes. Since these clinical data were more severe for PLP EAE model, a more increased BBB leakage was as expected. Furthermore, BBB leakage in the brain was observed mainly along the pia mater, and in the brain around ventricles and in the white matter of the cerebellum (Figure 14). In normal conditions, ventricular zones and pia mater regions have the weakest BBB properties when compared to capillaries. Therefore, in EAE models BBB leakage around these areas is expected. Also, when PLP and MOG EAE models were compared in terms of early stage and late stage, MOG EAE showed a progressive BBB

leakage (covering larger area over time) whereas PLP EAE showed a decrease in BBB leaked area over time. The latter is most possible due to the relapsing remitting characteristic of the PLP model.

Inflammation was assessed with H&E and by lymphocyte and macrophage staining and it was revealed that inflammatory cells were accumulated in cell clusters close to the pia mater in the spinal cord white matter, next to ventricular zones in the brain and in the white mater in the cerebellum.

Another key feature of MS/EAE is demyelination. This phenomenon was shown with LFB staining and with MBP staining. Both methods, showed notable myelin loss in the white matter areas of spinal cord and cerebellum. MOG EAE model showed a progressive trend in myelin loss over time, however, PLP model also showed signs of remyelination in the late stage.

Gliosis was shown in EAE with GFAP+ activated astrocytes/microglial cells (83). GFAP positive projecting astrocytes were progressively increased over time along the outer areas of the white matter close to the pia mater in both models, however were minimal merged with cell accumulations/lesions. They mostly formed a perimeter around these areas. On the other hand, astrocytes were increased in the gray matter of spinal cord sections and in the white matter areas in the cerebellum. Increased astrocytes in the gray matter were seen only in PLP EAE model. Additionally, axonal loss was observed as decreased MAP2 stained areas, especially in spinal cord sections of MOG EAE 40 model (Figure 21).

Then, pericytes were analyzed with several markers in brain and spinal cord sections of both EAE models. Generally when MOG and PLP models were compared, PLP model possessed lesions which were more stable and PDGFRB+ pericytes were accumulated around the vascular structure, whereas in MOG EAE model these lesions sites were scattered and PDGFRB+ pericytes were scattered appearing.

In the SHAM group, PDGFRβ+ pericytes were found co-localized around the vascular bed, wrapping the endothelium (Figure 31). This pattern was uniformly observed in the spinal cord tissue and in line with literature (84). However, in the MOG EAE 15 group, this order was deteriorated, whereas in the MOG EAE 40 group, PDGFRβ+ pericytes were increased and scattered around endothelium within and around the lesion sites. Particularly, pericytes separated from the endothelium were observed in the lesioned areas with increased cell infiltrations. In MOG EAE 40 group, there was a remarkable increase in αSMA cells throughout the spinal cord tissue. NG2, marking pericytes, showed a similar trend as PDGFRβ+ cells. There was simultaneously also increased and scattered IB4 staining at lesion sites, indicating either neovascularization or ruptured vessel residues or activated microglia. IBA1 staining for microglia revealed increased and accumulated microglia at lesion sites and gray matter of spinal cord sections.

Pericytes are cells of mesenchymal origin, normally contractile cells found in the walls of the microvessels, but also in close contact with the underlying endothelium. These cells play an important role in the integrity of the microvascular system. According to the literature, injured pericytes that break off from endothelial cells migrate to the interstitium. Pericytes leaving the endothelium lead to decreased pericyte coverage on the endothelium and weakening of the vessel wall leads to disruption of its integrity (85). Under normal conditions, the wrapping pattern is dominant but in disturbed conditions pericytes can detach and migrate with the formation of finger-like projections followed by retraction of projections (36).

According to our immunofluorescence studies with *in vivo* data from especially PLP EAE model, we hypothesized that pericytes might be triggered by factors leaking from the BBB and proliferate along the vessels thickening and wrapping up the infiltrating bulk of cells. Therefore we exposed pericytes in culture to MS and healthy human serum and found that pericytes proliferate faster upon contact with MS patient serum. The latter indicates, that after BBB leakage, or

even before if pericytes senses or detects (yet unknown) factors from the luminal side of the vessel, it may respond by proliferating and thickening the vessel wall. However, this mechanism would be valid for PLP EAE. In case of MOG EAE we found scattered pericytes distributed over the lesion areas, and no wall thickening was found, in contrary pericytes were detached from the vessels. These findings however indicate that there are possible different mechanisms involved in the occurrence and progression of both MOG and PLP models *in vivo*. Based on the pathway of these mechanisms, pericytes will adjust themselves in either leaving the vessel, or proliferating and thickening the vessel. The mechanisms on how pericytes mediate vessel stability in injured conditions remains unclear (86). However, to underline the necessity of pericytes, in a study of depleted pericytes in PDGFRβ−/− animals it was found that newly formed vessels rupture and collapse (45).

Changes in pericytes were detected in our *in vivo* EAE model and together with the obtained *in vitro* data of proliferative behavior of pericytes upon MS serum exposure, we hypothesized that immune events occurring in the blood are triggering pericytes to proliferate and are most probably causing pericytes to produce ECM at the lesion sites.

According to literature, TGFβ1 was found to induce fibronectin and collagen deposits by epithelial and mesenchymal cells *in vitro* (87). TGFβ1 is able to promote collagen accumulation and a fibrotic tissue response (69) but also induces pericyte-myofibroblast trans-differentiation and causes fibrosis (68). In addition, it is known that the interaction of pericytes with the endothelium promote TGFβ1 production which subsequently stimulates perivascular cell proliferation (88).

We next tested whether pericytes are releasing ECM upon exposure to MS serum and TGFB1 *in vitro*. After exposing pericytes to MS serum, it was found that pericytes *in vitro* are releasing Collagen I, Collagen IV and Fibronectin in the same trends as in MOG and PLP EAE *in vivo* models. In line with other studies, increased PDGFRβ+ cells were found in the *in vivo* EAE lesions, where

simultaneously also Collagen is accumulated, suggesting a possible contribution of these cells to fibrosis in EAE (89).

Pericytes did however produce more Collagen IV than Collagen I in EAE models *in vivo* and upon exposing to TGFB1 in cell culture experiments.

To assess which cell causes Collagen crosslinking/deposits in the EAE models, we next stained for LOXL2 and LOXL3. LOXL2 is more abundant in endothelial cells and fibroblasts, and LOXL3 in pericytes. We found that in lesion regions with infiltrated bulk of cells, LOXL3 was more abundant within the core, whereas LOXL2 was also present but in less amount. These LOXL2+ areas was remarkable colocalized with IB4, indicating endothelial cells.

To summarize, all MS/EAE features were shown in MOG and PLP EAE models. Although both models have the majority of these features in common, they distinguish in several factors indicating different mechanisms of EAE development are present. In addition to these key features, this study investigated the role of pericytes in this pathologic frame. Importantly, it was found that pericytes play a role in fibrosis and act different in both EAE models in terms of BBB involvement and disease progression.

5 Conclusion

In conclusion, it can be said that pericytes play a crucial role in the development of MS and that detachment of pericytes from the surrounding of the vessel has a negative effect on the disease progression such as presented in MOG EAE model which has a typical PPMS presentation. However, proliferating pericytes found around disturbed vessels may have a positive effect on sustaining the disease progression. By acting as a wall defensing the leaking BBB and thickening the barrier it may actually work literally as a band aid, also explaining the relapsing remitting form of PLP EAE model. All these data are observational and in fact insufficient to explain whether pericytes have a primary effect on the pathogenesis of the disease. In order to explore the underlying molecular mechanisms, pericytes should be investigated in detail in further studies for proteomics, transcriptomics and epigenetic changes in both EAE models. Pericytes contributing to fibrosis together with Collagen IV as a BBB wall amplifier may be explored as a therapeutic target to improve recovery after MS/EAE attacks.

Funding

This project was performed with the support and funding from the Scientific and Technological Research Council of Turkey (TUBITAK) with project numbers 116S552 and 216S627.

References

1. Frohman EM, Racke MK, Raine CS. Multiple Sclerosis — The Plaque and Its Pathogenesis. New England Journal of Medicine. 2006;354(9):942-55. PubMed PMID: 16510748.
2. Bennett JL, Stüve O. Update on Inflammation, Neurodegeneration, and Immunoregulation in Multiple Sclerosis: Therapeutic Implications. Clinical Neuropharmacology. 2009;32(3):121-32. PubMed PMID: 00002826-200905000-00001.
3. Ebers GC. Environmental factors and multiple sclerosis. The Lancet Neurology. 2008;7(3):268-77.
4. Ascherio A. Environmental factors in multiple sclerosis. Expert Review of Neurotherapeutics. 2013 2013/12/01;13(sup2):3-9.
5. 't Hart BA, Massacesi L. Clinical, Pathological, and Immunologic Aspects of the Multiple Sclerosis Model in Common Marmosets (Callithrix jacchus). Journal of Neuropathology & Experimental Neurology. 2009;68(4):341-55.
6. Traugott U, Reinherz E, Raine C. Multiple sclerosis: distribution of T cell subsets within active chronic lesions. Science. 1983;219(4582):308-10.
7. Hauser SL, Bhan AK, Gilles F, Kemp M, Kerr C, Weiner HL. Immunohistochemical analysis of the cellular infiltrate in multiple sclerosis lesions. Annals of Neurology. 1986;19(6):578-87.
8. Hohlfeld R, Wekerle H. Immunological update on multiple sclerosis. Current Opinion in Neurology. 2001;14(3):299-304. PubMed PMID: 00019052-200106000-00006.
9. Sospedra M, Martin R. IMMUNOLOGY OF MULTIPLE SCLEROSIS. Annual Review of Immunology. 2005;23(1):683-747. PubMed PMID: 15771584.
10. Madsen LS, Andersson EC, Jansson L, Krogsgaard M, Andersen CB, Engberg J, et al. A humanized model for multiple sclerosis using HLA-DR2 and a human T-cell receptor. Nature Genetics. 1999 1999/11/01;23(3):343-7.
11. Friese MA, Fugger L. Pathogenic CD8+ T cells in multiple sclerosis. Annals of Neurology. 2009;66(2):132-41.

12. Dhib-Jalbut S, Kufta CV, Flerlage M, Shimojo N, McFarland HF. Adult human glial cells can present target antigens to HLA-restricted cytotoxic T-cells. Journal of Neuroimmunology. 1990;29(1):203-11.
13. Dhib-jalbut S, Gogate N, Jiang H, Eisenberg H, Bergey G. Human microglia activate lymphoproliferative responses to recall viral antigens. Journal of Neuroimmunology. 1996;65(1):67-73.
14. Massa PT, ter Meulen V, Fontana A. Hyperinducibility of Ia antigen on astrocytes correlates with strain-specific susceptibility to experimental autoimmune encephalomyelitis. Proc Natl Acad Sci U S A. 1987;84(12):4219-23. PubMed PMID: 3495802. eng.
15. Aloisi F, Ria F, Adorini L. Regulation of T-cell responses by CNS antigen-presenting cells: different roles for microglia and astrocytes. Immunology Today. 2000;21(3):141-7.
16. Hayes GM, Woodroofe MN, Cuzner ML. Microglia are the major cell type expressing MHC class II in human white matter. Journal of the Neurological Sciences. 1987;80(1):25-37.
17. Prat E, Martin R. The immunopathogenesis of multiple sclerosis. Journal of rehabilitation research and development. 2002;39(2):187-200.
18. Hafler DA. Multiple sclerosis. J Clin Invest. 2004;113(6):788-94. PubMed PMID: 15067307. eng.
19. Magliozzi R, Howell O, Vora A, Serafini B, Nicholas R, Puopolo M, et al. Meningeal B-cell follicles in secondary progressive multiple sclerosis associate with early onset of disease and severe cortical pathology. Brain. 2007;130(4):1089-104.
20. Lucchinetti C, Brück W, Parisi J, Scheithauer B, Rodriguez M, Lassmann H. Heterogeneity of multiple sclerosis lesions: Implications for the pathogenesis of demyelination. Annals of Neurology. 2000;47(6):707-17.
21. Lassmann H, Brück W, Lucchinetti C. Heterogeneity of multiple sclerosis pathogenesis: implications for diagnosis and therapy. Trends in Molecular Medicine. 2001;7(3):115-21.

22. Probert L, Akassoglou K, Pasparakis M, Kontogeorgos G, Kollias G. Spontaneous inflammatory demyelinating disease in transgenic mice showing central nervous system-specific expression of tumor necrosis factor alpha. Proc Natl Acad Sci U S A. 1995;92(24):11294-8. PubMed PMID: 7479982. eng.
23. Griot C, Vandevelde M, Richard A, Peterhans E. Selective degeneration of oligodendrocytes mediated by reactive oxygen species. Free radical research communications. 1990;11(4-5):181-93.
24. Linington C, Bradl M, Lassmann H, Brunner C, Vass K. Augmentation of demyelination in rat acute allergic encephalomyelitis by circulating mouse monoclonal antibodies directed against a myelin/oligodendrocyte glycoprotein. Am J Pathol. 1988;130(3):443-54. PubMed PMID: 2450462. eng.
25. Lucchinetti CF, Parisi J, Bruck W. The pathology of multiple sclerosis. Neurologic Clinics. 2005 2005/02/01/;23(1):77-105.
26. Barnett M, Parratt J, Pollard J, Prineas J. MS: is it one disease. Int MS J. 2009;16(2):57-65.
27. Kilic AK, Esendagli G, Sayat G, Talim B, Karabudak R, Kurne AT. Promotion of experimental autoimmune encephalomyelitis upon neutrophil granulocytes' stimulation with formyl-methionyl-leucyl-phenylalanine (fMLP) peptide. Autoimmunity. 2015;48(6):423-8.
28. Baker D, Jackson SJ. Models of multiple sclerosis. ACNR. 2007;6(6):10-2.
29. Dore-Duffy P. Isolation and characterization of cerebral microvascular pericytes. The Blood-Brain Barrier: Springer; 2003. p. 375-82.
30. Winkler EA, Sengillo JD, Bell RD, Wang J, Zlokovic BV. Blood–spinal cord barrier pericyte reductions contribute to increased capillary permeability. Journal of Cerebral Blood Flow & Metabolism. 2012;32(10):1841-52.
31. Armulik A, Genové G, Mäe M, Nisancioglu MH, Wallgard E, Niaudet C, et al. Pericytes regulate the blood–brain barrier. Nature. 2010;468(7323):557.

32. Bell RD, Winkler EA, Sagare AP, Singh I, LaRue B, Deane R, et al. Pericytes control key neurovascular functions and neuronal phenotype in the adult brain and during brain aging. Neuron. 2010;68(3):409-27.
33. Daneman R, Zhou L, Kebede AA, Barres BA. Pericytes are required for blood–brain barrier integrity during embryogenesis. Nature. 2010;468(7323):562.
34. Gerhardt H, Betsholtz C. Endothelial-pericyte interactions in angiogenesis. Cell and tissue research. 2003;314(1):15-23.
35. Gerhardt H, Betsholtz C. How do endothelial cells orientate? Mechanisms of angiogenesis: Springer; 2005. p. 3-15.
36. Dore-Duffy P, Cleary K. Morphology and properties of pericytes. The Blood-Brain and Other Neural Barriers: Springer; 2011. p. 49-68.
37. Göritz C, Dias DO, Tomilin N, Barbacid M, Shupliakov O, Frisén J. A pericyte origin of spinal cord scar tissue. Science. 2011;333(6039):238-42.
38. Lin S-L, Kisseleva T, Brenner DA, Duffield JS. Pericytes and perivascular fibroblasts are the primary source of collagen-producing cells in obstructive fibrosis of the kidney. Am J Pathol. 2008;173(6):1617-27.
39. Ren S, Johnson BG, Kida Y, Ip C, Davidson KC, Lin S-L, et al. LRP-6 is a coreceptor for multiple fibrogenic signaling pathways in pericytes and myofibroblasts that are inhibited by DKK-1. Proceedings of the National Academy of Sciences. 2013;110(4):1440-5.
40. Holm A, Heumann T, Augustin HG. Microvascular Mural Cell Organotypic Heterogeneity and Functional Plasticity. Trends in Cell Biology. 2018 2018/04/01/;28(4):302-16.
41. Diaz-Flores L, Gutierrez R, Varela H. Behavior of postcapillary venule pericytes during postnatal angiogenesis. Journal of morphology. 1992;213(1):33-45.
42. Schrimpf C, Xin C, Campanholle G, Gill SE, Stallcup W, Lin S-L, et al. Pericyte TIMP3 and ADAMTS1 modulate vascular stability after kidney injury. Journal of the American Society of Nephrology. 2012;23(5):868-83.

43. Lin S-L, Chang F-C, Schrimpf C, Chen Y-T, Wu C-F, Wu V-C, et al. Targeting endothelium-pericyte cross talk by inhibiting VEGF receptor signaling attenuates kidney microvascular rarefaction and fibrosis. Am J Pathol. 2011;178(2):911-23.
44. Guillemin GJ, Brew BJ. Microglia, macrophages, perivascular macrophages, and pericytes: a review of function and identification. Journal of leukocyte biology. 2004;75(3):388-97.
45. Bjarnegård M, Enge M, Norlin J, Gustafsdottir S, Fredriksson S, Abramsson A, et al. Endothelium-specific ablation of PDGFB leads to pericyte loss and glomerular, cardiac and placental abnormalities. Development. 2004;131(8):1847-57.
46. Zlokovic BV. The blood-brain barrier in health and chronic neurodegenerative disorders. Neuron. 2008;57(2):178-201.
47. Armulik A, Abramsson A, Betsholtz C. Endothelial/pericyte interactions. Circulation research. 2005;97(6):512-23.
48. Wong S-P, Rowley JE, Redpath AN, Tilman JD, Fellous TG, Johnson JR. Pericytes, mesenchymal stem cells and their contributions to tissue repair. Pharmacology & Therapeutics. 2015;151:107-20.
49. Crisan M, Yap S, Casteilla L, Chen C-W, Corselli M, Park TS, et al. A perivascular origin for mesenchymal stem cells in multiple human organs. Cell stem cell. 2008;3(3):301-13.
50. Crisan M, Corselli M, Chen WC, Péault B. Perivascular cells for regenerative medicine. Journal of cellular and molecular medicine. 2012;16(12):2851-60.
51. Özen I, Boix J, Paul G. Perivascular mesenchymal stem cells in the adult human brain: a future target for neuroregeneration? Clinical and translational medicine. 2012;1(1):30.
52. Hurtado-Alvarado G, Cabañas-Morales AM, Gómez-Gónzalez B. Pericytes: brain-immune interface modulators. Front Integr Neurosci. 2014;7:80-. PubMed PMID: 24454281. eng.
53. Kovac A, Erickson MA, Banks WA. Brain microvascular pericytes are immunoactive in culture: cytokine, chemokine, nitric oxide, and LRP-1

expression in response to lipopolysaccharide. Journal of neuroinflammation. 2011;8(1):139.

54. Alvarez JI, Teale JM. Evidence for differential changes of junctional complex proteins in murine neurocysticercosis dependent upon CNS vasculature. Brain research. 2007;1169:98-111.
55. Shimizu F, Sano Y, Tominaga O, Maeda T, Abe M-a, Kanda T. Advanced glycation end-products disrupt the blood–brain barrier by stimulating the release of transforming growth factor–β by pericytes and vascular endothelial growth factor and matrix metalloproteinase–2 by endothelial cells in vitro. Neurobiology of aging. 2013;34(7):1902-12.
56. Thanabalasundaram G, Schneidewind J, Pieper C, Galla H-J. The impact of pericytes on the blood–brain barrier integrity depends critically on the pericyte differentiation stage. The international journal of biochemistry & cell biology. 2011;43(9):1284-93.
57. Hamilton NB, Attwell D, Hall CN. Pericyte-mediated regulation of capillary diameter: a component of neurovascular coupling in health and disease. Frontiers in neuroenergetics. 2010;2:5.
58. Schrimpf C, Teebken OE, Wilhelmi M, Duffield JS. The role of pericyte detachment in vascular rarefaction. Journal of vascular research. 2014;51(4):247-58.
59. Hinz B. Formation and function of the myofibroblast during tissue repair. Journal of Investigative Dermatology. 2007;127(3):526-37.
60. Humphreys BD, Lin S-L, Kobayashi A, Hudson TE, Nowlin BT, Bonventre JV, et al. Fate tracing reveals the pericyte and not epithelial origin of myofibroblasts in kidney fibrosis. Am J Pathol. 2010;176(1):85-97.
61. Kisseleva T, Brenner DA. Mechanisms of fibrogenesis. Experimental biology and medicine. 2008;233(2):109-22.
62. McAnulty RJ. Fibroblasts and myofibroblasts: their source, function and role in disease. The international journal of biochemistry & cell biology. 2007;39(4):666-71.

63. Arimura K, Ago T, Kamouchi M, Nakamura K, Ishitsuka K, Kuroda J, et al. PDGF receptor β signaling in pericytes following ischemic brain injury. Current neurovascular research. 2012;9(1):1-9.
64. Sharp AJ, Polak PE, Simonini V, Lin SX, Richardson JC, Bongarzone ER, et al. P2x7 deficiency suppresses development of experimental autoimmune encephalomyelitis. Journal of neuroinflammation. 2008;5(1):33.
65. Guo B, Chang EY, Cheng G. The type I IFN induction pathway constrains Th17-mediated autoimmune inflammation in mice. J Clin Invest. 2008;118(5):1680-90.
66. Trapp BD, Nave K-A. Multiple sclerosis: an immune or neurodegenerative disorder? Annu Rev Neurosci. 2008;31:247-69.
67. Terry RL, Ifergan I, Miller SD. Experimental autoimmune encephalomyelitis in mice. Multiple Sclerosis: Springer; 2014. p. 145-60.
68. Wu C-F, Chiang W-C, Lai C-F, Chang F-C, Chen Y-T, Chou Y-H, et al. Transforming growth factor β-1 stimulates profibrotic epithelial signaling to activate pericyte-myofibroblast transition in obstructive kidney fibrosis. Am J Pathol. 2013;182(1):118-31. PubMed PMID: 23142380. eng.
69. Kim KK, Sheppard D, Chapman HA. TGF-β1 signaling and tissue fibrosis. Cold Spring Harbor perspectives in biology. 2018;10(4):a022293.
70. Özen I, Deierborg T, Miharada K, Padel T, Englund E, Genové G, et al. Brain pericytes acquire a microglial phenotype after stroke. Acta Neuropathol. 2014;128(3):381-96. PubMed PMID: 24848101. Epub 05/22. eng.
71. Sakuma R, Kawahara M, Nakano-Doi A, Takahashi A, Tanaka Y, Narita A, et al. Brain pericytes serve as microglia-generating multipotent vascular stem cells following ischemic stroke. Journal of Neuroinflammation. 2016 2016/03/07;13(1):57.
72. Rustenhoven J, Jansson D, Smyth LC, Dragunow M. Brain Pericytes As Mediators of Neuroinflammation. Trends in Pharmacological Sciences. 2017;38(3):291-304.
73. Wynn TA. Cellular and molecular mechanisms of fibrosis. J Pathol. 2008;214(2):199-210. PubMed PMID: 18161745. eng.

74. van Horssen J, Bö L, Dijkstra CD, de Vries HE. Extensive extracellular matrix depositions in active multiple sclerosis lesions. Neurobiology of disease. 2006;24(3):484-91.
75. Sobel RA, Mitchell ME. Fibronectin in multiple sclerosis lesions. Am J Pathol. 1989;135(1):161.
76. Kawano H, Kimura-Kuroda J, Komuta Y, Yoshioka N, Li HP, Kawamura K, et al. Role of the lesion scar in the response to damage and repair of the central nervous system. Cell and tissue research. 2012;349(1):169-80. PubMed PMID: 22362507. Epub 02/25. eng.
77. Cox TR, Bird D, Baker A-M, Barker HE, Ho MWY, Lang G, et al. LOX-mediated collagen crosslinking is responsible for fibrosis-enhanced metastasis. Cancer Res. 2013;73(6):1721-32. PubMed PMID: 23345161. Epub 01/23. eng.
78. Ribeiro AL, Kaid C, Silva P, #x00ED, G. cB, Cortez BA, et al. Inhibition of Lysyl Oxidases Impairs Migration and Angiogenic Properties of Tumor-Associated Pericytes. Stem Cells International. 2017;2017:10.
79. Riew T-R, Choi J-H, Kim HL, Jin X, Lee M-Y. PDGFR-β-Positive Perivascular Adventitial Cells Expressing Nestin Contribute to Fibrotic Scar Formation in the Striatum of 3-NP Intoxicated Rats. Frontiers in Molecular Neuroscience. 2018 2018-November-05;11(402). English.
80. Birbrair A, Zhang T, Files DC, Mannava S, Smith T, Wang Z-M, et al. Type-1 pericytes accumulate after tissue injury and produce collagen in an organ-dependent manner. Stem Cell Research & Therapy. 2014 2014/11/06;5(6):122.
81. Bittner S, Afzali AM, Wiendl H, Meuth SG. Myelin oligodendrocyte glycoprotein (MOG35-55) induced experimental autoimmune encephalomyelitis (EAE) in C57BL/6 mice. J Vis Exp. 2014 (86):51275. PubMed PMID: 24797125. eng.
82. Terry RL, Ifergan I, Miller SD. Experimental Autoimmune Encephalomyelitis in Mice. Methods Mol Biol. 2016;1304:145-60. PubMed PMID: 25005074. eng.

83. Matsumoto Y, Ohmori K, Fujiwara M. Microglial and astroglial reactions to inflammatory lesions of experimental autoimmune encephalomyelitis in the rat central nervous system. Journal of Neuroimmunology. 1992;37(1):23-33.
84. Dias DO, Göritz C. Fibrotic scarring following lesions to the central nervous system. Matrix Biology. 2018 2018/08/01/;68-69:561-70.
85. Varga J, Lafyatis R. Etiology and pathogenesis of systemic sclerosis. Rheumatology: Sixth Edition: Elsevier Inc; 2014. p. 1177-89.
86. Jain RK, Booth MF. What brings pericytes to tumor vessels? J Clin Invest. 2003;112(8):1134-6.
87. Ignotz RA, Massague J. Transforming growth factor-beta stimulates the expression of fibronectin and collagen and their incorporation into the extracellular matrix. Journal of Biological Chemistry. 1986;261(9):4337-45.
88. Jo DH, Kim JH, Heo J-I, Kim JH, Cho C-H. Interaction between pericytes and endothelial cells leads to formation of tight junction in hyaloid vessels. Molecules and cells. 2013;36(5):465-71.
89. Iacobaeus E, Sugars RV, Andrén AT, Alm JJ, Qian H, Frantzen J, et al. Dynamic changes in brain mesenchymal perivascular cells associate with multiple sclerosis disease duration, active inflammation, and demyelination. Stem cells translational medicine. 2017;6(10):1840-51.

Appendix

1. Materials and catalog numbers
2. Ethical approval form *in vivo* experiments - Koç University
3. Ethical approval form blood serum collection - Istanbul University
4. Curriculum Vitae